Universidade do Minho
Escola de Ciências

Andreia Maria Azevedo da Silva

Production of silk-elastin-like composite materials with antimicrobial properties

Tese de Mestrado em Bioquímica Aplicada

Trabalho efetuado sob a orientação de
Doutor Raul Machado
Doutor Vitor Sencadas
Professora Doutora Margarida Casal

Janeiro de 2015

DECLARAÇÃO

Nome: Andreia Maria Azevedo da Silva

Endereço electrónico: amazevedosilva@gmail.com

Telefone: 911895757

Número do cartão de Cidadão: 13538504

Título da Tese de Mestrado:
Production of silk-elastin-like composite materials with antimicrobial properties

Orientadores:
Doutor Raul Machado
Doutor Vitor Sencadas
Professora Doutora Margarida Casal

Instituições de Acolhimento:
Centro de Biologia Molecular Ambiental (CBMA)

Ano de Conclusão: 2015

Designação do Mestrado:
Mestrado em Bioquímica Aplicada

Universidade do Minho, 31 de Janeiro de 2015

_____
Andreia Maria Azevedo da Silva

Acknowledgments/Agradecimentos

Este trabalho não é apenas resultado de um empenho individual, mas sim de um conjunto de esforços que tornaram possível a finalização desta etapa ao longo da qual adquiri competências pessoais e profissionais com todos aqueles que me acompanharam ao longo deste percurso. Desta forma, expresso a minha gratidão a todos pelos ensinamentos, ajuda, compreensão e pelo apoio nos momentos mais difíceis.

Aos meus orientadores, Doutor Raul Machado, Doutor Vitor Sencadas e Professora Doutora Margarida Casal, agradeço a oportunidade de realização do presente trabalho, toda a disponibilidade e conhecimentos transmitidos. Em primeiro lugar, agradeço ao Doutor Raul Machado pela dedicação na orientação, pelas conversas produtivas, amizade, incentivo, boa disposição e constante disponibilidade. Ao Doutor Vitor Sencadas pela simpatia, incentivo, paciência, ajuda e atenção prestada. À Professora Doutora Margarida Casal, pela amabilidade, por me ter acolhido no seu grupo de investigação e ter tornado a realização deste trabalho possível.

Ao Departamento de Biologia, particularmente ao Laboratório de Biotecnologia Molecular. Aos meus colegas do LBM pela amizade, ajuda, incentivo e pelo excelente ambiente de trabalho. Um agradecimento especial ao André pelo ensinamento, amizade, ajuda, paciência, apoio e por estar sempre presente. À Margarida, obrigada pela amizade, pelos conselhos e pelas boas conversas nos momentos certos.

Ao Laboratório de Biologia Animal, particularmente à Professora Andreia Gomes e ao André Costa por ter proporcionado a realização dos ensaios de citotoxicidade.

Queria agradecer ao Departamento de Física, pela disponibilidade, simpatia e pela disponibilização de equipamentos necessários para a realização deste trabalho.

Aos funcionários do Centro de Biologia Molecular e Ambiental pela simpatia e por toda a ajuda prestada.

Aos meus Pais, por serem os melhores pais do mundo, pelo apoio incondicional, por nunca deixarem de acreditar em mim, pela amizade, carinho e por possibilitarem a realização desta etapa, que representa um importante marco na minha vida.

Ao meu irmão por todo o apoio, carinho, simplesmente por ser quem é. À minha cunhada pelo carinho. Ao meu afilhado por me fazer sorrir nos momentos mais difíceis e por ser um dos Homenzinhos mais importantes da minha vida.

Aos meus amigos de infância, especialmente Elisabete e Ana, verdadeiros amigos, pela amizade incondicional, pelos bons conselhos e pelo apoio. Estiveram sempre presentes nos bons momentos e, o mais importante, estiveram comigo nos momentos mais difíceis.

Quero também agradecer a todos os meus amigos com os quais criei laços durante o meu percurso académico. Obrigada pelo apoio e pelos momentos inesquecíveis que me proporcionaram. Em especial a Andreia e a Cidália que se tornaram indispensáveis na minha vida. Um agradecimento especial também ao meu padrinho Marco por toda a ajuda, apoio e amizade nesta fase.

A todos, o meu muito Obrigada!

Production of silk-elastin-like composite materials with antimicrobial properties

Abstract

Pathogenic microorganisms can cause several infectious diseases in humans and, in a more dangerous situation, these microorganisms can acquire resistance over time due to excessive and inappropriate use of the pharmaceutical drugs used to cure such infections.

Currently, there is a great interest in the research of new antimicrobial agents to overcome the increasing problem associated with antibiotic resistance and therefore, the discovery of new effective antimicrobial agents will contribute to improve life quality. Antimicrobials of natural origin have attracted special interest for various biomedical applications due to its biocompatibility, availability and broad spectrum of action in combating microbial infections.

Considering the therapeutic potential shown by silver nitrate ($AgNO_3$) and bovine lactoferrin (bLF), this work is devoted to the production of novel biopolymer composites based on recombinant Silk-Elastin-Like Proteins (SELPs) and silver nitrate and lactoferrin as active fillers.

Initially, SELPs were produced and purified, and used for the fabrication of composite materials by solvent casting and electrospinning techniques. The materials were then characterized by analytical techniques and evaluated for their antimicrobial performance against bacteria and fungi. Furthermore, the cytotoxicity of the SELP/Ag materials was also evaluated using normal human skin fibroblasts.

Produção de copolímeros do tipo seda-elastina com propriedades antimicrobianas

Resumo

Os microrganismos patogênicos podem causar diversas doenças infeciosas em seres humanos e, numa situação mais perigosa, esses microrganismos podem adquirir resistência ao longo do tempo devido ao uso excessivo e inadequado dos medicamentos usados para tratar essas infeções.

Atualmente, existe um grande interesse na pesquisa de novos agentes antimicrobianos para superar o problema associado com o aumento da resistência aos antibióticos pelo que, a descoberta de novos agentes antimicrobianos mais eficazes poderá contribuir para melhorar a qualidade de vida. Os antimicrobianos de origem natural têm despertado especial interesse para várias aplicações biomédicas devido à sua biocompatibilidade, disponibilidade e largo espectro de ação no combate a infeções microbianas.

Considerando o potencial terapêutico demonstrado pelo nitrato de prata ($AgNO_3$) e lactoferrina bovina (bLF), este trabalho é dedicado à produção de novos compósitos de biopolímeros com base em Proteína Recombinante do Tipo Seda-Elastina (SELPs) e os agentes ativos nitrato de prata e lactoferrina.

Inicialmente, SELPs foram produzidos e purificados, e usados para a fabricação de materiais compósitos por técnicas de evaporação do solvente e eletrofiação. Os materiais foram depois caracterizados por técnicas analíticas e avaliados quanto ao seu desempenho antimicrobiano contra bactérias e fungos. Além disso, a citotoxicidade dos materiais de SELP/Ag também foi avaliada utilizando fibroblastos de pele humana normais.

Index

List of abbreviations

[$(NH_4)_2SO_4$]- ammonium sulphate
A- L-alanine
$AgNO_3$- silver nitrate
AGNPs- silver nanoparticles
Al- aluminum
Au- gold
***B. subtilis*-** *Bacillus subtilis*
BJ-5ta- telomerase-immortalized normal human skin fibroblasts cell line
bLF- bovine lactoferrin
C- carbon
***C. albicans*-** *Candida albicans*
***C. glabrata*-** *Candida glabratta*
CDR1 and CDR2- Candida drug resistance 1 and 2
CFUs- Colony forming units
DMEM- Dulbecco's modified Eagle's medium
DMSO- Dimethyl sulfoxide
DNA- Deoxyribonucleic acid
***E. coli*-** *Escherichia coli*
EBS- Electron Backscattering
EDS- Energy Dispersive Spectrometer
EDTA- Ethylenediamine tetraacetic acid disodium salt dihydrate
ERG11- gene encoding the target enzyme for azoles
ESEM- Environmental Scanning Electron Microscope
FA- formic acid
FdUMP- 5-fluoro-deoxyuridine monophosphate
FKS1- the gene encoding for the major and presumed catalytic subunit of 1,3-β-D-glucan synthase
FTIR- Fourier Transform Infrared Spectroscopy
FUMP- 5-fluorouridine monophosphate
FUTP- fluorouridine triphosphate
G- glycine
H_2O or dH_2O- deionized water
HCl- hydrochloric acid
IPTG- Isopropyl β-D-1-thiogalactopyranoside
LB + lac- LB medium supplemented with lactose
LB- Lysogeny Broth
LF- Lactoferrin
LPS- lipopolysaccharides
MDR1- MultiDrug Resistance 1
MFS- major facilitator superfamily
MTS- Tetrazolium salt assay (3-(4,5-dimethylthiazol-2-yl)-5-(3-carboxymethoxyphenyl)-2-(4-
NB- Nutrient broth
O- oxygen
OD- Optical density
OD_{600}- Optical density measured at a wavelength of 600 nm

OD_f – Final OD (0.05, value optimized for staining copper)

OD_i – OD of the culture cells

P- L-proline

***P. aeruginosa*-** *Pseudomonas aeruginosa*

PBS- Phosphate Buffered Saline

RNA- Ribonucleic acid

rPBPs- recombinant protein-based polymers

S- L-serine

***S. aureus*-** *Staphylococcus aureus*

SDS-PAGE- Sodium dodecyl sulphate-polyacrilamide gel electrophoresis

SELPs- Silk-elastin-like proteins

SEM- Scanning electron microscopy

SPR- surface plasmon resonance

sulfophenyl)-2H-tetrazolium)

TB + lac- TB medium supplemented with lactose

TB- Terrific Broth

TE- Tris EDTA

UPRTase- uracil phosphoribosyltransferase

UV-vis- Ultraviolet-visible spectroscopy

V- L-valine

XRD- x-ray diffraction

YPD- Yeast Peptone Dextrose medium

List of figures

temperature. **(B)** Inset graphic represents the degree of swelling determined during the first 5 min of immersion.

Figure 4.37- (A) Degree of swelling obtained for H_2O-SELP, H_2O-SELP/Ag (5 wt%) and H_2O-SELP/LF (5 wt%) films for a total of 60 min of immersion in deionized water at room temperature. **(B)** Inset graphic represents the degree of swelling determined during the first 5 min of immersion.

Figure 4.38- Hydrolytic degradation profile of SELP, SELP/Ag (3 wt%) and SELP/LF (5 wt%) fibres in PBS at different time periods. **(B)** SELP/Ag membranes removed from the PBS after 15 days of incubation. (**C)** SELP/LF membranes removed from the PBS after 15 days of incubation.

Figure 4.39- Hydrolytic degradation profile of SELP, SELP/Ag (5 wt%) and SELP/LF (5 wt%) films in PBS at different time periods.

Figure 4.40- Growth curves of *Gram-negative bacteria* (*Escherichia coli* and *Pseudomonas aeruginosa*) (blue), *Gram-positive bacteria* (*Staphylococcus aureus* and *Bacillus subtilis*) (black) and yeast (*Candida glabrata* and *Candida albicans*) (red).

Figure 4.41- Growth inhibition against *E .coli* for **(A)** FA-SELP/Ag films, **(B)** H_2O-SELP/Ag films and **(C)** SELP/Ag fibre mats. Bars represent means ± SD. **** $p<0.0001$.

Figure 4.42- Growth inhibition rates against *E. coli* and *P. aeruginosa* by SELP/Ag fibre mats. Bars represent means ± SD. **** $p<0.0001$.

Figure 4.43- Halo of inhibition of FA-SELP/Ag films (1- 0 wt%; 2- 1 wt%); 3- 3 wt%); 4- 5 wt%) against *E. coli*, *P. aeruginosa*, *S. aureus* and *B. subtilis*.

Figure 4.44- Graphical representation comparing the diameter of the halos of inhibition found for FA-SELP/Ag films against different bacteria. Results are expressed by calculating the diameter of zones of inhibition (mm).

Figure 4.45- Halo of inhibition of H_2O-SELP/Ag films (1- 0 wt%; 2- 1 wt%); 3- 3 wt%); 4- 5 wt%) against *E. coli*, *P. aeruginosa*, *S. aureus* and *B. subtilis*.

Figure 4.56- Growth inhibition against *E.coli* of **(A)** FA-SELP/LF films, **(B)** H_2O-SELP/LF films and **(C)** SELP/LF fibre mats. Bars represent means ± SD. ** p<0.01and **** p<0.0001.

Figure 4.57- Halo of inhibition of SELP/LF fibres (1- 0 wt%; 2- 1 wt%); 3- 3 wt%); 4- 5 wt%) against *E. coli, P. aeruginosa, S. aureus,* and *B. subtilis*.

Figure 4.58- Halo of inhibition of FA-SELP/LF films (1- 0 wt%; 2- 1 wt%); 3- 3 wt%); 4- 5 wt%) against four *E. coli, P. aeruginosa, S. aureus* and *B. subtilis*.

Figure 4.59- Halo of inhibition of H_2O-SELP/LF films (1- 0 wt%; 2- 1 wt%); 3- 3 wt%); 4- 5 wt%) against four *E. coli, P. aeruginosa, S. aureus* and *B. subtilis*.

Figure 4.60- Indirect contact cytotoxicity test of pristine FA-SELP and FA-SELP/Ag films on normal human skin fibroblasts (BJ-5ta cell line) with positive (control) and negative controls (30% DMSO) for cell viability after 24 and 72 h of cell culture. Results are expressed as % of viability compared to the control. Bars represent means ± SD. ns- non-significant,* p<0.05,** p<0.01, *** p<0.001 and **** p<0.0001.

Figure 4.61- Indirect contact cytotoxicity test of pristine H_2O-SELP and H_2O-SELP/Ag films on normal human skin fibroblasts (BJ-5ta cell line) with positive (control) and negative controls (30% DMSO) for cell viability after 24 and 72 h of cell culture. Results are expressed as % of viability compared to the control. Bars represent means ± SD. ns- non-significant,* p<0.05,** p<0.01, *** p<0.001 and **** p<0.0001.

Figure 4.62- Indirect contact cytotoxicity test of pristine SELP and SELP/Ag fibres on normal human skin fibroblasts (BJ-5ta cell line) with positive (control) and negative controls (30% DMSO) for cell viability after 24 and 72 h of cell culture. Results are expressed as % of viability compared to the control. Bars represent means ± SD. ns- non-significant,* p<0.05,** p<0.01, *** p<0.001 and **** p<0.0001.

List of tables

1. INTRODUCTION

The infectious diseases are a major cause of mortality in the world with more than 15 million deaths per year due to infections (Spížek *et al.,* 2010). For some years, chemical antibiotics have demonstrated to be part of the "solution" for the treatment of infectious diseases. However, bacteria and fungi have developed antibiotic and antifungal resistance, making the medical treatments very difficult and expensive. Thus, it is extremely important to improve the medical care as well as to find alternatives in order to overcome this resistance (Rai *et al.,* 2012; Spížek *et al.,* 2010).

1.1. Antibiotic resistance

Pathogens can be found everywhere *i.e.,* in the air, soil and water; and since the beginning of history, humans have handled a war against microorganisms that caused infections and diseases. Regardless of the great discoveries in the 20th century that contributed to infection control such as the discovery and commercialization of penicillin in the 40's, bacteria quickly demonstrated various forms of resistance. In fact, despite the development of new antimicrobial agents, microorganisms continue to develop new mechanisms of resistance (Harbottle *et al.,* 2006; Tenover, 2006). Presently, we are susceptible to various microorganisms that acquired resistance to different drugs (Alekshun and Levy, 2007) and therefore, the study of antibiotic resistance has had priority due to the following main factors: i) bacteria are mainly responsible for community and nosocomial infections and ii) the development of several classes of antibiotics often results in diverse mechanisms of resistance (Ghannoum and Rice, 1999).

The antimicrobial therapy used against bacterial infections may be grouped, according to their principal mechanism of action, in i) cell wall perturbation, ii) inhibition of protein synthesis, iii) interference with nucleic acid synthesis, and iv) inhibition of a metabolic pathway (Tenover, 2006).

Microorganisms may express resistance by several mechanisms which are associated to intrinsic or acquired resistance (Harbottle *et al.,* 2006; Kenneth and Ray, 2004; Tenover, 2006). The intrinsic resistance is considered a natural trait, associated with the genome of a bacterial specie and thus is present in all the elements of a specie (Harbottle *et al.,* 2006; Shanks and Peteroy-Kelly, 2009). Examples of such intrinsic

mechanism include the multi-drug resistant (MDR) phenotype of Gram-negative bacteria and the production of β-lactamases that are responsible for innate resistant against β-lactam antibiotics (Alekshun and Levy, 2007).

Of greater concern are the cases of acquired resistance (Tenover, 2006). This resistance mechanism arises from the mutation of regulatory or structural genes or from the horizontal acquisition of new genes that confers defense to a particular antimicrobial agent (Hogan and Kolter, 2002). This phenotype is not common to all elements of the specie, but rather is present in the individuals of a bacterial strain derived from a previously susceptible organism (Harbottle *et al.*, 2006; Shanks and Peteroy-Kelly, 2009).

The mutations associated with antibiotic resistance may include i) modifications of the target protein to which the antibacterial agent binds. For example, resistance to erythromycin, a ribosome inhibitor, is caused when adenosine in the bacterium's rRNA is methylated which results in alterations in the binding site (Shanks and Peteroy-Kelly, 2009); ii) downregulation or alteration of a membrane protein channel required by the antimicrobial agent to enter the cell. For example, decreased permeability via porin alterations (eg, OmpF in *E. coli*), can develop resistance to several antibiotics (Harbottle *et al.*, 2006; Tenover, 2006); iii) upregulation of the production of enzymes that inactivate the drug such as β-lactamases. These enzymes hydrolyze the ring structure of β-lactam antibiotics such as penicillins and cephalosporins (Shanks and Peteroy-Kelly, 2009; Tenover, 2006); or iv) upregulation of pumps that expel the antimicrobial agent out of the bacterial cell. For example, the efflux of tetracyclines in both Gram-positive and Gram-negative bacteria (Poole, 2002; Tenover, 2006).

Regarding horizontal gene transfer the main mechanisms are conjugation, transformation and transduction (Figure 1.1). Conjugation is the most frequent mechanism and is mediated by circular plasmids (DNA fragments) and conjunctive transposons. The plasmids are transferred between bacteria through a structure denominated "pilus" formed by the proximity of bacteria, connecting them and allowing the passage of the genetic material. Transformation is another transmission mechanism of bacterial resistance and occurs when there is a direct passage of free DNA from one cell to another. The receiving bacterium then incorporates the free DNA in its own genome, spreading the resistance. The third mechanism is named transduction and

arises through bacteriophages. The virus containing the bacterial antibiotic resistance gene infects a new cell by introducing the genetic material (Alanis, 2005).

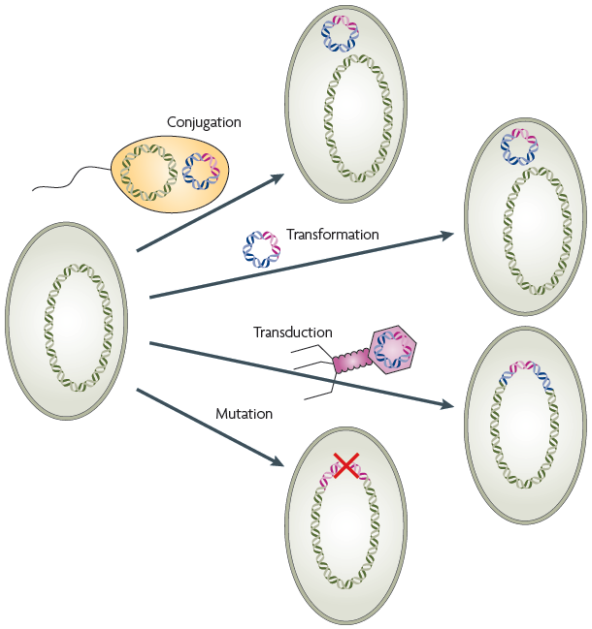

Figure 1.1- Mechanisms of antibiotic resistance by gene transfer mechanisms. DNA from the biosphere containing an antibiotic resistance gene (pink) can be transmitted by horizontal transfer through several mechanisms: conjugation, transformation and transduction. Resistance can also appear by *de novo* mutation (red cross) (Andersson and Hughes, 2010).

1.2. Antifungal resistance

Presently, the fungal infections represent a global health threat (Vandeputte *et al.*, 2012). In the last decades, the incidence of fungal infections has increased dramatically due to the increase in the number of vulnerable immunocompromised individuals to fungal infection (LaFayette *et al.*, 2010; Mishra *et al.*, 2007).

The antifungal treatment and the selection of drug are determined by various fundamental aspects such as the status of the host immune system, the location of the infection, evaluation of characteristics of the infection (fungi species present and their different susceptibility to antifungal drugs) and pharmacokinetic properties of the drug (e.g. absorption, excretion and toxicity) (Loeffler and Stevens, 2003).

The different classes of antifungal use different means to kill or inhibit the growth of fungi (Pfaller, 2012). The mode of action for the principal antifungals can be distributed in four classes namely, i) polyenes that result in modification of membrane functions; ii) azoles that inhibit the 14α-lanosterol demethylase, a fundamental enzyme

in ergosterol biosynthesis; iii) DNA and RNA synthesis inhibitors (flucytosine); and iv) 1,3-β-glucan synthase inhibitors (echinocandins) (Loeffler and Stevens, 2003).

The fungi can be intrinsically resistant to antifungal agents prior to drug exposure (primary resistance) or can acquire resistance when exposed to the antifungal drug during treatment (secondary resistance) (Perea and Patterson, 2002). The fungal pathogens develop mechanisms to neutralize the fungicidal or fungistatic action of the antifungal drugs based on the following principal mechanisms: i) reduction in the accumulation of the antifungal inside the fungal cell; ii) decrease the affinity of the drug for its target and iii) changes in the metabolism to nullify the effect of the antifungal agents (Vandeputte *et al.*, 2012).

Accordingly, the resistance mechanisms of the main antifungals are described.

Azole Resistance

Several mechanisms related to resistance to azoles in *Candida* species have been described. The first mechanism is associated with the induction of efflux pumps leading to a decrease in the accumulation of the antifungal inside the fungal cell (Pfaller, 2012). The over-expression of efflux pumps belonging to the family of ATP-binding cassette (ABC) encoded by the *CDR1* and *CDR2* genes, and the major facilitator superfamily (MFS) encoded by *MDR1* gene have been associated with azole resistance in *Candida albicans* (Lewis *et al.*, 2012). A second mechanism relates with point mutations in the *ERG11* gene that codes for the target enzyme lanosterol 14α-demethylase, inducing modifications in the target such as decreased affinity or the inability to bind to azoles (Pfaller, 2012).

Polyene Resistance

The polyenes binds to sterol, preferably ergosterol, in cell membrane causing alterations in the permeability of the membrane and cell death (Prasad and Kapoor, 2004). Resistance to polyenes arises as a consequence of considerable modifications in the lipid composition of the plasma membrane (Loeffler and Stevens, 2003). One example can be a decrease of ergosterol content due to a lack of the $\Delta^{8,7}$-sterol isomerase. Thus, this condition results in a lower affinity of the antifungal (amphotericin B) to the plasma membrane, possibly the result of a lack of the binding site (Ghannoum and Rice, 1999; Loeffler and Stevens, 2003). Another reason for

amphotericin B resistance may be a modified content β-1,3 glucans in the fungal cell wall. These constituents that influence the stability of the cell wall, induce access of large molecules such as amphotericin B to the plasma membrane (Loeffler and Stevens, 2003).

Echinocandins Resistance

This antifungal class inhibits 1,3-β-D-glucan synthase and thereby disrupts the biosynthesis of 1,3-β-D-glucan, a fundamental component of the fungal cell wall. This results in the formation of a defective cell wall that relates with cellular instability and lysis in yeasts (Pfaller, 2012). Mutations in the glucan synthase gene *FKS1* are able to drastically reduce the susceptibility to echinocandins in yeast and molds. In fact, mutations in the FSK1 resulting in a single amino acid change in the protein, of *Candida parapsilosis*, *Candida orthopsilosis*, and *Candida metapsilosis* shows up as a possible cause of intrinsic reduced susceptibility to echinocandins in these species (Marie and White, 2009).

5-fluorocytosine Resistance

The 5-fluorocytosine enters cells through cytosine permease and is deaminated to the active form 5-fluorouracil, by cytosine deaminase. In turn, 5-fluorouracil is then converted to 5-fluorouridine monophosphate (FUMP) by uracil phosphoribosyltransferase (UPRTase). FUMP can be converted into fluorouridine triphosphate (FUTP) or 5-fluoro-deoxyuridine monophosphate (FdUMP), which inhibits protein synthesis or DNA synthesis, respectively (Mishra *et al.*, 2007; Prasad and Kapoor, 2004). The 5-fluorocytosine or flucytosine resistance is associated with loss or mutation of enzymes (cytosine permease) involved in absorption of drugs (Bossche, 1997) or loss of enzymatic activity responsible for conversion to FUMP. The interruption in the formation of FUMP by the absence of cytosine deaminase activity or loss of UPRTase activity provides 5-fluorocytosine resistance (Ghannoum and Rice 1999).

In opposition to bacteria, fungi do not appear to have ability to transfer resistance genes from one organism to another. Therefore, development of resistance is remarkably slower than that verified for bacteria, and is related to the antifungal

pressure to propel mutations or reveal previously suppressed resistance genes within a given fungal strain (Klepser *et al.*, 1997).

1.3. Antimicrobial agents

Commonly, pathogenic microorganisms represent a public health problem therefore, a way of preventing this problem is essential (Azam *et al.*, 2012). The use of antimicrobial agents plays a significant role in biomedicine wherein the fundamental prerequisite of these materials is based on the capacity to perform a specific application associated to a specific and reproducible response. The antimicrobial agents can be of chemical or biological origin and one can find several examples of these. However, and considering the scope of this work, only silver (chemical origin) and bovine lactoferrin (biological origin) will be described.

1.3.1. Silver as an antimicrobial agent

Noble metals have attracted interest not only due to its versatile reactivity, but also to the compatibility and non-toxicity towards eukaryotic cells. From this group, silver is the preferred choice for application in the biomedical field owing to its attractive physicochemical properties, lower cost and particularly low toxicity to humans when present in lower concentrations (Saengmee-Anupharb *et al.*, 2013).

Silver is a basic element, very ductile and malleable, displaying higher electrical and thermal conductivity with minimum contact resistance (Rai *et al.*, 2012). The antimicrobial activity of silver is known since ancient times and its use remained until nowadays. In fact, Egyptians, Romans and Greeks used silver salts to clean wounds and silver threads in sutures to promote healing. Silver was (and still is) used in wound dressings to treat open infected wounds, skin ulcers, compound fractures, and burn injuries (Knetsch and Koole 2011). Silver was also the most widely used therapy for the treatment of infections until the discovery of antibiotics; although it is still applied due the increase of bacterial resistance to antibiotics (Knetsch and Koole, 2011; Monteiro *et al.*, 2009; Prabhu and Poulose, 2012). Silver presents antimicrobial effects of large spectrum against *Gram-negative* and *Gram-positive* bacteria, including strains resistant

to antibiotics, fungi, protozoa and certain viruses, even at lower concentrations (Monteiro *et al.*, 2009).

Silver mechanism of action

This chemical element is widely used due to its bacteriostatic and bactericidal ability towards microorganisms however, its mechanisms of action are not fully understood and several theories were developed to explain such behavior (Egger *et al.*, 2009).

Silver immediately interacts with sulfhydryl groups (-SH) on the surface of the bacteria, replacing the hydrogen atoms and giving origin to an S-Ag bond. This interrupts respiration and electron transfer, which hinders the induction of rescue mechanisms (Mijnendonckx *et al.*, 2013). Furthermore, interruption of respiration and electron transfer induces a collapse of the proton motive force, leading to the de-energization of the membrane and consequently cell death (Cao and Liu, 2010; Mijnendonckx *et al.*, 2013). The disruption of the cell membrane allows the entrance of silver ions in the cytoplasm, where it may affect many steps. The silver ions interact with nucleic acids, particularly with the nucleosides, rather than with phosphate groups (Jung *et al.*, 2008). Binding to the guanine base (N^7 atom), which is perturbed by methylation, enhances pyrimidine dimerization and affects the DNA replication (Mijnendonckx *et al.*, 2013). The suspension of replication for bacteria proliferation results in a decrease or absence of cells or promotes the formation of reactive oxygen species (ROS) within the cell, causing cellular damage and subsequent death of the bacterial structures (Cao and Liu, 2010). However, the effect which is considered most effective of silver ions is their interaction with thiol groups. Since the thiol group of cysteine residues is essential for the function of various enzymes, interaction leads to conformational changes and to inactivation of enzymatic functions (Mijnendonckx *et al.*, 2013). The steps of antibacterial actions of silver ions are summarized in Figure 1.2.

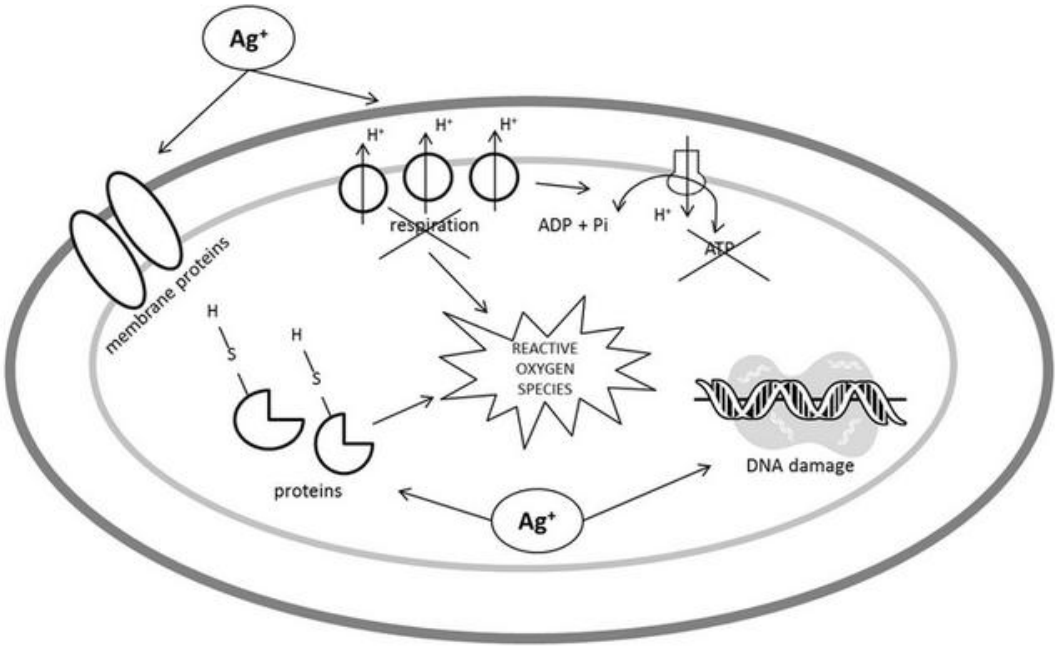

Figure 1.2- Mechanisms of action of silver ions in bacteria (Mijnendonckx *et al.*, 2013).

Silver nanoparticles show great antimicrobial activity due to the large surface area available, which promotes a better interaction between Ag^+ and the microorganisms. The nanoparticles can bind to the cell membrane and are also able to penetrate into the bacteria (Rai *et al.*, 2009).

The action of silver nanoparticles has been described by the following mechanisms:

(1) Adhesion of silver nanoparticles onto the surface of the bacterium, which induces an increase in membrane permeability, causing structural alterations and thereby cell death. The small size and large surface area of the nanoparticles provides a strong contact with the bacterium surface;

(2) Formation of free radicals, which are derived from the surface of the silver nanoparticles that interact with bacteria causing damage to the cell membrane, which becomes permeable leading to cell death;

(3) Decomposition of silver nanoparticles releases Ag^+ ions which can interact with sulphur-containing proteins in the bacterial cell walls inactivating them. The contact between the bacterial cells and silver interferes with the normal functions of the cell, resulting in the production of reactive oxygen species;

(4) Silver nanoparticles penetrate inside the bacterial cell and attack proteins that contain sulfur as well as phosphorus-containing compounds such as DNA. Nanoparticles cause DNA damage that will induce cell death. The interaction of the nanoparticles with DNA may hinder replication resulting in cell death (Egger *et al.*, 2009; Prabhu and Poulose, 2012; Reidy *et al.*, 2013).

The mechanisms for antibacterial action of silver nanoparticles as reported above are summarized in Figure 1.3.

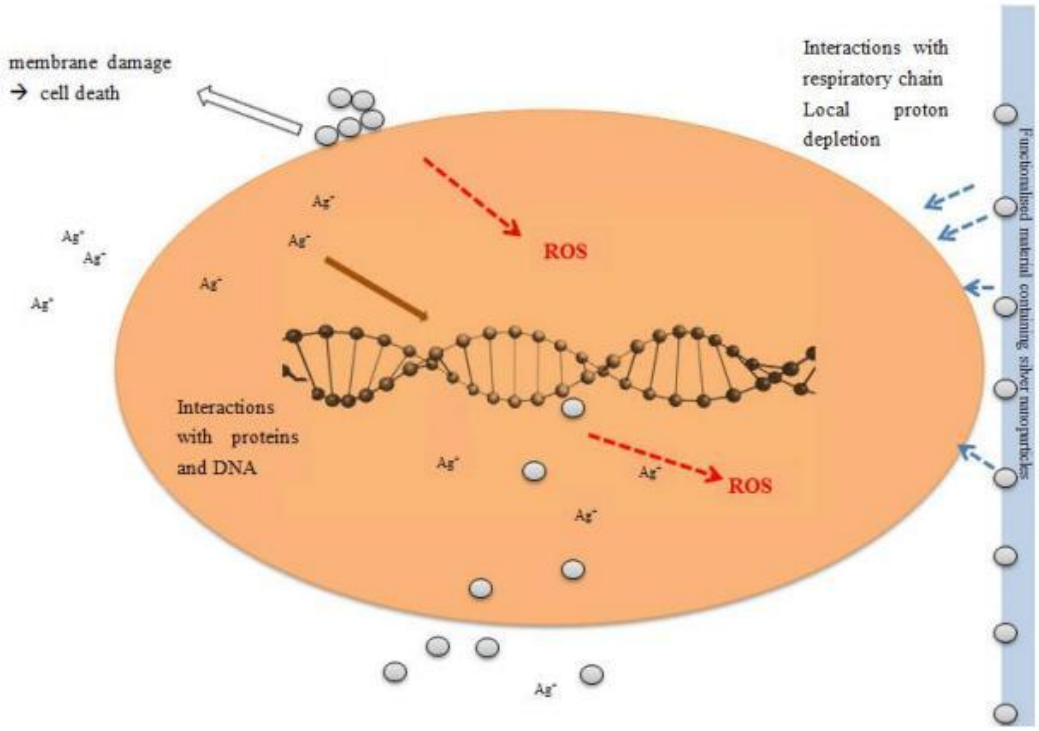

Figure 1.3- Schematic representation of the mechanisms for antibacterial action of silver nanoparticles. Grey circles indicate silver nanoparticles and Ag^+ are silver ions released from the nanoparticles (Reidy *et al.*, 2013).

Antifungal action of silver

Silver action mechanism in fungi has not been the subject of much study and its potential is not totally clear. Silver nanoparticles acts on fungi, targeting and disrupting the cell membrane, which results in formation of pores and subsequently causing cell death (Rai and Bai, 2011). It has been proposed that the silver nanoparticles affect transport systems of the cell, leading to accumulation of silver ions, causing complications in cellular processes such as metabolism and respiration. The silver ions

produce reactive oxygen species that are harmful to cell, causing damage to proteins, lipids and nucleic acids (Gavanji, 2013).

Silver applications

As mentioned, in small concentrations, silver is a compound having low toxicity, high thermal stability and low volatility to human cells and high antimicrobial activity against a broad spectrum of microorganisms (Rai *et al.,* 2009; Raja *et al.,* 2012). Nowadays, silver ions are used to control/inhibit bacterial growth in various medical applications, such as catheters, dental practice, wound healing, coating of medical devices and even in cosmetics (eg. hydrating creams, antiperspirants) (Jung *et al.,* 2008).

Silver dressings play an important role in wound treatment. These make use of delivery systems that release silver in different concentrations. Other factors, such as the silver disposal in the dressing, its chemical and physical state form, affinity of the dressing to moisture are also involved the killing of microorganisms (Rai *et al.,* 2009). Silver is also used in topical creams for the treatment of burn wounds, in dental amalgam, eye care and in silk impregnated polymers to inhibit the growth of microorganisms on medical devices, including catheters and heart valves. The use of silver has also been used in water systems acting as a disinfectant such as in swimming pools, hot water equipment in hospitals and potable water apparatus (Mijnendonckx *et al.,* 2013).

1.3.2. Lactoferrin as an antimicrobial agent

Lactoferrin (LF) was firstly reported in 1960 and is a glycoprotein that belongs to the transferrin family with a molecular weight of ~80 kDa showing a high affinity for iron (Adlerova *et al.,* 2008). Structurally, lactoferrin is a polypeptide with approximately 700 amino acids, folded into two globular lobes, each situated in one of the terminals, denominated N and C-lobe; each lobe consists of two subunits (N1, N2, C1 and C2) connected by an α-helix (Figure 1.4). Each lobe can bind a metal atom, in cooperation with the carbonate ion, which is fundamental for the binding of iron

(Adlerova *et al.,* 2008; García-Montoya *et al.,* 2012; Strate *et al.,* 2001). This glycoprotein is found in several mammalian mucosal surfaces including man, cattle, goats, dogs, among others. Lactoferrin is present in the mucosal secretions including saliva, tears, vaginal secretions, semen, bronchial and nasal secretions, gastrointestinal fluids, urine and more intensely in milk and colostrum, designating it as the second most abundant protein in milk after casein (García-Montoya *et al.,* 2012; González-Chávez *et al.,* 2009; Strate *et al.,* 2001).

Lactoferrin is considered a multifunctional protein presenting a diversity of physiological functions including the control of the amount of iron absorbed from the intestine; immune response; antioxidants, anticancer and anti-inflammatory properties. However, until the present moment, their antimicrobial capability is the most studied subject (García-Montoya *et al.,* 2012; González-Chávez *et al.,* 2009).

Figure 1.4- Structure of Lactoferrin bonded to iron (Fe_2LF) (Baker and Baker, 2012).

Antimicrobial activity

The presence on the mucosal surface makes lactoferrin a major form of defense against microorganisms that invade the body through mucosal tissues. Lactoferrin inhibits the growth of a broad spectrum of microorganisms capable of attacking humans and promote the appearance of diseases, including *Gram-positive* and *Gram-negative*

bacteria, viruses, protozoa, or fungi (Adlerova *et al.*, 2008; Jenssen and Hancock, 2009; Legrand *et al.*, 2008).

The antimicrobial activity of lactoferrin is primarily related with two mechanisms: the first is based on the ability of lactoferrin to remove the iron, essential nutrient for the growth of potential pathogens at sites of infection, acting as a bacteriostatic agent and the second mechanism is the direct effect of lactoferrin against a variety of microorganisms (García-Montoya *et al.*, 2012).

Antibacterial activity

The bacteriostatic effect of LF is due to its ability to sequester the Fe^{3+} ion resulting in the inhibition of microorganism growth (González-Chávez *et al.*, 2009). However, various bacteria can develop resistance mechanisms to overcome the sequestration of iron. Some *Gram-negative* bacteria synthesize siderophores, which function is to remove the iron from lactoferrin and transport it to zones of interest in the bacterium (Ward, 2002).

The bactericidal effect has been demonstrated by direct interaction of lactoferrin with the bacterial surface (Figure 1.5). In *Gram-negative* bacteria, LF damages the outer membrane by interacting with anionic lipid A, a constituent of the lipopolysaccharides (LPS) or porins. The positively charged N-terminal of lactoferrin prevents the interaction between LPS and bacterial cations (Ca^{2+} and Mg^{2+}), leading to the release of LPS from the cell wall, triggering the membrane permeabilization and consequential bacterial damage. The interaction of LF and LPS develops the action of natural antibacterial agents, lysozyme is one of the agents is secreted from the mucosa in parallel with LF. On the other hand, in *Gram-positive* bacteria, LF binds to positively charged anionic molecules located on the surface of bacteria, namely lipoteichoic acid, contributing in a reduction of negative charge on the cell wall and subsequently promoting the action of antibacterial agents, namely the contact between lysozyme and underlying peptidoglycan over which it exerts an enzymatic action (González-Chávez *et al.*, 2009).

Besides the aforementioned antimicrobial actions. LF contains a N-terminal domain with serine protease activity which inactivates proteins of the outer membrane of

bacteria that are essential for the adherence to host cells. Thus, LF has several antimicrobial actions for the protection of mucosal surfaces against infections caused by infectious agents (Jenssen and Hancock, 2009; Ward, 2002).

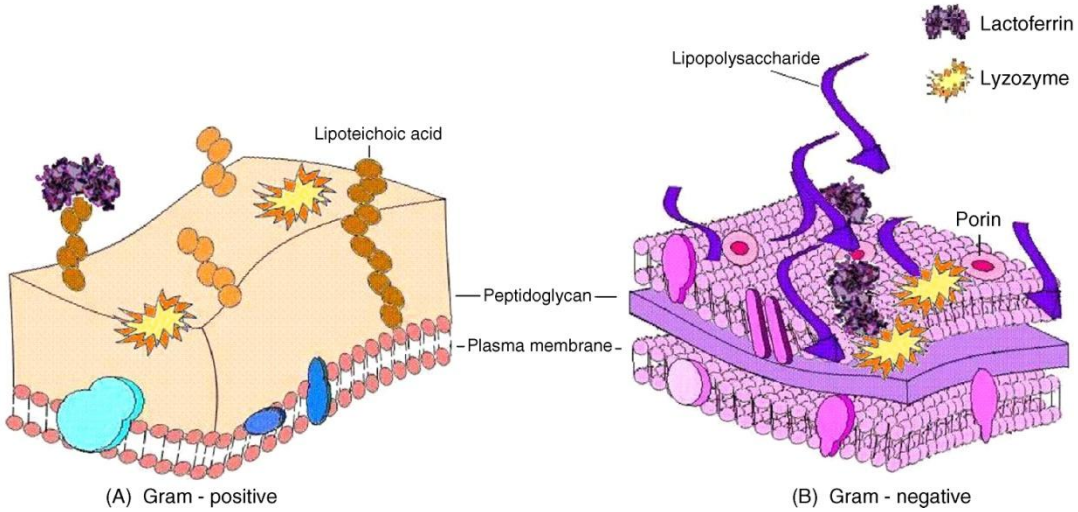

Figure 1.5- Mechanism of antibacterial action lactoferrin (González-Chávez *et al.*, 2009).

Antifungal activity

The antifungal activity of lactoferrin has been attributed to its ability to trap Fe^{3+} ions leading to changes in cell surface permeability (García-Montoya *et al.*, 2012). Due to its direct interaction with surface glycoproteins, lactoferrin induces changes in the fungal cell wall with the occurrence of surface bubbles that lead to swelling and failure (Jenssen and Hancock, 2009).

Lactoferrin applications

The various LF properties make this protein promising for clinical and industrial applications. The most widely used application is as supplement of infant formula, such as drinks and milk. Presently, it has been used in cosmetics, toothpaste, pet food supplements and drinks (García-Montoya *et al.*, 2012; Legrand *et al.*, 2008; Wakabayashi *et al.*, 2006). These products are reported as anti-inflammatory, antioxidant and anti-infection, and have the ability to improve oro-gastrointestinal microflora.

Lactoferrin has also been used in the maintenance and food protection by retarding lipid oxidation or reducing the growth of microorganisms. One example, is to obtain edible films or sprays with lactoferrin, providing a physical barrier or acting as an antimicrobial agent. In addition, clinical studies have shown good efficacy of LF for the treatment of infections and inflammatory diseases (García-Montoya *et al.*, 2012; Legrand *et al.*, 2008). Lactoferrin may also be used as a clinical marker of inflammatory diseases, once its concentration in blood and fluids may increase considerably in septicemia or during a very severe acute respiratory syndrome (García-Montoya *et al.*, 2012; Legrand *et al.*, 2008).

1.4. Silk-elastin-like proteins (SELPs)

The search for effective antimicrobial compounds with capacity to reduce and/or avoid infections has become a priority area. Due to their intrinsic properties, polymers are interesting candidates as substrates for the development of antimicrobial materials devoted for biomedical applications, either by incorporation or functionalization with antimicrobial agents. Characteristics such mechanical properties, hydrophilicity or molecular weight are important factors for antimicrobial activity, particularly in aspects such as the release rate of the biocide (Muñoz-Bonilla and Fernández-García, 2012).

The recombinant protein-based polymers (rPBPs) are a class of macromolecules obtained by recombinant DNA technology. These polymers mimic the characteristics of natural proteins, but can also display functions and properties that are not present in the natural counterparts. The silk-elastin-like proteins are an example of such macromolecules which composition is based on *tandem* repeats of silk-like (GAGAGS; G: glycine, A: L-alanine, S: L-serine) and elastin-like (VPGVG; V: L-valine, P: L-proline) blocks (Machado *et al.*, 2013a). The size of each block as well as the silk:elastin block ratio are crucial to the physicochemical properties of SELP copolymers (Machado, 2012).

Elastin is present in the extracellular matrix, providing strength and elasticity to mammalian tissues and organs, in particular in blood vessels, cartilage, ligaments, skin, and lungs. The combination of silk with elastin confers unique mechanical and biological properties to the macromolecule. The silk blocks provide strength, chemical

and thermal stability due to the formation of antiparallel beta-sheet stabilized by hydrogen bonds; whereas the periodic insertion of elastin blocks reduces the overall crystallinity of the polymeric molecule and increases its flexibility and water solubility (Machado *et al.,* 2013a). Indeed, SELPs with large silk blocks and small elastin blocks precipitate in aqueous solution even at relatively low concentrations, while the inclusion of elastin blocks with adequate size renders SELPs soluble in water (Machado *et al.,* 2013a). This characteristic is fundamental for protein purification as well as for the conception of the polymer when directed for biomedical applications.

Due to their biocompatibility and ability to self-assemble into hydrogels, SELPs have been explored as matrix-mediated delivery systems for gene therapy (Gustafson *et al.,* 2010; Gustafson *et al.,* 2009; Greish *et al.,* 2010; Megeed *et al.,* 2002; Price *et al.,* 2012), drug delivery systems (Cappello *et al.,* 1998; Dinerman *et al.,* 2002) and as scaffolds for encapsulation and chondrogenesis of human mesenchymal stem cells (Haider *et al.,* 2008). The SELP-59-A (composition S5E9, where S represents the silk block and E the elastin block) used in this study differs from the most frequent SELPs as the sequence of the elastin-like block is altered to VPAVG. This simple substitution of the central glycine by an L-alanine demonstrated to dramatically change the thermal properties of elastin-like polypeptides and have been suggested to change the mechanical response from elastic to plastic (Machado *et al.,* 2009; Urry, 2006). Furthermore, electrospun fibre mats produced from SELP-59-A showed promising properties for application in skin tissue engineering namely, for wound healing (Machado *et al.,* 2013b). In this sense, the production of SELP fibre membranes can be explored for several applications, such as in the development of artificial muscles, biosensors, dressings, protective materials and drug administration systems (Ner *et al.,* 2009).

1.5. Fabrication of composite materials with antimicrobial properties

A composite material is defined when two or more different materials are combined together, normally with different properties that, when combined, produce a material with unique characteristics. The individual components remain separate and distinct within the composite structure (Sahay *et al.,* 2012). In recent years, composite materials have been shown to be effective candidates for technological and research applications,

especially those with advantageous characteristics such as good mechanical and electrical properties, and chemical and thermal stability (Sahay *et al.*, 2012).

Solvent casting

Solvent casting is a commonly used technique for the production of films and porous membranes. This technique improved the hydrophilicity of a surface forming netted pours inside membranes which are generally used for biomaterials and tissue engineering applications (Lin *et al.*, 2012). This technique involves the solubilization, in a solvent, casting and drying whereas the solvent used confers different properties to the dried films (Byun *et al.*, 2011). The procedure to obtain films is simple: the lyophilized compound (polymer) is dissolved in a solvent, cast into a mold and usually evaporated at room temperature. The concentration and volume of the solution determines the thickness of the film (Machado, 2012).

Electrospinning

The most common methods for the production of fibrous membranes used in biomedical applications are the techniques of electrospinning, phase separation and self-assembly (Beachley and Wen, 2010). Electrospinning is a very versatile technique that allows a controlled process for the production of nano and micro fibres from different polymer solutions at laboratory scale; nevertheless, this process also allows an up-scale of materials production. The hydrodynamic stability of a liquid jet when submitted to an applied electric field was studied in 1897 by Rayleigh (Bhardwaj and Kundu, 2010). However, the fundamental idea of electrospinning dates back to 1934 when Anton and Formhals published a series of patents related with the production of fibres using an electrostatic force (Garg and Bowlin, 2011). Despite its antiquity, this technique is still used in research and industry due to its versatility and potential for applications in many areas such as nanoscience and nanotechnology. The electrospinning technique consists in the production of fibres with different diameters ranging between a few tens of nanometers to a few micrometres, through application of electrostatic forces between a capillary and a collector (Bhardwaj and Kundu, 2010; Rutledge and Fridrikh, 2007).

The fibres resulting from this process are removed in the form of a porous membrane with an elevated specific surface area (Bhardwaj and Kundu, 2010).

Regarding the nature of the polymers used in this processing technique, natural or synthetic polymers, or a mixture of both, involving nucleic acids, proteins, polysaccharides, have been processed into electrospun nanofibres (Bhardwaj and Kundu, 2010). Considering biomedical applications, natural polymers are often most appropriate as they show a better biocompatibility and low immunogenicity when compared to synthetic ones. However, the natural polymers have some disadvantages such as delicate mechanical properties and its difficult processing (Kundu *et al.*, 2013; Bhardwaj and Kundu, 2010). Characteristic natural polymers include collagen, chitosan and silk protein (fibroin) (Bhardwaj and Kundu, 2010). Among others, electrospun nanofibres have been used in biomedical applications as scaffolds for tissue engineering, drug delivery systems, wound healing and prosthetic vascular implants (Bhardwaj and Kundu, 2010).

Basic principles of the processing

In a general way, the electrospinning apparatus is composed of a high voltage source which generates a high potential difference between a capillary (metallic needle) and a grounded metal collector, a pump to control polymer flow and a deposition place (grounded metal collector) where the as-spun fibres are deposited (McCann *et al.*, 2005).

Initially, a polymer is dissolved in a suitable solvent and after complete dissolution, the solution is transferred into a syringe and mounted in a flow pump (Bhardwaj and Kundu, 2010) that connects to the high voltage source. In the electrospinning process, mutual repulsion of charge induced by the electric field causes an opposite force to the surface tension of the polymer fluid. As the electric field intensity is increased, the hemispherical surface of the fluid at the tip of the capillary tube elongates to obtain a conical shape designated as "Taylor Cone." With the increasing electrostatic field, the electrostatic repulsive force exceeds the surface tension of the polymer solution and a jet-loaded fluid is ejected from the tip of the "Taylor cone" (Huang *et al.*, 2003; Martins *et al.*, 2008; McCann *et al.*, 2005).

The polymer solution jet is in this way directed from the capillary to the metal collector, and along the way, the external electric field forces accelerates and stretch the polymer chains. With the stretch and the fast evaporation of the solvent, the jet radius becomes smaller and the radial load forces become large enough to overcome the cohesive forces of the fiber dividing it into two or more smaller fiber. This process occurs several times in rapid succession and produces a large number of small electrically charged fibres moving towards the collector (Martins *et al.*, 2008). A schematic of the electrospinning technique is represented in Figure 1.6.

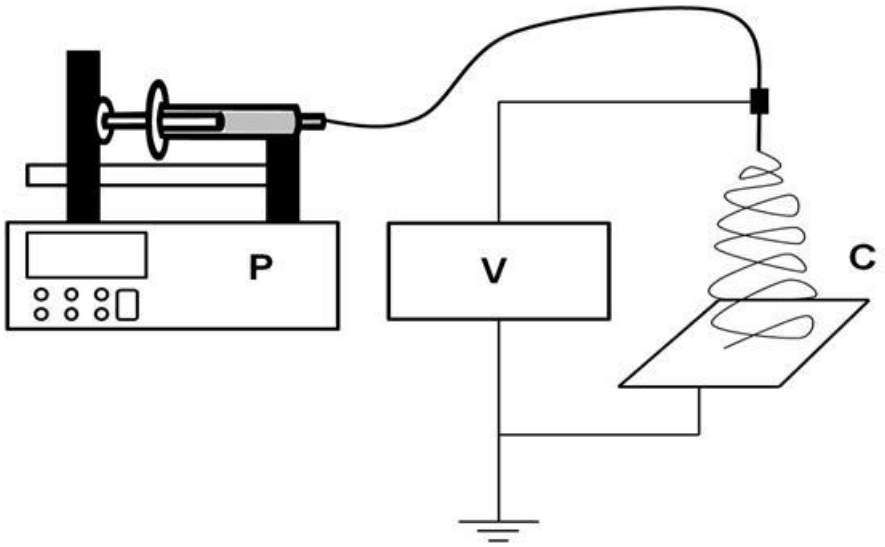

Figure 1.6- Schematic representation of the electrospinning equipment configuration. The syringe is mounted in a flow pump (P) and connected to a needle by a capillary tube which in turn is connected to a high voltage source (V). The collector (C), where the polymer fibres are collected is grounded (Machado, 2012).

During the electrospinning process, several parameters must be taken in account as they can interfere with the fibre morphology. These include sample properties such as viscosity, conductivity, molecular weight and surface tension of the polymeric solution; parameters inherent to the process such as applied electric field, the capillary diameter and the distance between the tip of the capillary and the collector; as well as environmental parameters such as humidity and temperature (Bhardwaj and Kundu, 2010; Huang *et al.*, 2003).

Important aspects of the technique

The material used is an essential component and there is a wide variety of polymers that can be processed (Bhardwaj and Kundu, 2010). The polymer concentration is also an essential variable as it is directly related to fiber diameter and inversely related to the existence and number of beads or particles which lead to the deposition of defective fibres (Huang *et al.*, 2003).

The solvent used also plays a fundamental role in this process as it must provide an adequate dissolution of the polymer while maintaining the integrity of the polymer sample. Furthermore, other characteristics include good volatility and vapor pressure (Bhardwaj and Kundu, 2010). The vapor pressure requires a determination of the rate of evaporation and the crystallization time for the materials. The volatility is fundamental in the formation of structures due to interference demonstrated in the process of phase separation. In summary, the solvent has two main functions in electrospinning, first to dissolve the polymer molecules for the formation of an electrified jet and secondly, to transport the dissolved polymer molecules towards the collector (Bhardwaj and Kundu, 2010).

2. OBJECTIVES

The present work was developed in the scope of the 2nd year of the Master Course in Applied Biochemistry, in the Department of Biology of University of Minho, under the supervision of Doctor Raul Machado (CBMA, Department of Biology), Doctor Vitor Sencadas (CFUM, Physics Department) and Prof. Doctor Margarida Casal (CBMA, Department of Biology). Experimental work was performed in the Laboratories of Molecular Biotechnology and Animal Biology from the Department of Biology, as well as in the laboratory of Electroactive smart materials group from the Physics Department, all from University of Minho.

The main objective of this project was to obtain materials displaying antimicrobial properties through the use of electrospinning and solvent cast techniques, aiming at applications directed for skin tissue engineering, namely wound healing. Due to the enormous potential of SELPs such as biocompatibility, biodegradability (as they are composed of amino acids), the ability to be fully customized for specific applications as well as the high versatility of processing into different types of materials, these recombinant biomolecules were used as base material. Antimicrobial functionality was achieved by adding two antimicrobial agents during material processing namely, bovine lactoferrin and silver nitrate.

The main objectives for this work comprised:

1. Production and purification of SELP copolymers using genetic constructions previously obtained in Margarida Casal's research group and established methodologies.
2. Production of SELP composites with antimicrobial agents (lactoferrin and silver nitrate) by electrospinning and solvent casting techniques
3. Characterization of the materials by analytical techniques
4. Evaluation of antimicrobial activity of the processed material
5. Evaluation of cytotoxicity using normal human skin fibroblasts

3. MATERIAL AND METHODS

For a clear understanding and separation of the different materials and methods used, this section is divided into different main topics. The first one describes the production and purification of silk-elastin-like proteins. The second is dedicated to materials processing, namely films and fibres by solvent casting and electrospinning techniques. Subsequently, the characterization of these materials and antimicrobial activity performance was assessed and finally, the cytotoxicity was also evaluated.

3.1. Protein production and purification

In this work, *E. coli* BL21(DE3) cells harboring the plasmid pCM13$(S_5E_9)_9$ were used for production of SELP-59-A. Pre-inoculums of *E. coli* BL21(DE3) were made in 10 mL of Terrific Broth (TB, Table 3.1) or Lysogeny Broth (LB, Table 3.1) supplemented with ampicillin (100 mg/mL) and allowed to grow at 37 °C and 200 rpm in an incubator for 18 h. The pre-cultures were then used to inoculate 250 mL of TB or LB supplemented with ampicillin (in 1 L *Erlenmeyer* flasks, 1:4 volume ratio) for an initial optical density (OD_{600nm}) of 0.01.

Table 3.1 – Culture media used and composition.

Medium	Composition
Terrific Broth (TB)	Tryptone (BD Difco) 1.2% (w/v), Yeast Extract (Hi-Media) 2.4% (w/v), K_2HPO_4 (Panreac) 0.07M, KH_2PO_4 (Panreac) 0.02 M, Glycerol (José M. Vaz Pereira, S.A.)
Lysogeny Broth (LB)	Yeast Extract (Hi-Media) 0.5% (w/v), NaCl (Panreac) 0.5% (w/v), Tryptone (BD Difco) 1.0% (w/v)

For protein expression, induction was performed by adding lactose (auto-induction) to the culture medium before inoculation (2.0 g/L) or with isopropyl β-D-1-thiogalactopyranoside (IPTG, 1 mM). For auto-induction, the cells were allowed to grow at 37 ºC, 200 rpm for 24 h; whereas, for IPTG induction, cells were grown until an OD_{600nm} of 0.6-0.8 and then induced with IPTG for 4 h. Cells from each condition were then collected by centrifugation at 10000 xg for 7 min at 4 °C and frozen at -20 ºC until purification.

3.1.1. Production screening

Protein expression levels in cells cultured in TB or LB were accessed by polyacrylamide gel electrophoresis in denaturating conditions (SDS-PAGE). Visualisation of protein bands was performed after negative gel staining with 0.3 M copper chloride. For this, 1 mL of cell culture was taken at different production times (6, 8, 10, 12, 14, 16, 18, 20, 22 and 24 h), centrifuged, resuspended in 100 µL TE buffer (50 mM Tris, 1 mM EDTA at pH 8.0) and supplemented with additional 25 µL of protein loading buffer (5x concentrated, 10% w/v SDS, 10 mM β-mercaptoethanol, 20% v/v glycerol, 0.2 M Tris-HCl pH 6.8, 0.05% w/v bromophenol blue). The samples were kept on ice and centrifuged for 20 min at 14000 xg. For electrophoresis, the samples were normalized for the same cell density and the volume of supernatant to be applied in the gel was calculated using the following expression:

$$OD_i * V_i = OD_f * V_f \quad (1)$$

where OD_i is the OD_{600nm} of the cell culture, OD_f is 0.05 (value optimized for copper staining), V_f is 125 (100 µL of the TE + 25 µL of loading buffer) and V_i is the volume of supernatant to apply on the gel. Assessment of protein expression was visually estimated by comparison between lanes.

3.1.2. Protein purification

The frozen cell pellets were thawed and resuspended in 50 mL TE buffer followed by ultrasonic cell disruption using an ultrasonic processer (Fisher S. Bioblock Scientific Model Vibra-cell 75043, 750 watts) to lyse the cells. Cell disruption was carried out using the following conditions: an amplitude of 60% for 3 s of pulse-on, followed by 6 s pulse-off delay with a total sonication time of 20 min. Samples were kept on ice throughout the entire process. The pH of the cell lysate was then adjusted to 3.5-4.0 with 1M HCl to precipitate most of the *E.coli* proteins and centrifuged at 11600 xg for 20 min at 4 ºC. The clear supernatant was then transferred and separated in new tubes. Ammonium sulphate (Panreac, p.a.) at various saturation concentrations (10, 15, 20, 25, 30 and 35%) was slowly added to the solution while on ice and constant stirring, to find the optimal concentration for the purification of the recombinant SELP copolymers.

Ammonium sulphate amounts were calculated by using the online ammonium sulphate calculator (http://www.encorbio.com/protocols/AM-SO4.htm, Encor Biotechnology, Inc.). The solutions were kept under agitation for 30 min followed by centrifugation at 11600 xg for 20 min at 4 ºC. The pellet was resuspended in deionized water (dH_2O) and centrifuged once again to remove insoluble cellular debris. The translucent polymer solution was dialyzed against dH_2O at 4 ºC under agitation for 3 days using membranes with a molecular weight cut off of 12-14 KDa (Medicell Internation Lda), filtered with a syringe filter of 0.45 µm (PES, Millipore) and lyophilized (CHRIST Model ALPHA 2-4 LD plus).

3.2. Materials processing

3.2.1. Production of films by solvent casting

Films were prepared by dissolving pure lyophilized SELP-59-A in deionized water or formic acid (Panreac, 98%) with $AgNO_3$ (Merck, p.a) or lactoferrin as a filler. Film thickness was controlled by the solution concentration and volume used. Solutions were prepared with 5 mL of SELP-59-A 3 wt% in formic acid or water with $AgNO_3$ or lactoferrin at different concentrations (1, 3 and 5 wt%). The solution was poured on the surface of a Petri plate and the solvent evaporated at room temperature.

3.2.2. Production of fibres by electrospinning

For electrospinning, solutions were prepared in the same way as the films but with a SELP-59-A concentration of 20% (w/v). The prepared solution was transferred to a plastic syringe fitted with a metallic needle with an inner diameter of 0.5 mm to initiate the electrospinning process. Electrospinning was conducted at an applied electric field of 1.7 $kV.cm^{-1}$ with a PS/FC30P04 power source from Glassman. A syringe pump (Syringepump) fed the polymer solution into the tip at a rate of 0.1 $ml.h^{-1}$. The electrospun samples were collected on aluminium foil by putting this collector on a grounded metallic collector placed at 150 mm from the needle tip.

3.2.3. Post-processing treatment

Films and fibres of SELP-59-A are soluble when in contact with aqueous environments. In order to stabilize the materials a chemical treatment with methanol vapor was performed. The materials were exposed to methanol-saturated air at room temperature for 48 hours in a vacuum desiccator (Figure 3.1). Three glass plates were placed on the bottom chamber of the desiccator, each plate containing approximately 15 mL of methanol (99.8%, Panreac). The processed materials were placed in a perforated ceramic plate located in the upper chamber and exposed to the methanol-saturated environment for 48 h.

Figure 3.1- Post- processing treatment with methanol.

3.3. Materials characterization

This section describes the various methodologies and techniques used to characterized the processed materials and in this way, evaluate the materials performance.

3.3.1. Scanning electron microscopy (SEM)

General description

The scanning electron microscopy (SEM) allows the characterization of heterogeneous materials, organic and inorganic at the micrometer (μm) or submicrometer level and is a widely used analytical technique not only in research but

also in technological industry (Smith, 1998). SEM consists in the incidence of an electron beam on the sample and when the electron beam impacts with the sample surface, a number of radiation is emitted in particular backscattered electrons, secondary electrons and x-rays, among other effects. These radiations are then detected by a detector and provide information about sample topography, chemical composition, and other material characteristics (Chong *et al.*, 2014).

Experimental analysis conditions

Microscopy samples were previously placed in a conductive carbon tape and coated with a gold thin layer (few nanometers thick). SEM characterization was performed with the help of a Cambridge S360 microscope (Leica) with an accelerating voltage of 15 kV and with magnifications of 5000x and 10000x. The average diameter and distribution of the fibres in the electrospun fibre mats was calculated with 100 randomly selected fibres with *ImageJ* image processing software (Schneider *et al.*, 2012). The Energy Dispersive Spectrometer (EDS) of silver materials was evaluated with an acceleration voltage of 8 kV and a magnification of 5000x with an acquisition time of 6 s. The distribution of the silver particles in the polymer matrices was assessed through back-scattered electrons with an accelerating voltage of 15 kV and a magnification of 10000x. SEM characterization was also done with the help of an Environmental Scanning Electron Microscope (ESEM) (FEI - Quanta 200FEG) with a landing voltage of 3-7 keV and with magnifications of 50000x, 100000x, 150000 and 200000x.

3.3.2. Fourier transform infrared spectroscopy (FTIR)

General description

The Fourier Transform Infrared Spectroscopy (FTIR) is a very useful technique for the structural analysis of compounds. The main objective is the determination of functional chemical groups present in the material as they possess characteristic absorption bands. In this technique, the sample is submitted to infrared radiation and the absorbed radiation stimulates vibratory movements, thereby generating an infrared spectrum. The energy of each particular absorption band that appears in the spectrum

corresponds to the frequency of vibration of a given chemical bond present in the sample (Duygu *et al.*, 2009).

Conditions of experimental analysis

Infrared (FTIR) spectra of films and fibres were acquired at room temperature in attenuated total reflectance mode (ATR, Alpha from Bruker) from of 4000 to 600 cm^{-1}. FTIR spectra were collected after 64 scans with a resolution of 4 cm^{-1}. Analysis of the obtained spectra was performed using the OriginPro 9.1 software (OriginLab).

3.3.3. Ultraviolet-visible spectroscopy

General description

The Ultraviolet-visible spectroscopy (UV-vis) is a characterization technique that measures the absorption of radiation by a material as a function of the wavelength. The spectrophotometer is used to measure the amount of ultraviolet or visible radiation absorbed by a sample. The radiation has energy capable of causing the interaction of photons with electrons of the sample, causing excitation of electrons to orbital of higher energy (Behera, 2012; Oudhia, 2012).

Conditions of experimental analysis

The analysis was performed either in the liquid or solid form in the UV-1700 (Shimadzu) and UV-2501PC (Shimadzu) spectrophotometers, respectively, at a wavelength range of 200 nm to 700 nm at room temperature. For solid analysis (films) specific solid support was used while for solutions analysis a 3 mL cuvette was used.

3.3.4. X-ray diffraction (XRD)

General description

The x-ray diffraction is amply used to obtain information about the structure, composition and orientation of the crystalline structure of a material. This technique studies how the crystal structures diffract incident X-ray radiation in which the

wavelength is of the same order of magnitude as the interatomic distances in the crystal lattice (Jenkins, 2000).

Conditions of experimental analysis

The X-ray diffractograms were obtained with an Analytical X-Ray Phillips Model PW 1710 BASED with a cathode current of 30 mA and a voltage of 40 kV with 1.5418740 Å (Cu-Kα) radiation. The X-ray diffraction data was collected at room temperature over the range 5–80º in increments of 0.02º.

3.3.5. Degree of swelling

Determination of the water uptake capability (degree of swelling) was assessed gravimetrically in methanol-treated samples. The materials were immersed in 10 mL of dH_2O in a glass container for different time periods (1, 2, 3, 5, 15, 30 and 60 min) at room temperature. At the end of each time interval the sample was removed and the excess of water was gently removed on both sides with the help of a paper tissue and weighted (Mettler Toledo, error ± 0.01 mg). The degree of swelling was calculated according to:

$$\text{Degree of swelling} = \left(\frac{W_t - W_d}{W_d}\right) * 100 \quad (2)$$

where W_t is the weight of the swollen sample at time t and W_d is the initial dry mass.

3.3.6. Hydrolytic degradation

Methanol-treated samples were immersed in 10 mL of Phosphate Buffered Saline (PBS) for 0, 1, 5 and 15 d at 37 °C in an oven. At the end of each time period, the samples were removed, washed with ultrapure water and air-dried at room temperature for at least 48 hours before weighting. The extent of weight loss was determined by:

$$Weigh\ Loss = \frac{W_t}{W_d} * 100 \quad (3)$$

where W_t is the weight of the material immersed in the solution at time t and W_d the initial dry.

3.4. Evaluation of antimicrobial activity

3.4.1. Biological material

Microorganisms

The microorganism used in this study were obtained from the Biology Department (University of Minho) collection and are presented in Table 3.2. All strains were preserved at -80 ºC in glycerol (30% w/v).

Table 3.2 – List of microorganisms used in the antimicrobial susceptibility tests.

Microorganisms	Species	Strain
Bacterial species	*Escherichia coli*	HB101
	Bacillus subtilis	48886
	Staphylococcus aureus	ATCC6538
	Pseudomonas aeruginosa	ATCC10145
Fungal species	*Candida albicans*	PYCC 3436
	Candida glabratta	CBS 138
	Aspergillus nidulans	FGSC A4

Culture media

Depending of the microorganism, different types of culture media were used. Bacterial cells were grown in nutrient broth (NB) [peptone 0.5% (w/v), meat extract

0.3% (w/v)]. Yeast strains were grown in yeast peptone dextrose (YPD) medium [peptone 1.0% (w/v), yeast extract 1.0% (w/v), glucose 2.0% (w/v)]. Filamentous fungi were grown in complete media [salt solution 2.0% (v/v), vitamin solution 1% (v/v), casamino acids 0.1% (w/v), yeast extract 0.1% (w/v), bactopeptone 0.2% (w/v), glucose 1.0% (w/v)]. For growth in solid media, agar 1.5% (w/v) was added to all culture media.

Growth curves

The growth curves of the bacterial species were assessed with cells grown at 37 °C for 24 h in NB medium with a volumetric ratio of 1:4 and an initial OD_{600nm} of 0.05. Measurements were made at OD_{600nm} every two hours. At an OD_{600nm} of approximately 0.6, the bacterial cell cultures were diluted in sterile PBS and plated on NB agar medium followed by overnight incubation at 37 °C. Similarly, yeast cultures were grown at 30 °C in YPD medium and OD measurements were performed at 640 nm. At an OD_{640nm} between 0.5-0.9 the yeast cell cultures were diluted in sterile PBS and plated on YPD agar medium followed by incubated at 30 ºC for 48 h. The number of colony forming units (CFUs) was then correlated with the optical density for determination of the number of cells used in the antimicrobial assays. Experiments were performed in triplicate.

3.4.2. Antimicrobial assays

Direct contact assay

This protocol is an adaptation of the ISO 22196 method "Plastics - Measurement of antibacterial activity on plastics surfaces" and is described elsewhere (da Costa *et al.*, 2015). Circular material samples with 15.4 mm of diameter were sterilized with ultraviolet light, for at least 15 min and placed in 24-well plates. For the antimicrobial assay, 50 µL of a cell suspension prepared from a 18 h pre-culture ($1.0x10^6$ CFU's.mL^{-1} per cm^2, NB medium, 37 ºC, 200 rpm) were placed in contact with the surface of the materials and incubated at 37 ºC for 2 h. A well with cell culture and no testing material was used as negative control. After incubation, 950 µL of sterile PBS were added, followed by agitation in an orbital shaker for at least 1 min. Finally, serial dilutions of

100 µL were plated in NB agar plates and incubated overnight at 37 °C. Results were expressed as % kill by the following equation:

$$\% \text{ kill} = \left[\frac{A-B}{A}\right] * 100 \quad (4)$$

where A is the number of CFUs in the negative control and B the number of CFUs after exposure to the materials samples. All experiments were performed in triplicate.

For the filamentous fungus *Aspergillus nidulans*, spores were collected with a sterile toothpick and placed in complete media plates. The materials to be tested (Ø15 mm) were placed near the spores and the plates incubated at 37 ºC for 3 d.

Dynamic shake tests

The antimicrobial properties of the electrospun fibres were evaluated by following the ASTM E2149-01 (Standard Test Method for Determining the Antimicrobial Activity of Immobilized Antimicrobial Agents under Dynamic Contact Conditions) (Varesano *et al.*, 2011). The testing cell cultures were incubated in NB and grown at 37 ºC, 200 rpm for approximately 16h. Fibre mats of 1x1cm, previously sterilized by exposure to ultraviolet light for about 15 min, were placed in a 50 mL *Erlenmeyer* flask containing 10 mL of the cell culture diluted in PBS for a final concentration of $1x10^6$ $CFUs.mL^{-1}$. The flasks were placed in an incubator for 2 h at 37 ºC and 200 rpm. After a series of dilutions in PBS, 100 µL were plated in nutrient agar and incubated overnight at 37 ºC for. The percentage of reduction was determined according to the equation 4. All experiments were performed in triplicate.

Diffusion method/halo of inhibition

The antimicrobial activity of silver and lactoferrin composites was evaluated by diffusion using 10 mm diameter sample discs previously sterilized by exposure to ultraviolet light for 15 min. Cell cultures in 0.85% agar (w/v) medium with a concentration of $1x10^6$ $CFUs.mL^{-1}$(bacteria) and $5x10^5$ $CFUs.mL^{-1}$(yeast) were prepared and poured on the top of agar plates. The composite material samples were then added to the top of the solidified layer and incubated overnight at the adequate temperature for

each microorganism. After the incubation period, the diameter of the inhibition zone (halo of inhibition) was recorded.

For the filamentous fungus *Aspergillus nidulans*, spores were collected with a sterile toothpick and placed in 5 mL of Complete Media with 0.85% agar (w/v). The materials to be tested were placed on the top of the solidified layer and incubated at 37 ºC for 3 d.

3.5. Cytotoxicity evaluation/cell viability

The cytotoxicity of the materials was evaluated with BJ-5ta cell line (telomerase-immortalized normal human skin fibroblasts) by the MTS (3-(4,5-dimethylthiazol-2-yl)-5-(3-carboxymethoxyphenyl)-2-(4-sulfophenyl)-2H-tetrazolium) proliferation assay (Promega). The MTS proliferation assay is a colorimetric method for determining the number of viable cells in proliferation and thus is an indirect cytotoxicity assay. Viable cells reduce tetrazolium compounds into intensely colored formazan products that can be detected measuring the absorbance with a spectrophotometer. The amount of formazan is directly proportional to the number of viable cells in standard culture conditions (Celis, 2006).

The materials (previously sterilized) were placed in 24-well plates with 750 µL of culture medium (4 parts of Dulbecco's modified Eagle's medium (DMEM) containing 4 mM L-glutamine, 4.5 g L−1 glucose, 1.5 g L−1 sodium bicarbonate, and 1 part of Medium 199, supplemented with 10% (v/v) of fetal bovine serum, 1% (v/v) penicillin/streptomycin solution and 10 μg mL−1 hygromycin B). The plate was incubated for 24 h at 37 ºC, 5% CO_2 in humidified environment. In parallel, cells were seeded at a density of $6.6x10^4$ cells per mL in 96-well plates and incubated for 24 h at 37 ºC, 5% CO_2 in humidified environment. After 24 h of cell growth, the medium was removed from the 96-well plates and replaced by 100 µL of the medium conditioned by contact with composite materials. Cells were incubated for an additional 24 h and 72 h at 37 °C, 5% CO_2 in humidified environment and cell viability was measured using the MTS proliferation assay. The medium was replaced by 100 µL of fresh medium and 20 µL of MTS solution was added to each well. The plate was incubated at 37 ºC for 2 h and the absorbance at 490 nm was recorded using a microplate reader (SpectraMax Plus

(Molecular Devices)). 30% DMSO and cells cultured in standard culture medium were used as negative and positive controls for cell viability, respectively. Each experiment was done in triplicate.

Statistics and data analysis. One-way and two-way analysis of variance (ANOVA) was carried out to compare the means of different data sets within each experiment in GraphPad Prism 6 software. A value of $p < 0.05$ was considered to be statistically significant.

4. RESULTS AND DISCUSSION

4.1. Protein production

Protein production studies were assessed with *E. coli* BL21(DE3) transformed with the vector pCM13$(S_5E_9)_9$, previously obtained from Margarida Casal´s research group. SELP-59-A with composition $(S_5E_9)_9$ was designed to have a molecular weight of approximately 55 kDa and consists in 9 tandem repetitions of 5 silk blocks (GAGAGS) and 9 elastin blocks (VPAVG). The expression vector pCM13 is a modified pET-25b(+) vector and contains a 6x Histidine-tag for protein purification by immobilized metal ion affinity chromatography (IMAC).

The most popular expression system in *E. coli* is based on the T7 promoter and is commonly induced by isopropyl-β-D-thiogalactopyranoside (IPTG). However, IPTG is toxic for the cells and highly expensive. Previously, it was demonstrated that protein expression induced by lactose was highly efficient while avoiding extra culture handling (Machado *et al.*, 2013a). In this work, initial protein expression studies were thus conducted using LB and TB media with and without lactose, for 24 h, 37 ºC and a 1:4 volume ratio. Supplementation with lactose showed to influence cell growth, leading to lower density values when compared with the same condition without the supplement. Indeed, for both LB (Figure 4.1) and TB (Figure 4.2), the highest cell density values were obtained in the conditions without lactose.

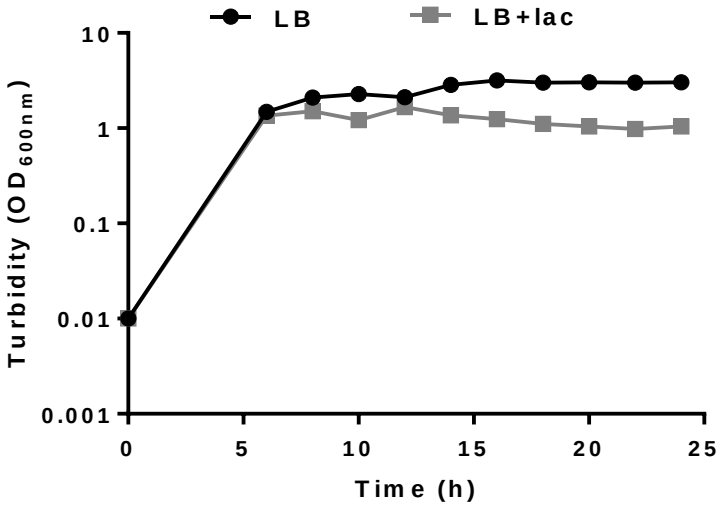

Figure 4.1- Cell growth of *E. coli* BL21(DE3) transformed with pCM13(S_5E_9) in LB medium without (LB) and with lactose (LB+lac) at different time periods for 24 h at 37 °C, 1:4 volume ratio and 200 rpm.

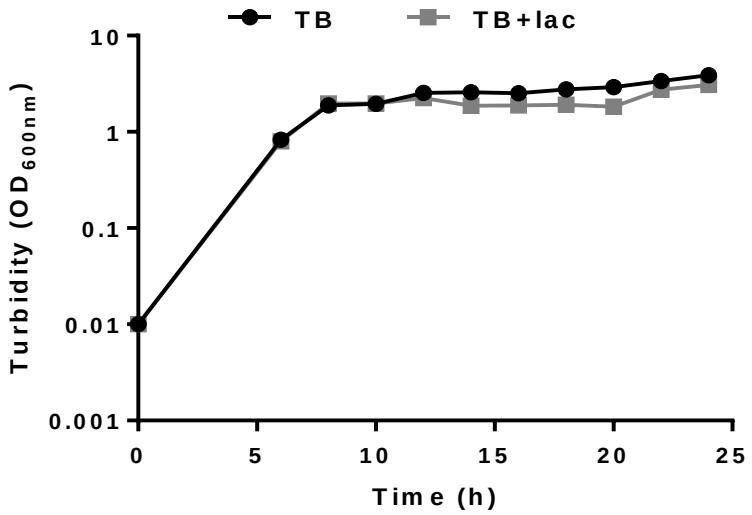

Figure 4.2- Cell growth of *E.coli* BL21(DE3) transformed with pCM13(S_5E_9) in TB medium without (TB) and with lactose (TB+lac) at different time periods for 24 h at 37 ºC, 1:4 volume ratio and 200 rpm.

Regarding protein production, expression levels were analyzed by SDS-PAGE using crude cell extracts taken at different fermentation time points (Figures 4.3 and 4.4). No overexpressed protein was observed in cells cultured in LB medium without lactose, despite the higher OD_{600nm} (approximately 3.0) (Figure 4.3A). However, for the culture in LB medium supplemented with lactose, a clear overexpression band around 66 kDa was observed (Figure 4.3B). The molecular weight was higher than the expected 55 kDa but this discrepancy was also observed by others authors and attributed to the hydrophobic nature of the protein (Machado *et al.*, 2013a; Teng *et al.*, 2009). The lower cell density obtained for the LB cultures with lactose can be explained by the metabolic burden exerted by recombinant protein production that implies a deviation of metabolic energy from cellular division to protein production.

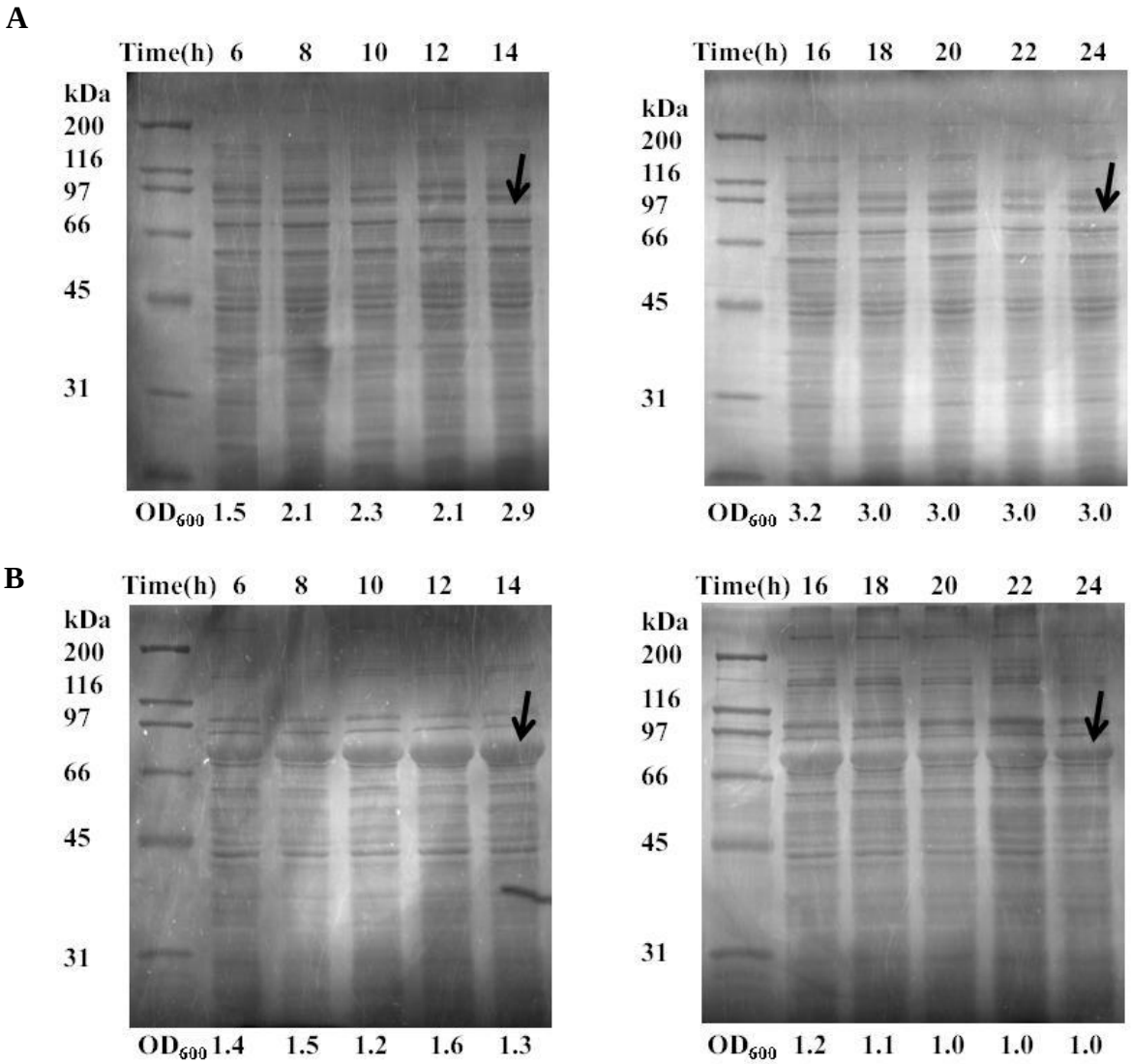

Figure 4.3- Protein production analyzed by SDS-PAGE (Copper staining) of soluble fractions of SELP-59-A at different time points. (A) Growth in LB, (B) Growth in LB+ lactose. The optical density is indicated below each fraction, and the arrow indicates the band correspondent to the recombinant protein.

Analysis of crude extracts from cells cultured in TB revealed that protein expression occurred not only in the medium supplemented with lactose but also in the non-lactose supplemented culture (Figure 4.4). In fact, the production levels in the non-lactose condition (Figure 4.4A) are apparently higher than those in the lactose-supplemented medium (Figure 4.4B). Protein expression may occur due to the nutrient rich, carbon source supplemented and buffered nature of TB. The composition and/or quality of the media ingredients can also influence this behavior likely due to lactose contamination in the yeast extract that can be responsible for this involuntary induction. In such case, the addition of lactose to TB could lead to an excess of this sugar that

might induce a stress in the host cells, leading to lower recombinant protein expression levels in the lactose-supplemented TB.

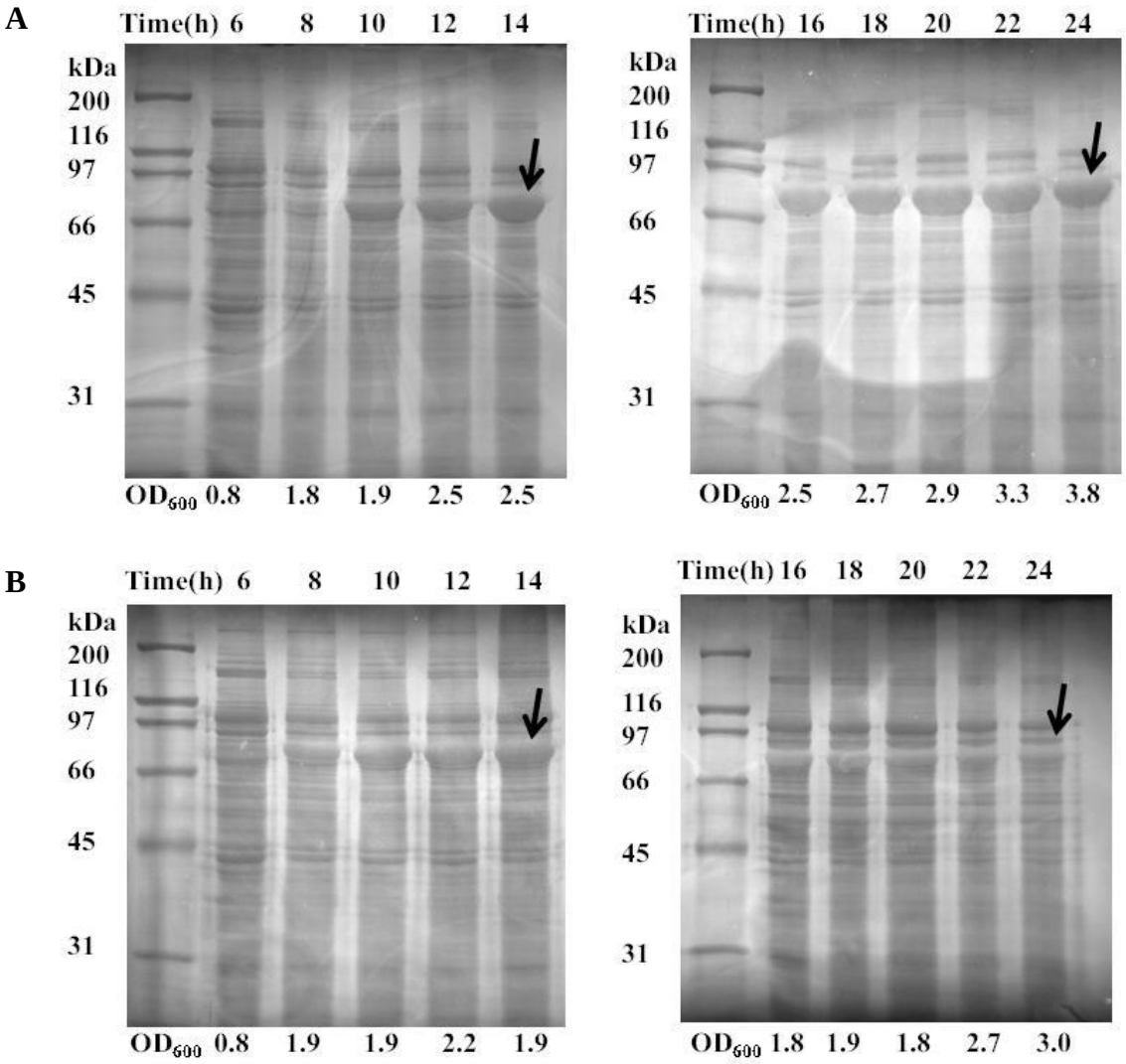

Figure 4.4- Protein production analyzed by SDS-PAGE (Copper staining) of soluble fractions of SELP-59-A at different time points. (A) Growth in TB, (B) Growth in TB+ lactose. The optical density is indicated below each fraction, and the arrow indicates the band correspondent to the recombinant protein.

To further compare the auto-induction conditions with the most commonly used inducer IPTG, and since protein expression was observable in TB medium even without induction, cells were cultured in LB medium. Using the pET system manual as reference, cells were grown in LB until reaching an OD_{600nm} between 0.6-0.8 and further induced with 1 mM IPTG for 4 h. As represented in Figure 4.5, the highest expression levels were observed after 4 h of induction with a final OD_{600nm} of 1.6.

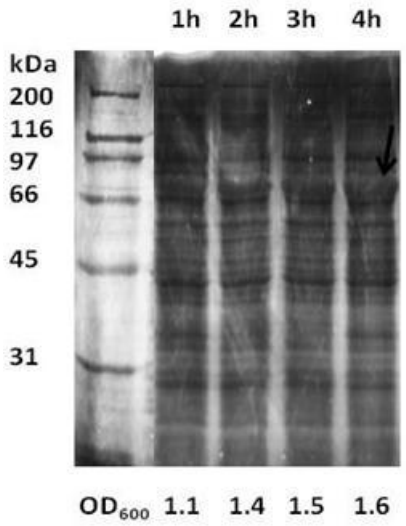

Figure 4.5- SDS-PAGE analysis of the expression levels of SELP-59-A in cell cultures induced with 1mM IPTG in LB medium at different times points (indicated on top of the gel). The optical density is indicated below each fraction. The arrow indicates the band correspondent to the recombinant protein.

Summing up the results, both induction methods allowed obtaining similar levels of overexpression. However, auto-induction is a more convenient system as there is not the need to follow growth and wait for the right time for induction. This avoids additional culture handling minimizing risks of culture contamination.

4.1.1. Protein purification

Purification with ammonium sulphate [$(NH_4)_2SO_4$] is a method that has been successfully used for the purification of many recombinant proteins (Machado *et al.*, 2013a; Scheller *et al.*, 2001; Xia *et al.* 2010). Recent studies have demonstrated the effectiveness of this method in purifying SELPs (Machado *et al.*, 2013a).

After cell disruption by sonication, the pH of the cell crude lysate was adjusted to pH 3.5 which, after centrifugation, allowed to remove most of *E. coli* endogenous proteins (Figure 4.6). The second step on the purification procedure involves the precipitation of SELP-59-A by salting out with ammonium sulphate. Figure 4.6 shows the pellet and the supernatant fractions resulting from increased concentrations of saturation with ammonium sulphate. Due to the hydrophobicity of SELP-59-A, the copolymer precipitated at relatively low concentrations of ammonium sulphate (Figure 4.6). Indeed, 20% of saturation was effective to promote the precipitation of SELP-59-A

from the soluble lysate. A highly pure protein fraction was obtained by solubilizing the precipitated copolymer in deionized water (ddH_2O) followed by centrifugation/filtration to remove the insoluble debris (Figure 4.7). This methodology allowed not only to increase the purity of the samples but also to concentrate it, leading to pure protein enriched fractions.

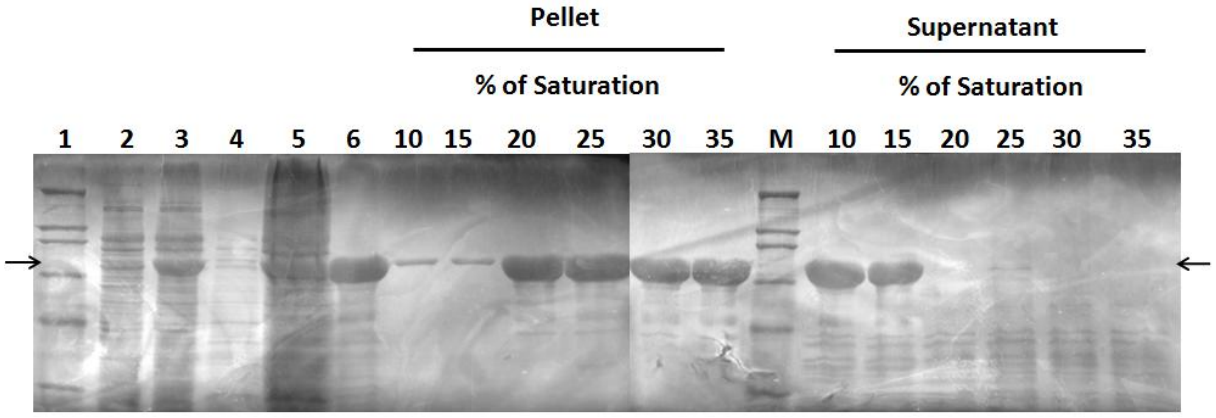

Figure 4.6- Purification of SELP-59-A by ammonium sulphate precipitation observed by SDS-PAGE (cooper staining). 1- Molecular Weight Marker (Broad Range, Bio-Rad); 2- Without production (cells transformed with empty vector); 3- Crude cell extract after induction; 4- Culture medium; 5- Crude cell lysate after sonication; 6- Supernatant of acidification. The acidified fraction was saturated with increasing concentrations of ammonium sulphate (indicated above the gel). The arrow indicates the recombinant protein band.

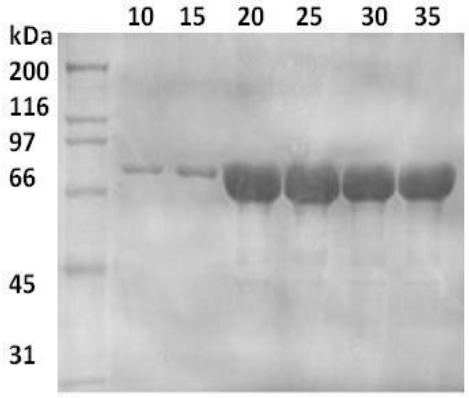

Figure 4.7- SDS-PAGE showing highly pure polymer fractions after resuspension of the precipitated copolymer in ddH_2O followed by centrifugation to remove insoluble debris. The different percentages of saturation are indicated above the gel.

After freeze-drying, the weight of pure recombinant SELP-59-A was measured and used to calculate the volumetric productivities (Table 4.1). Accordingly, the highest

level of production was obtained with TB medium. The general appearance of the freeze-dried SELP is shown in figure 4.8.

Table 4.1- Volumetric productivities of SELP-59-A using different media.

Fermentation (SELP-59-A)	LB+lactose	LB+IPTG	TB	TB+lactose	TB+IPTG
mg/L	24	80	320	130	100

Figure 4.8- Pure lyophilized SELP-59-A.

4.2. Fabrication and morphological characterization of free standing films

4.2.1. Production of films by solvent casting

Solvent casting is a technique amply used to obtain free standing films in which the solvent in the polymer solution is allowed to evaporate. Thus, the polymer needs to be soluble in the solvent to be used. The most commonly used solvents for film fabrication using SELPs as structural basis, are water (Machado, 2012; Teng *et al.*, 2009) and formic acid (Chul *et al.*, 2001; Machado *et al.*, 2013). However, formic acid has a greater ability to dissolve SELPs at higher concentrations (Machado *et al.*, 2013).

On a view of that, pure lyophilized SELP-59-A was dissolved in either formic acid or ddH_2O with corresponding filler, silver nitrate or lactoferrin, and used for film

production. Visually, the films with silver nitrate (SELP/Ag) acquired different colour intensities according to the solvent used and silver nitrate concentration (Figure 4.9A and Figure 4.9B). The films obtained with formic acid (FA-SELP/Ag) were more opaque with a stronger brownish colour than the water-based films (H_2O-SELP/Ag), with colour intensity proportional to the concentration of silver nitrate. This can be explained by the increased reduction of silver nitrate into metallic silver at higher concentrations in formic acid. The films of only SELP or composites of SELP with lactoferrin were optically transparent in both water and formic acid (Figure 4.9C and Figure 4.9D).

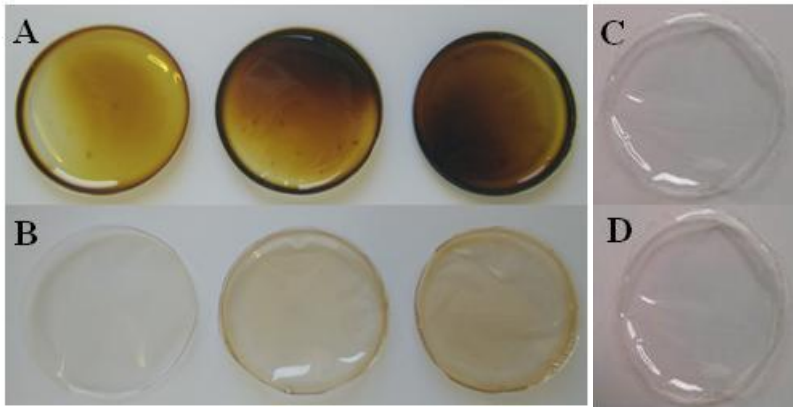

Figure 4.9 – Photograph showing colour changing of the films. **(A)** FA-SELP/Ag films (1, 3 and 5 wt %); **(B)** H_2O-SELP/Ag films (1, 3 and 5 wt %); **(C)** FA-SELP films; **(D)** FA-SELP/LF(5 wt%).

4.2.2. Scanning electron microscopy (SEM) of free standing films

The morphology of FA-SELP/Ag, H_2O-SELP/Ag and FA-SELP/LF films is shown in Figures 4.10, 4.11 and 4.12, respectively. In general, all the films showed similar surface morphology independently of the solvent or filler used. However, in the FA-SELP/Ag films it was possible to observe the presence of several brilliant dots which are indicative of the presence of silver depots.

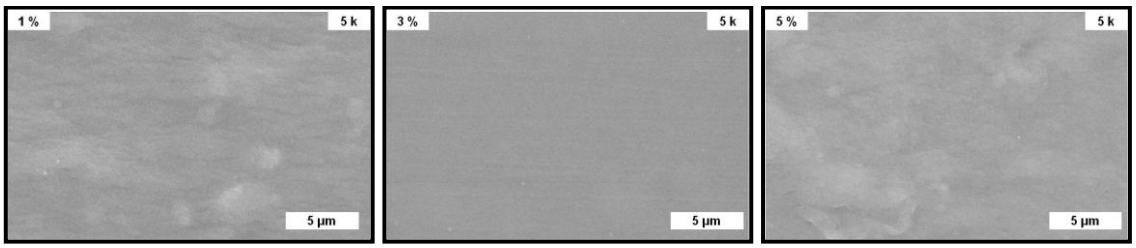

Figure 4.10- SEM micrographs of H_2O-SELP/Ag films with 1 wt%, 3 wt% and 5 wt% of silver.

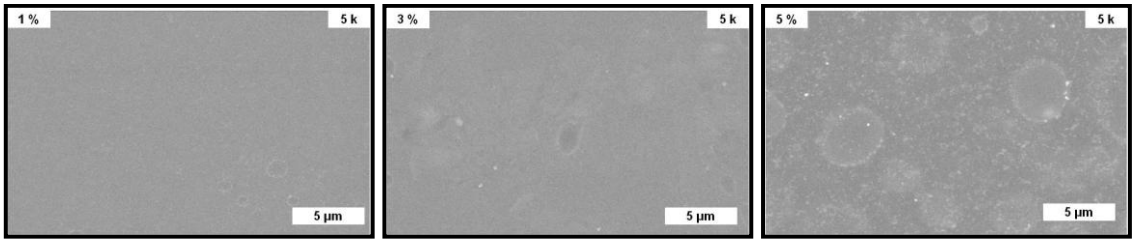

Figure 4.11- SEM micrographs of FA-SELP/Ag films with 1 wt%, 3 wt% and 5 wt% of silver.

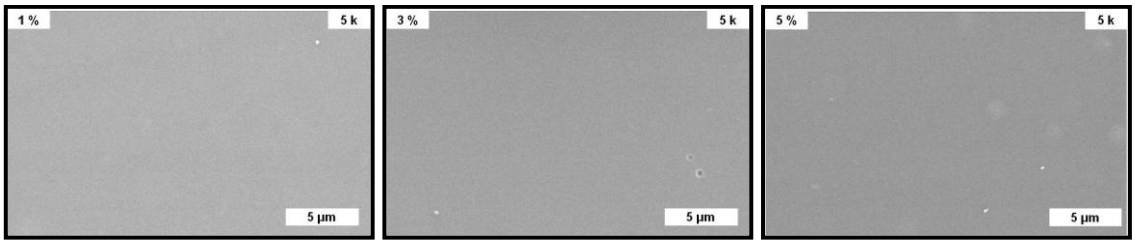

Figure 4.12- SEM micrographs of FA-SELP/LF films with 1 wt%, 3 wt% and 5 wt% of lactoferrin.

The results of SEM were not conclusive to understand the morphology of the silver depots in the film surface and so further analysis was done through environmental scanning electron microscopy (ESEM). The presence of the silver particles was very clear in the micrographs of FA-SELP/Ag films showing uniform distribution and size around 30 nm (Figure 4.13).

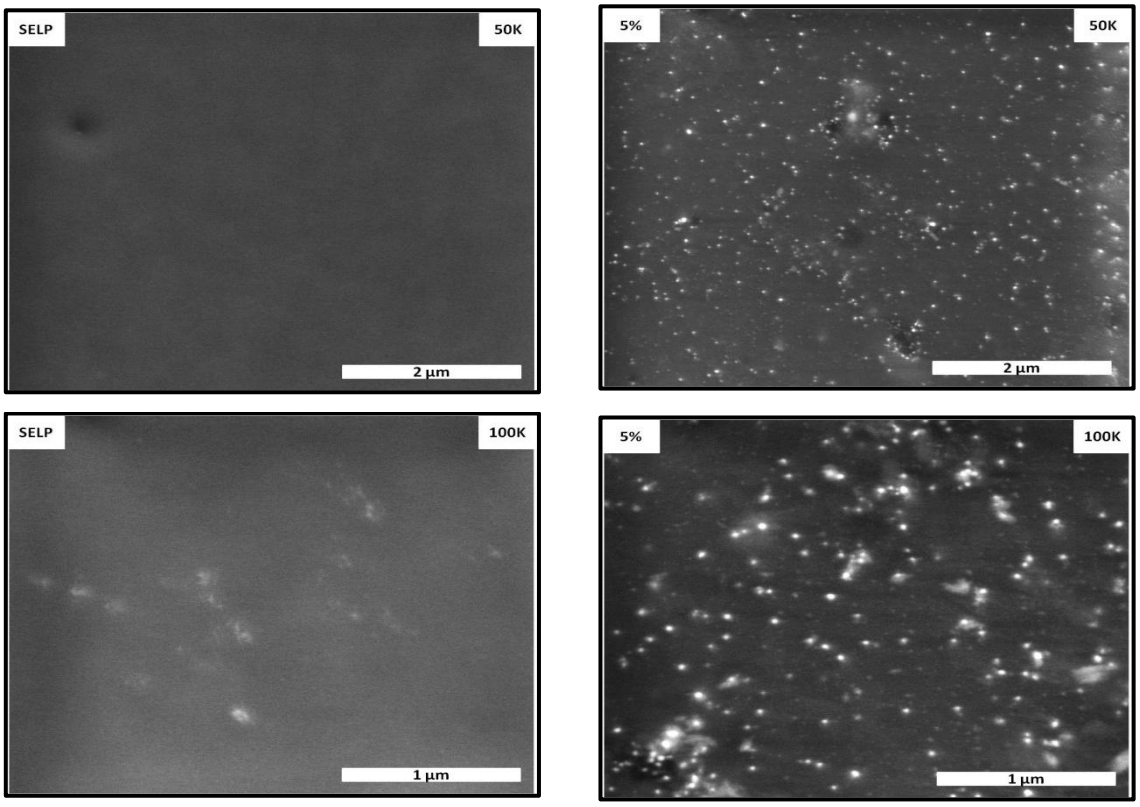

Figure 4.13 - Representative micrographs of FA-SELP films without (SELP) and with 5 wt% of silver nitrate (5%).

Shi *et al.* (2011) and Jeong and Park (2014) reported in their studies that aldehydes groups are able to reduce silver nitrate to metallic silver.

In the present study, the FA eventually has two functions, acting as a good solvent for the SELP copolymer and also working as a reducing agent for $AgNO_3$. The proposed mechanism of reaction is shown in Figure 4.14.

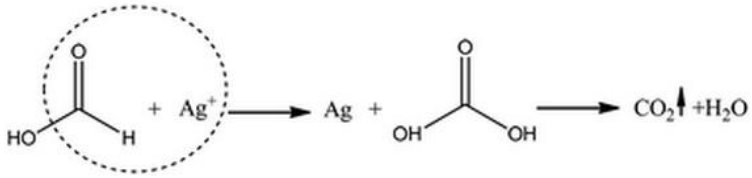

Figure 4.14 – Mechanism of silver reduction by formic acid (Shi *et al.*, 2011).

When silver nitrate combines with FA, the silver is reduced to metallic silver by the aldehyde group of formic acid. Simultaneously, the aldehyde group is oxidized to the carboxyl group to form carbonic acid which is unstable and immediately dissociates into water and carbon dioxide (Jeong and Park, 2014; Shi *et al.*, 2011). In the process of reduction of silver ions into metallic silver, first these are aggregated into clusters. Later, they aggregate into larger particles due to their small size and high surface energy (Jeong and Park, 2014; Shi *et al.*, 2011).

When analysed by energy dispersive spectroscopy (EDS), both H_2O- and FA-SELP/Ag films showed the characteristic peak of silver at about 3 keV (Figure 4.15 and Figure 4.16), which is typical of the absorption of metallic Ag nanocrystallites due to the surface plasmon resonance (Shahverdi *et al.*, 2007). Other X-ray emission peaks are labeled, including signs of carbon (C), oxygen (O) and gold (Au). The gold is the conductor medium used in the SEM, the carbon is due to the carbon tape used as conductive layer on the surface of the sample and the oxygen peak observed may suggest the presence of an oxide layer. The peaks of carbon and oxygen are also attributed of the chemical composition of amino acids and therefore the SELP. The slight increase in counts correlates with the increasing concentration of silver in the samples (Figure 4.15 and Figure 4.16).

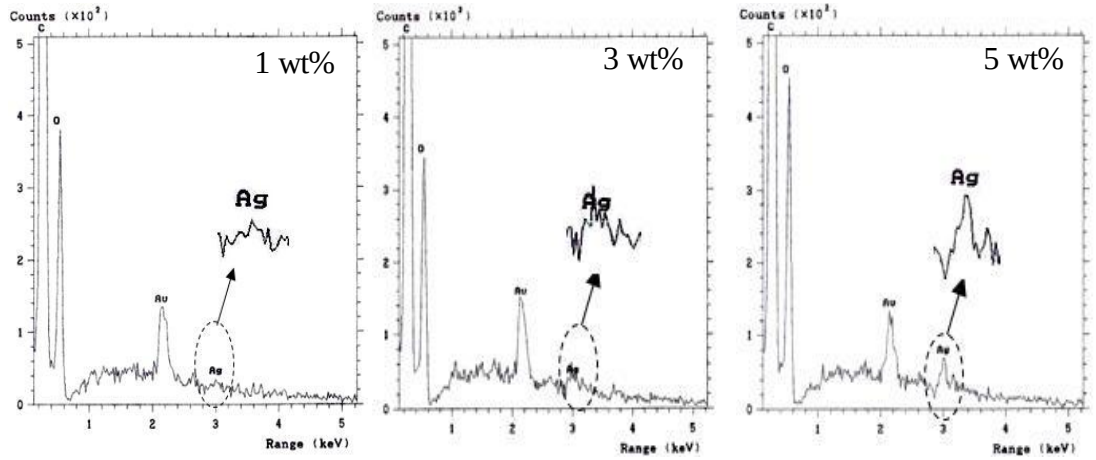

Figure 4.15- EDS analysis of FA-SELP/Ag films with different concentrations of silver showing characteristic elemental peaks.

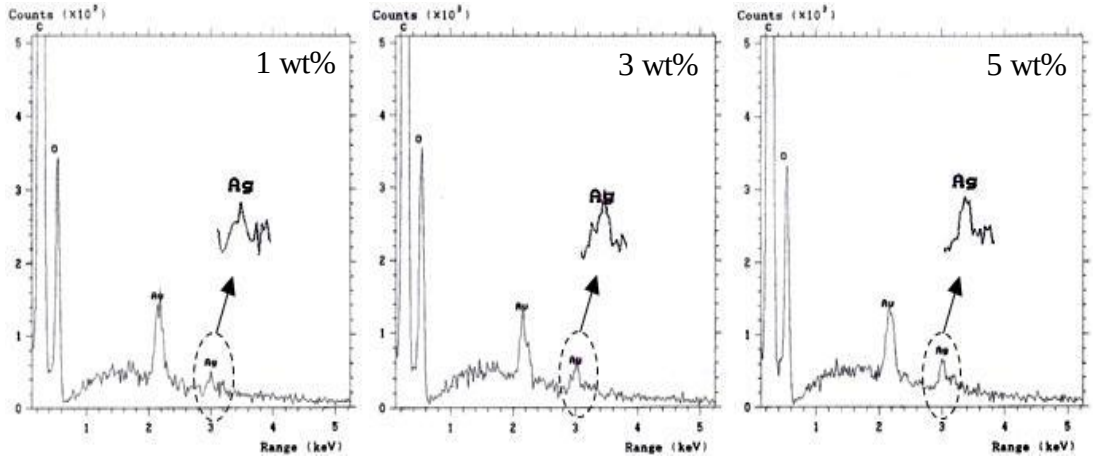

Figure 4.16- EDS analysis of H_2O-SELP/Ag films with different concentrations of silver showing characteristic elemental peaks.

4.2.3. X-ray diffraction (XRD) of silver-containing films

The X-ray diffraction (XRD) was performed to confirm the crystalline nature of the particles. The XRD patterns of FA-SELP/Ag and H_2O-SELP/Ag films are shown in Figures 4.17A and 4.17B. The obtained results were compared and interpreted using as reference data from the International Centre of Diffraction Data (ICDD) and Joint Committee on Powder Diffraction Standards (JCPDS).

The sample FA-SELP/Ag (0 wt%) showed to be amorphous while FA-SELP/Ag (5 wt%) film was characterized by the presence of five diffraction peaks, characteristic of silver nanoparticles, at approximately 32º, 38°, 44°, 64° and 77°, which correspond to the crystal facets of (101) (111) (200) (220) and (311) of silver, respectively (Ruparelia

et al., 2008; Khemani *et al.*, 2011). The XRD pattern shows that the silver nanoparticles formed by the reduction of Ag^+ ions in the FA-SELP/Ag solution are crystalline in nature. In fact, the XRD pattern of pure silver ions is known to display peaks at 2Θ = 7.9º, 11.4º, 17.8º, 30º, 32º, 38º, and 44º (Khemani *et al.*, 2011). However, in the SELP-H_2O/Ag films the same diffraction peaks are not present. H_2O-SELP/Ag (0 wt%) showed an amorphous state, while H_2O-SELP/Ag (5 wt%) was characterized by the presence of one diffraction peak characteristic of silver nanoparticles at approximately 32º.

These results mean that there is a higher crystallinity in the FA-SELP/Ag films relatively to the H_2O-SELP/Ag films. The crystallinity can influence the water-diffusion characteristics. Since water absorption is considered a determining factor for Ag^+ release, which mainly depends on the crystallinity of the sample (Kumar and Münstedt 2005), the FA-SELP/Ag films with a higher crystallinity possibly have a lower release of Ag^+ in comparison with H_2O-SELP/Ag films that are less crystalline. This means that the solvent for films processing affect the crystallinity of the polymeric matrix.

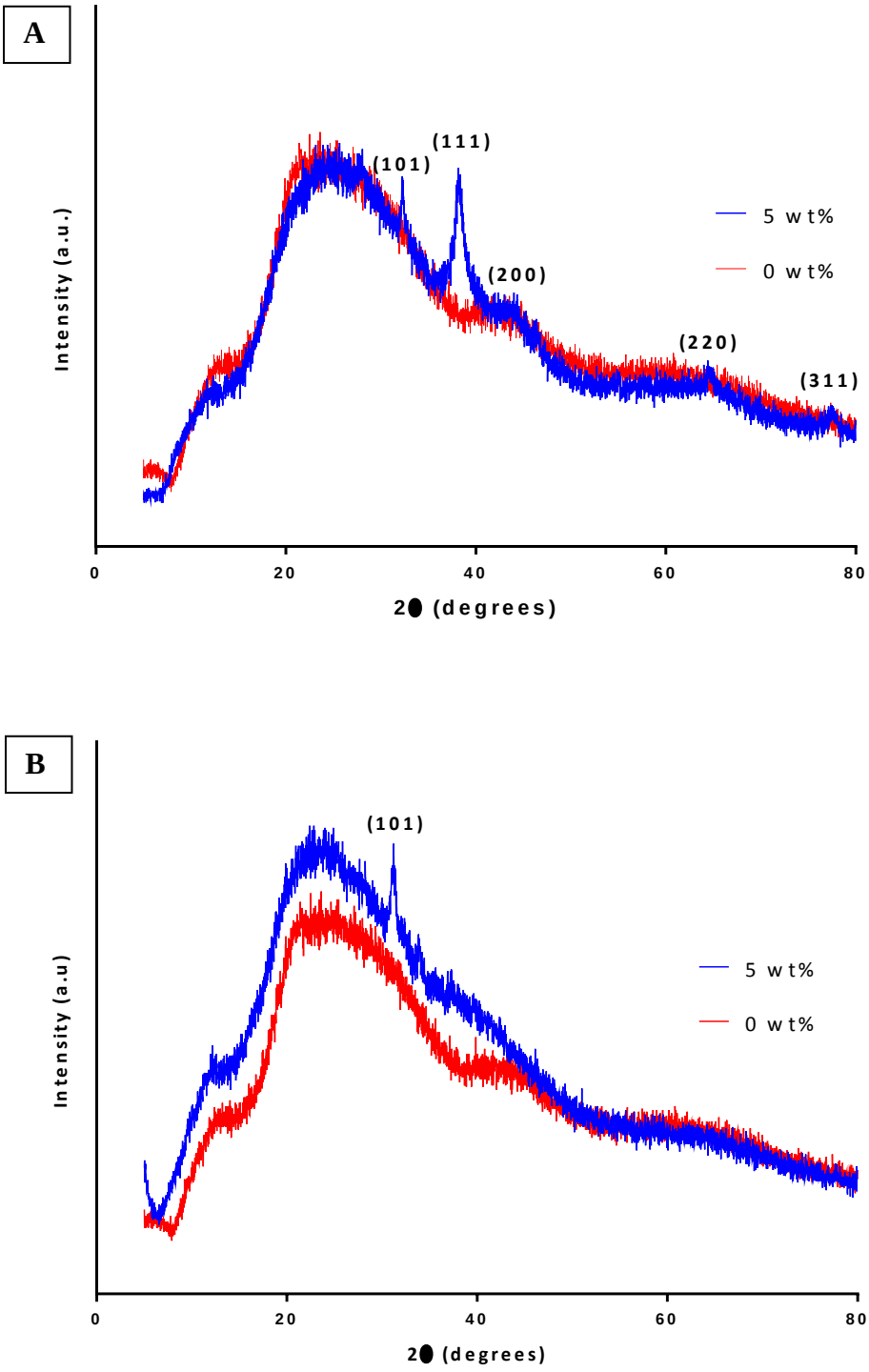

Figure 4.17- XRD spectra of **(A)** FA-SELP/Ag (0 and 5 wt%) films and **(B)** H_2O-SELP/Ag (0 and 5 wt%) films.

4.2.4. Ultraviolet-visible spectroscopy (UV-vis) of free standing films

Silver-containing film

SELP-59-A films with silver were characterized by UV–visible spectroscopy. The UV-visible absorption spectrum is described as sensitive to detect the formation of silver nanoparticles (Xu and Zhou, 2008). The interaction of light in suitable wavelength with electrons of silver nanoparticles (AgNPs) results in a phenomenon designated as surface plasmon resonance (SPR), originating optical SPR absorption peaks (Jeong and Park 2014).

The UV-vis absorption spectra for FA-SELP/Ag and H_2O-SELP/Ag films, with or without the post-processing treatment with methanol, are represented in Figures 4.18 and 4.19, respectively. The spectra show an absorption band with a steep peak at about 420 nm, corresponding to the plasmon resonance absorption band of silver. This characteristic surface plasmon absorption band indicates the presence of spherical or roughly spherical silver nanoparticles as the shape and position of plasmon absorption of AgNPs is related to the size and shape of the particles (Pal *et al.*, 2007). According to Pal *et al.* (2007), a single SPR band is shown in the absorption spectrum of spherical nanoparticles, while anisotropic particles could result in two or more SPR bands depending on the form of the nanoparticles. The nanoparticles in the region around 410–450 nm can be attributed to particles of size about 5 to 50 nm (Xu and Zhou, 2008). This size correlates to the particle size detected in the ESEM micrographs. The greater absorption at 420 nm may indicate that a larger number of silver particles were formed after evaporation of the solvent and subsequent film formation. The largest plasmon resonance peak was observed for films with 5 wt% of silver with methanol treatment whereas the intensity of the absorption band at 420 nm showed to increase proportionally with silver content. Nevertheless, the position of the maximum absorbance peak remained equal for each concentration thus indicating that the average size of silver nanoparticles is similar for every concentration.

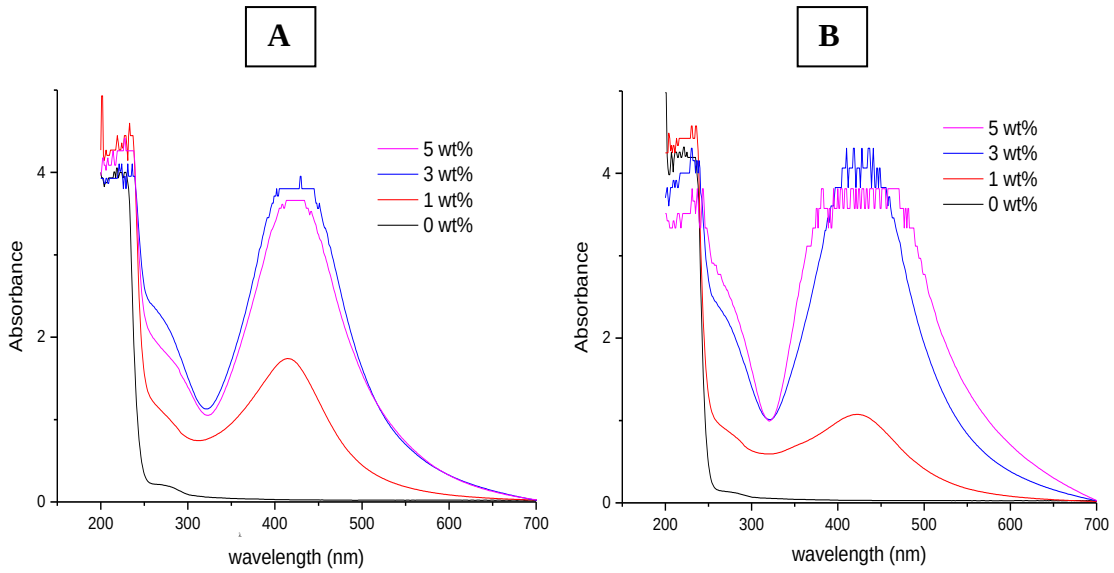

Figure 4.18 - UV-vis absorption spectra of FA-SELP/Ag films with different silver nitrate content (0, 1, 3 and 5 wt%). **(A)** non-treated FA-SELP/Ag films. **(B)** methanol-treated FA-SELP/Ag films.

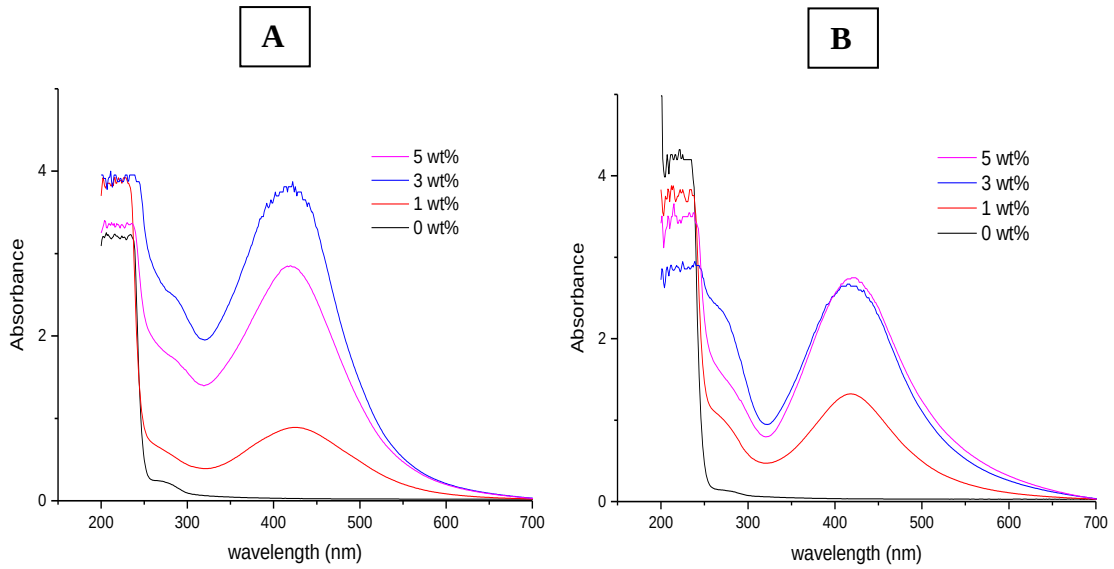

Figure 4.19- UV-vis absorption spectra of H_2O-SELP/Ag films with different silver nitrate content (0, 1, 3 and 5 wt%). **(A)** non-treated H_2O-SELP/Ag films. **(B)** methanol-treated H_2O-SELP/Ag films.

Lactoferrin-containing films

The UV-Vis absorption spectra of FA-SELP/LF and H_2O-SELP/LF films are shown in Figure 4.20 and Figure 4.21 respectively. A clear absorption band is visible at about 280 nm for both FA-SELP/LF and H_2O-SELP/LF films, being more pronounced at higher concentrations of LF. This absorption is characteristic of proteins and it is caused at great extent by the absorbance of aromatic amino acids (Schmid, 2001). As there is no aromatic amino acids with absorbance at 280 nm in the SELP sequence, this

peak is clearly attributable to the tryptophan and tyrosine residues present in the lactoferrin sequence which correlates with the increased absorbance at higher concentrations of LF. Interestingly, after treatment with methanol (Figures 4.20B and Figure 4.21B), a shift in the absorption band from the 280 to about 350 nm was observed, which may indicate a possible change in the structure of lactoferrin after the post-processing treatment.

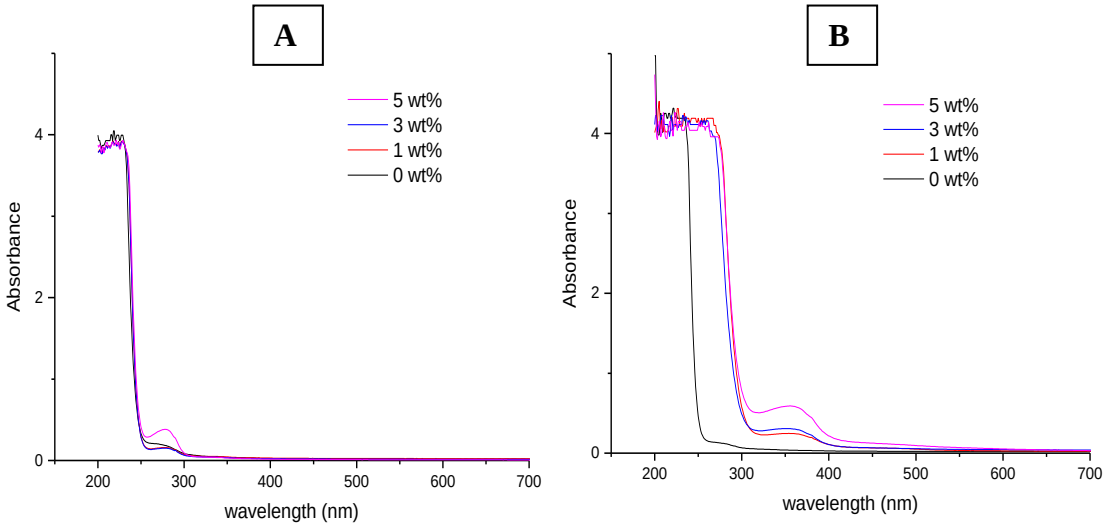

Figure 4.20- UV-vis absorption spectra of FA-SELP/LF films with different lactoferrin content (0, 1, 3 and 5 wt%). **(A)** non-treated FA-SELP/LF films. **(B)** methanol-treated FA-SELP/LF films.

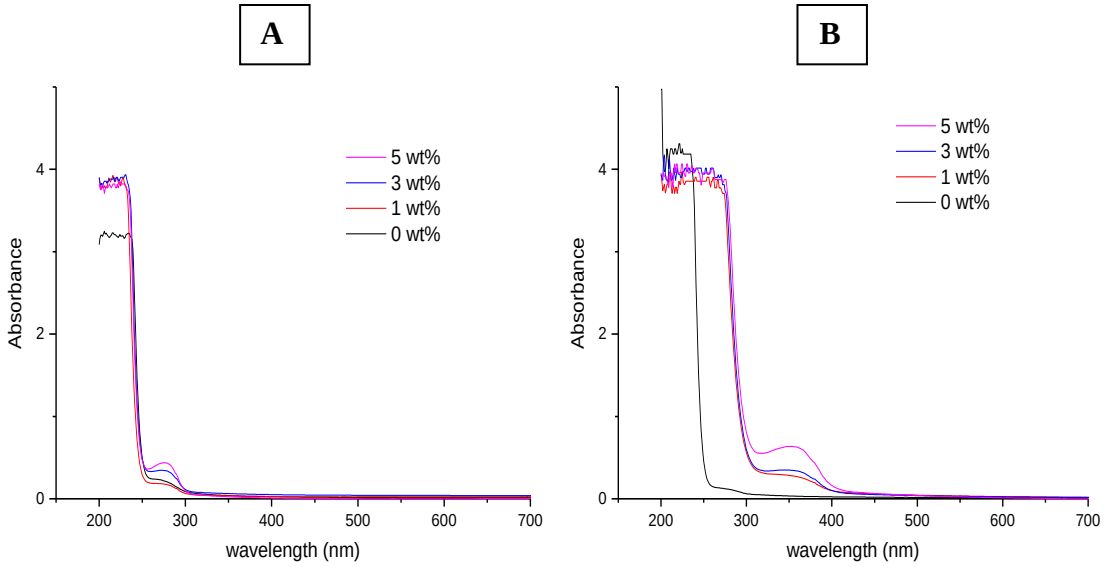

Figure 4.21 - UV-vis absorption spectra of H_2O-SELP/LF films with different lactoferrin content (0, 1, 3 and 5 wt%). (**A**) non-treated H_2O-SELP/LF films. **(B)** methanol-treated H_2O-SELP/LF films.

4.3. Fabrication and morphological characterization of electrospun fibre mats

4.3.1. Production of fibres by electrospinning

SELP electrospun mats were obtained by dissolving the copolymer in formic acid as described in previous chapter (3.2.2.). The polymer and the respective filler ($AgNO_3$ or bovine lactoferrin) were completely dissolved in FA at different concentrations resulting in a clear solution without visual signs of SELP aggregation or gelation.

In Figure 4.22, is possible to observe the general appearance of the pristine nanocomposite electrospun fibre mats. It was observed that the presence of silver nitrate led to yellowing of the fibres mats and similarly to the films, higher colour change was observed at increasing concentration of silver nitrate due to reduction of $AgNO_3$ into metallic silver. The samples with bLF showed a colour similar to the pristine SELP for all concentrations (0, 1, 3 and 5 wt%) tested in this work.

Figure 4.22 – Images showing the colour change of SELP-59-A fibres. (A) SELP/Ag fibres (from left to right) with 0, 1, 3 and 5 wt %); (B) SELP/LF fibres with 5 wt% bLF.

4.3.2. Scanning electron microscopy (SEM) of electrospun fibre mats

Silver-containing fibres

The morphology of the SELP/Ag electrospun fibres obtained from FA-SELP/Ag solutions is shown in Figure 4.23. For all the different silver nitrate concentrations, a smooth, continuous fibrous structure without defects such as beads was obtained.

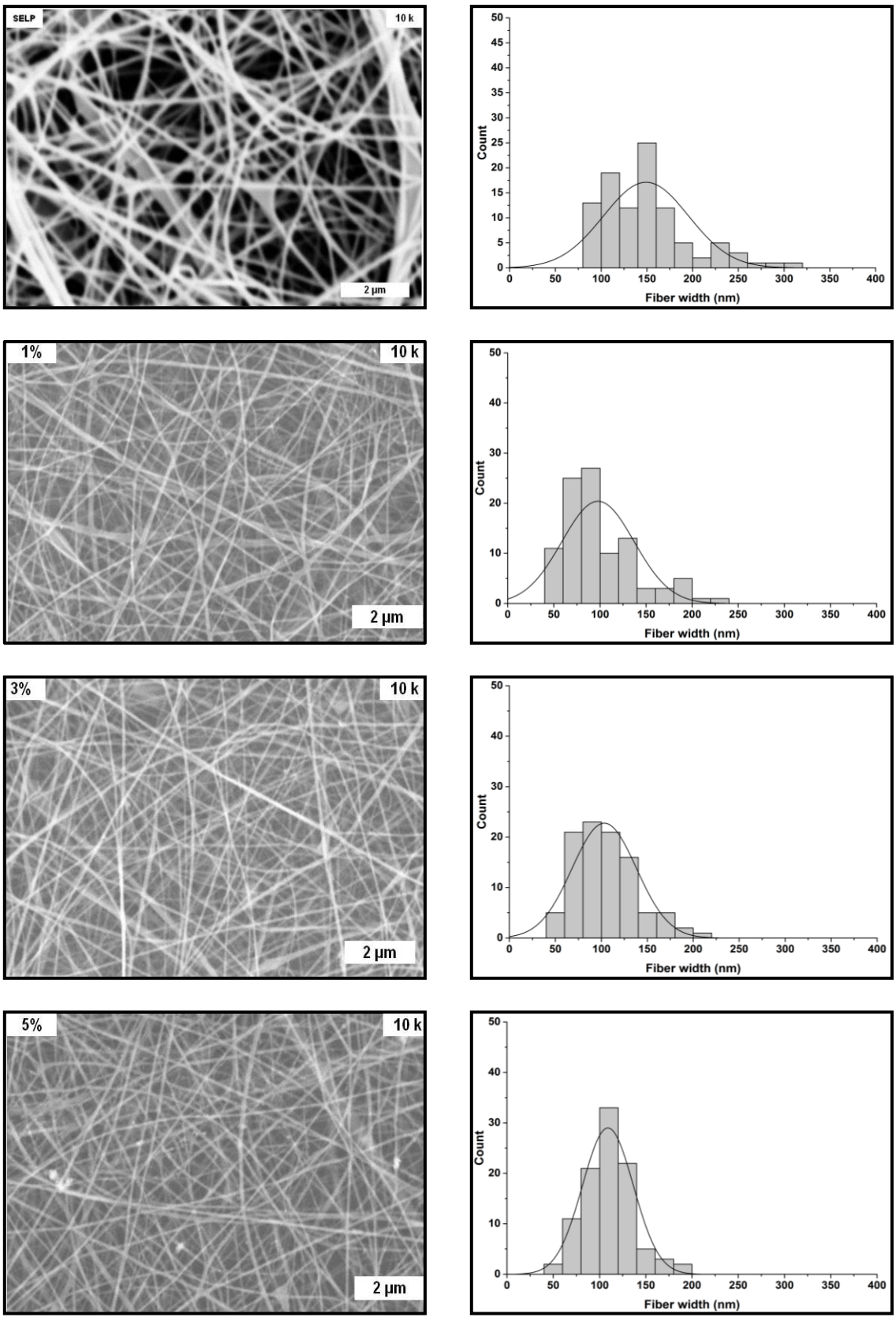

Figure 4.23- SEM micrographs of SELP/Ag electrospun fibres with different concentrations of silver nitrate: 0, 1, 3 and 5 wt%. The histograms represent fibre size distribution for each corresponding concentration. A normal distribution curve was applied for all histograms.

The effect of silver content in fibre diameter is represented in Figure 4.24. It was observed that the presence of $AgNO_3$ in the solution leads to a decrease of mean fibre diameter when compared to the pristine SELP fibres (0 wt%), decreasing from 149 ± 47 nm down to 98 ± 39 nm. This is most likely due to the increase of solution conductivity, increasing charge density and consequently promoting higher stretching forces exerted on the jet of the polymer that results in thinner fibres. Furthermore, it was also possible to observe a narrower distribution of fibre size as observable in the histograms (Figure 4.23). This same effect was also observed by other authors (Montazer and Malekzadeh, 2012; Park *et al.,* 2009).

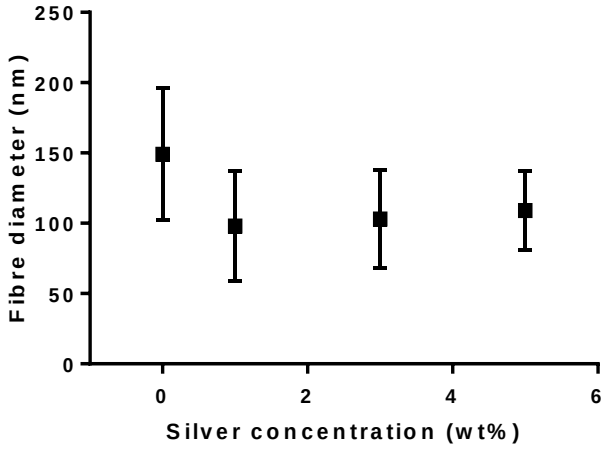

Figure 4.24- Graphical representation correlating the average fibre diameter with silver content.

The obtained electrospun fibres are highly soluble in aqueous environments limiting the range of their applicability. Therefore, in order to expand their use in liquid environments or environments with a high moisture level, there is the need to promote water insolubility. Exposure to methanol-saturated environment demonstrated to be a method that promotes the stability of the structure by inducing a molecular reorganization of the silk blocks into β-sheets thus increasing the stability of the materials when in contact with water (Machado *et al.*, 2013b).

After treatment with methanol-saturated atmosphere, the SELP/Ag fibres were assessed by SEM, showing to retain an integrity and morphology very similar to the non-treated ones (Figure 4.25). Similarly, no remarkable changes in fibre diameter were observed. The diameter of treated fibres was around 176 ± 53 nm for 0 wt% and 106 ±

31 nm for the sample with 5 wt% $AgNO_3$ which is in the same range of the mean diameter values found for the pre-treated samples (Figure 4.24).

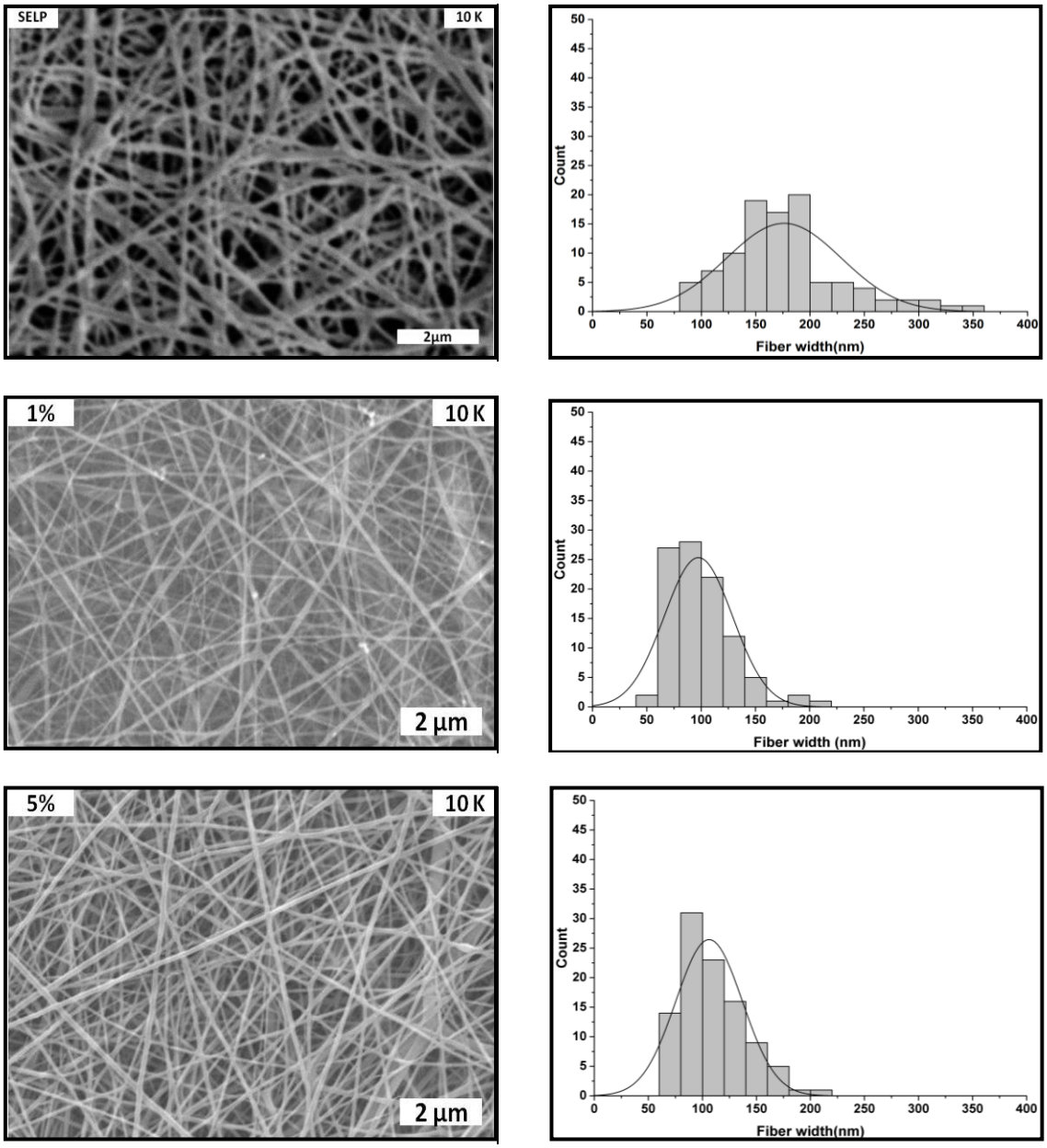

Figure 4.25- Representative SEM micrographs and histograms of fibre size distribution for methanol-treated SELP/Ag fibre mats with 0 wt% (SELP), 1 wt% (1%) and 5 wt% (5%).

Although it was possible to observe some small spots in the micrographs, the presence and confirmation of AgNPs in the fibres was also studied by SEM using an Electron Backscattering (EBS) detector (Figure 4.26). This analysis allowed a more clear detection of the presence of silver particles by the string reflection of the silver ions. As observed in the micrographs, the silver particles showing up as brilliant dots,

were not homogenously distributed in the fibre mat but rather aggregated forming silver depots in the fibre web.

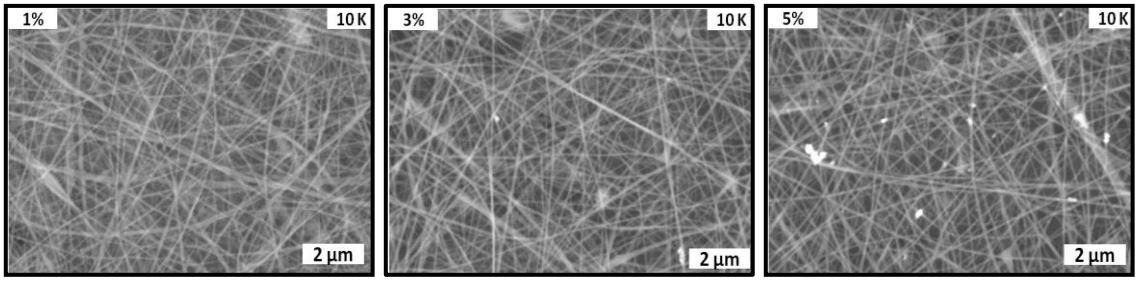

Figure 4.26- Electron Backscattering images of SELP/Ag electrospun fibres with different silver concentrations: 1 wt%, 3 wt% and 5 wt%.

The aforementioned SEM analysis clearly demonstrate the presence of AgNPs apparently at the fibre surface. However, the spatial distibution of these, in terms of fibre surface or fibre core, was still unclear. Therefore, the electrospun fibre mats were analysed by environmental scanning electron microscopy (ESEM). The ESEM micrographs of a representative section of the FA-SELP/Ag (5 wt%) fibres show the presence of silver particles distributed throughout the sample and, as expected, the silver particles appear to be located on the surface of the fibres (Figure 4.27). The measured size of the silver nanoparticles was approximately 10 nm which is lower than those observed earlier for the films. This phenomenom may be a consequence of the processing type (electrospinning) and needs to be more explored to better understand why this happens.

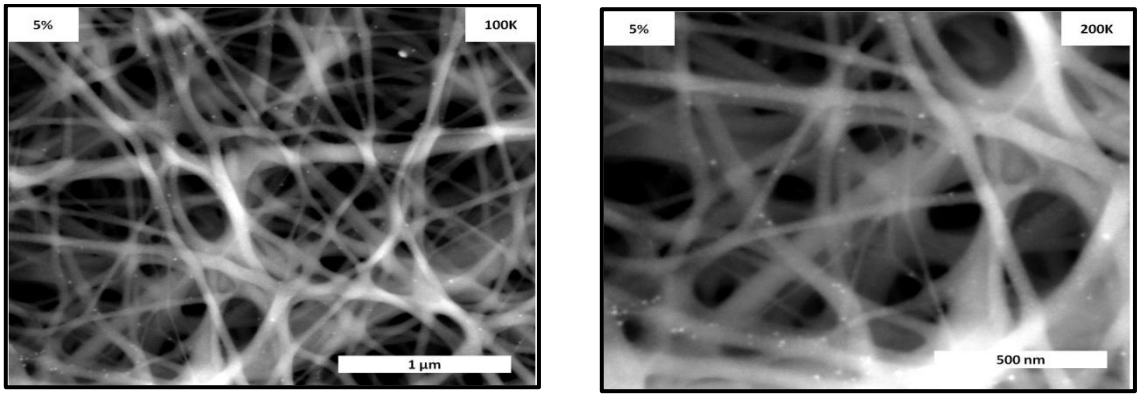

Figure 4.27 - Representative micrographs of the FA-SELP/Ag (5 wt%) fibres obtained after treatment with methanol-saturated air.

The EDS analysis of the SELP/Ag fibres is shown in Figure 4.28 showing the elemental profile and confirming the presence of the silver element. As previously mentioned, the optical absorption peak at 3 keV is characteristic to metallic silver nanocrystals due to their surface plasmon resonance (Shahverdi *et al.*, 2007). In this figure it was also possible to observe the presence of another X-ray emission peak corresponding to aluminium (Al), which was the metal used as base collector for fibre deposition. Moreover, and similar to the results obtained with SELP/Ag films, the intensity of the silver peak increased proportionally with the concentration of $AgNO_3$ in the sample. Interestingly, the sample with 5 wt% of silver presented two different peaks of Ag absorption. The additional smaller peak is most likely attributed to the silver nanoparticles (AgNPs) or other crystals originated from insoluble Ag salts (Figure 4.28) (Shahverdi *et al.*, 2007).

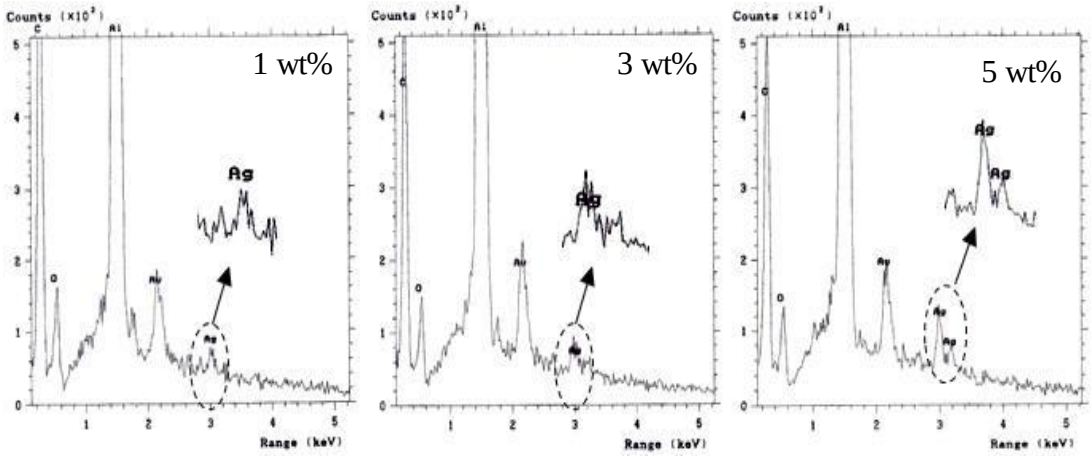

Figure 4.28- EDS analysis of fibres with different concentrations of silver showing characteristic elemental peaks.

Lactoferrin-containing fibres

Another aim of the present work was to produce fibres mats with a natural antimicrobial agent such as bovine lactoferrin (bLF). Similarly to the SELP/Ag, the fibres obtained from solutions with different concentrations of bLF showed a smooth and bead free fibrous structure (Figure 4.29). However, with 5 wt% of bLF it was possible to observe the formation of some ribbons structures among the electrospun fibres mats. This structural feature is a consequence of the formation of a thin solid skin around the liquid jet due to the fast evaporation of the solvent at the surface. As the liquid jet travels between the needle tip and the grounded collector, the liquid solvent

present in the fibre core evaporates leading to the formation of a hollow cylindrical structure that collapses into ribbon-like structures (Machado *et al.*, 2013b)

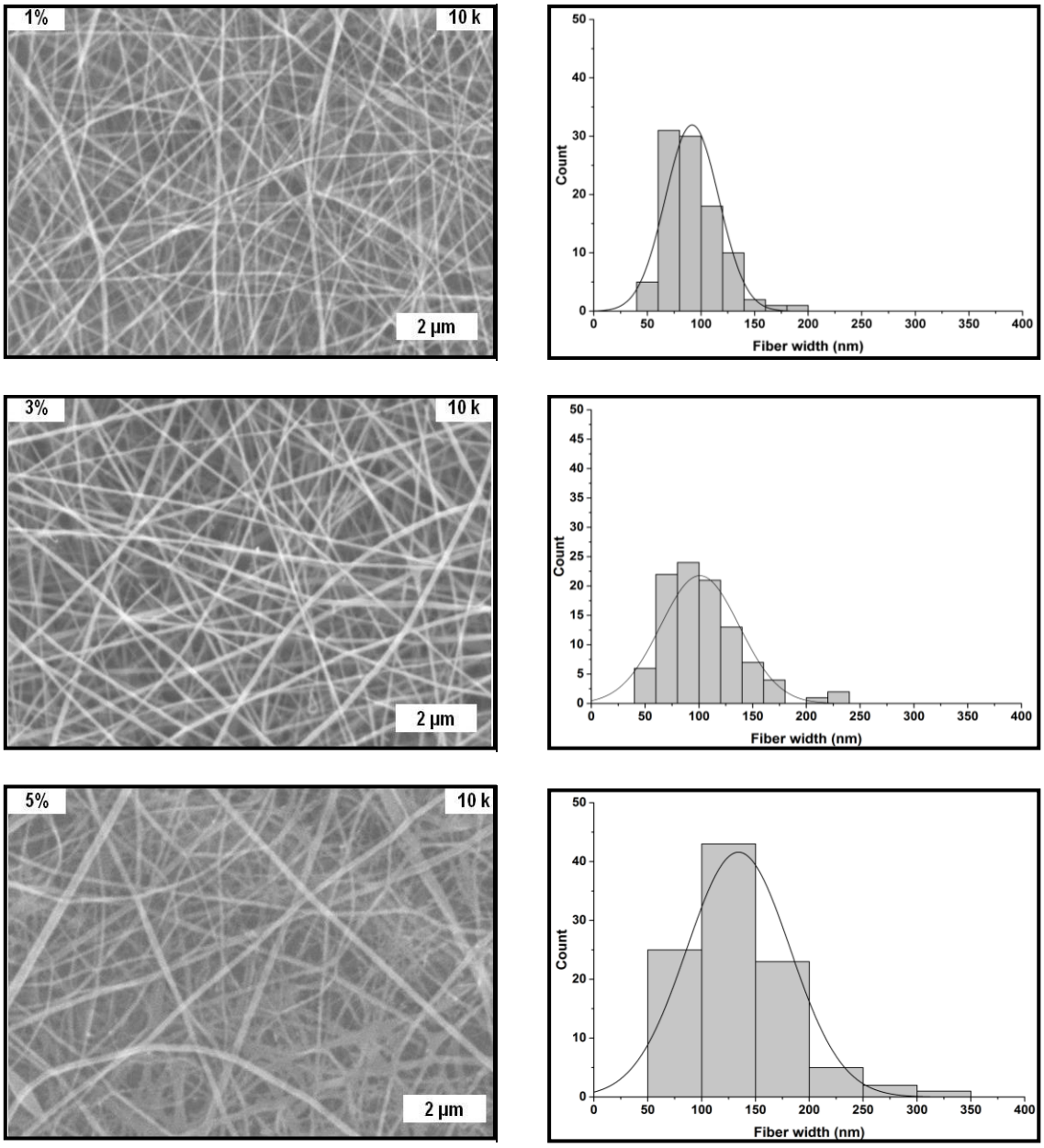

Figure 4.29- Representative SEM micrographs and histograms of fibre size distribution for SELP/LF fibre mats with 1 wt%, 3 wt% and 5 wt% of lactoferrin.

Comparing the effect of bLF in mean fibre diameter, the results are within those observed with SELP/Ag (Figure 4.30). However, as observed in the histograms, a broader diameter distribution is observed with increasing concentrations of lactoferrin. This can be explained by the presence of ribbons with increasing concentrations of bLF.

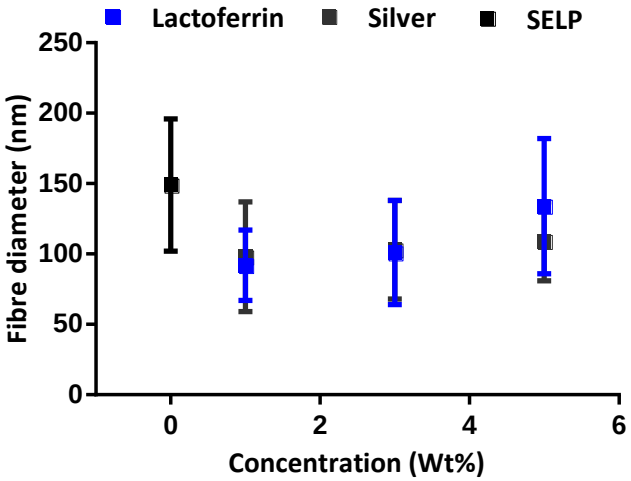

Figure 4.30- Graphical representation correlating the average fibre diameter with lactoferrin and silver content.

As previously described, in order to stabilize the structure of the fibres and to render water insolubility, the electrospun mats were exposed to a methanol-saturated atmosphere. After the chemical treatment, the SELP/LF fibres maintained its morphological integrity with some minor differences in fibre width, displaying average fibre diameters of 117 ± 53 nm and 110 ± 41 nm for 1 wt% and 5 wt%, respectively (Figure 4.31).

Summing up, regardless of the filler used, Ag or LF, the mean diameter of the fibres was similar with values around 100 nm. In general, the fillers did not significantly affect the morphology of the fibres, although higher concentrations of LF led to the formation of ribbons. Finally, the chemical treatment with methanol maintained fibre integrity for both SELP/Ag and SELP/LF fibres.

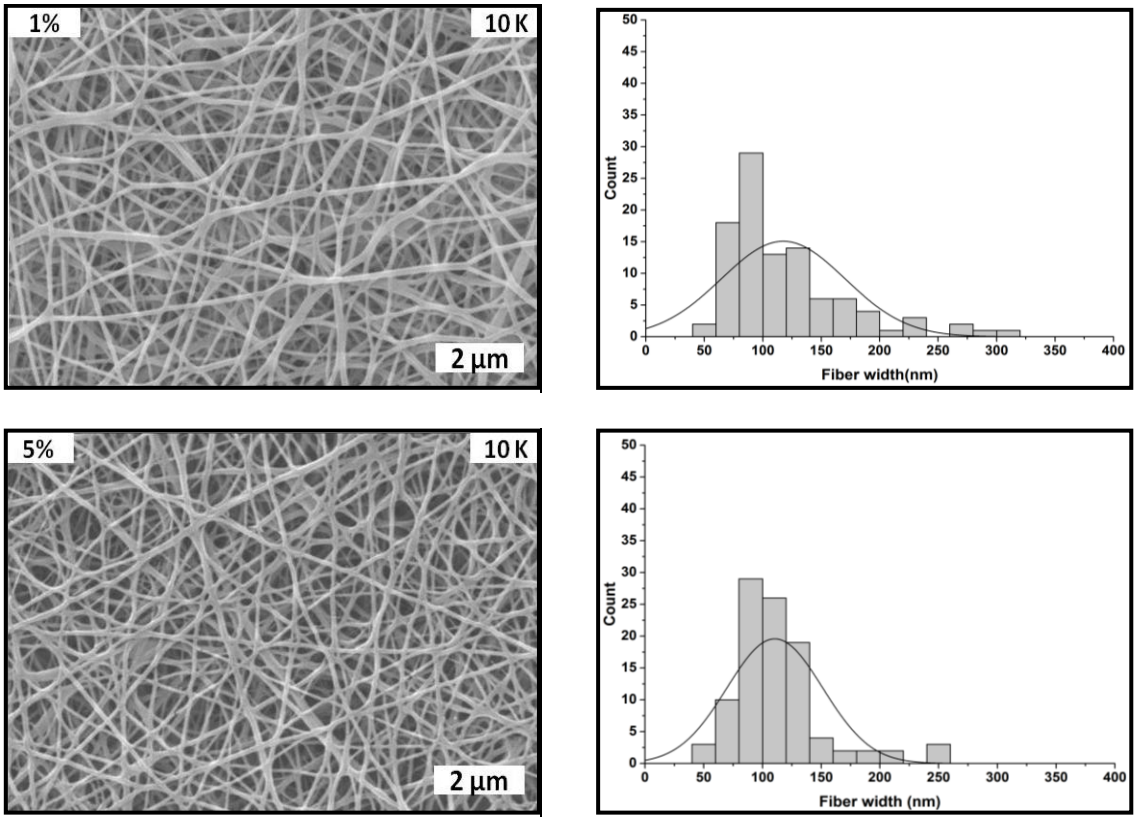

Figure 4.31- Representative SEM micrographs and histograms of fibre size distribution for methanol-treated SELP/LF fibres with 1 wt% and 5 wt% of lactoferrin.

4.4. Fourier transform infrared spectroscopy

Electrospun fibre mats and films were analysed by Fourier transform infrared spectroscopy in attenuated total reflectance (ATR-FTIR). This technique has been extensively applied to study the secondary structure of proteins and is frequently used to study the molecular conformation of silk fibroin fibres or films (Kim *et al.*, 2003).

Previous studies indicate that silk fibres and films processed with organic or aqueous solvents resulted in an amorphous structure mainly with random coil conformation. This is due to the crystallization rate of the silk β-sheet which is slower than solvent evaporation during the electrospinning or solvent casting (Ner *et al.*, 2009). The treatment of materials with methanol induces the formation of β-sheet structure and thus improves the crystalline structure of the material.

FTIR data of SELP/Ag fibres and films shows peaks in amide I band at 1644 cm^{-1} (C=O stretching), in amide II at 1532 cm^{-1} (N-H bending and C-N stretching), and in amide III at 1237 cm^{-1}(N-H in plane deformation) (Figure 4.32). A large portion of β-

sheets or sheet-like structures show an amide I peak below 1630 cm^{-1} and an amide III peak at 1230 cm^{-1} (Zeng *et al.*, 2014). The presence of a peak at 1625 cm^{-1} in the amide I region suggests the coexistence of β-sheets and unordered structures. The silver composite materials with and without methanol treatment showed similar FTIR spectra as represented in Figure 4.32, presenting only a slight deviation in peak centre. Also, no remarkable differences were found when compared with the spectrum of pristine SELP materials, with no additional peaks or spectral components due to the presence of the filler.

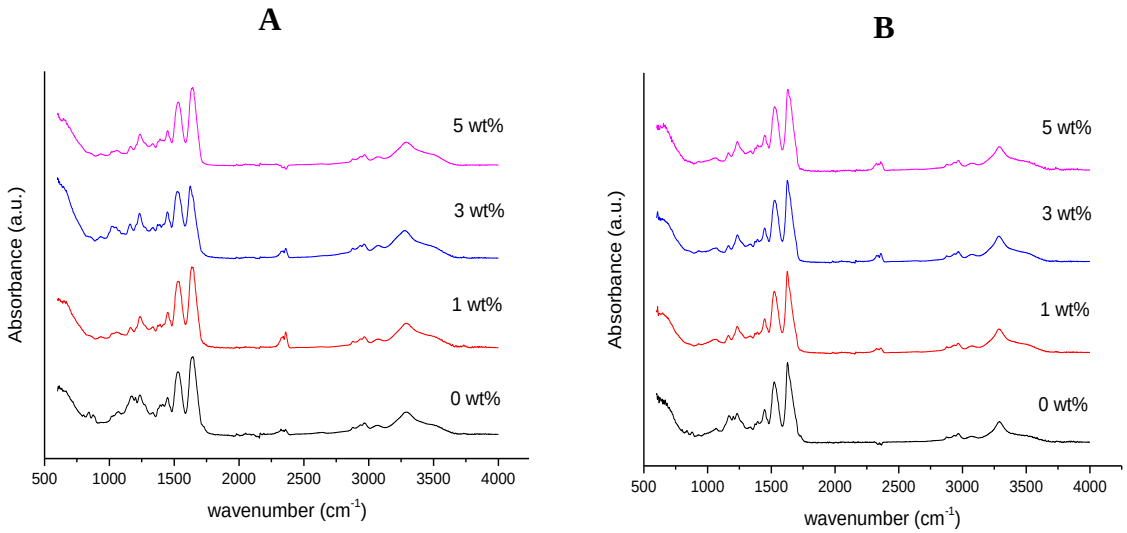

Figure 4.32- (A) FTIR spectra of SELP/Ag composite materials. **(B)** FTIR spectra of methanol-treated SELP/Ag composite materials.

The evaluation of secondary structural changes after treatment with methanol was performed by analysis of the amide I absorption band between 1644 cm^{-1}. In the amide I region, the C=O stretching frequency varies accordingly to the type of secondary structure due to the unique molecular geometry and hydrogen bonding pattern (Machado, 2012). For the materials treated with methanol it was found that the absorption band of the amide I dislocates to lower wavenumbers relatively to the non-treated sample (Figure 4.33). This suggests a changing from a disordered structure (random coil) to an ordered conformation (β-sheet). Further, for the $AgNO_3$ nanocomposite samples, the amide I band peak is similar for the different concentrations, indicating that the silver compound and its concentration do not affect the secondary structure of the SELP.

In order to study in more detail the secondary structure, second derivative and curve fitting analysis in the amide I band region were employed for determination of secondary structural content (*see* Annex). Accordingly, there was an increase of about 10% in the β-sheet content of methanol-treated samples when compared with the non-treated samples. This increase showed to be a consequence of a structural conversion of random coils to β-sheet whereas the content in turns and bends remained constant.

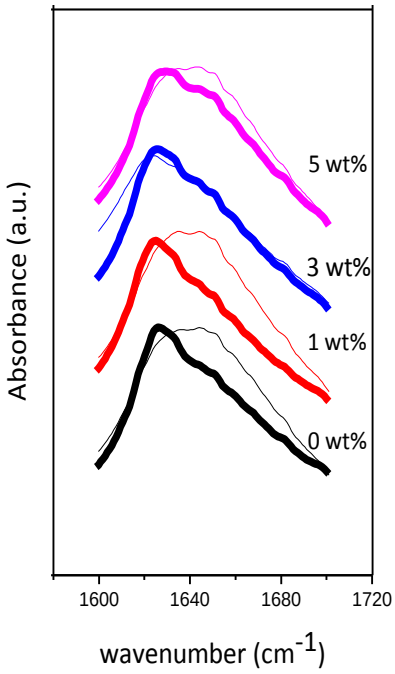

Figure 4.33- FTIR spectra in the amide I region of non-treated (normal line) and methanol-treated (intense line) SELP/Ag with different silver concentrations (0, 1, 3, 5 wt%).

Regarding the lactoferrin composite materials both SELP/LF films and fibres showed similar FTIR spectra as the pristine SELP material, without the presence of additional spectral bands (Figure 4.34).

Similarly to the results previously obtained for the silver composites, the methanol-treated samples presented a peak centre displacement of the amide I to lower wavenumber, indicating a conversion to a more ordered structure (Figure 4.35). Once again, no changes in the amide I region observed for all the concentrations of bLF, indicating that lactoferrin concentration does not affect the secondary structure of the composite material.

Second derivative and curve fitting analysis in the amide I region were also performed for the SELP/LF materials (*see* Annex). Again, the increase in β-sheet content, resulting from the conversion of random coils, was observed after the methanol treatment while the content in turn and bends remained constant.

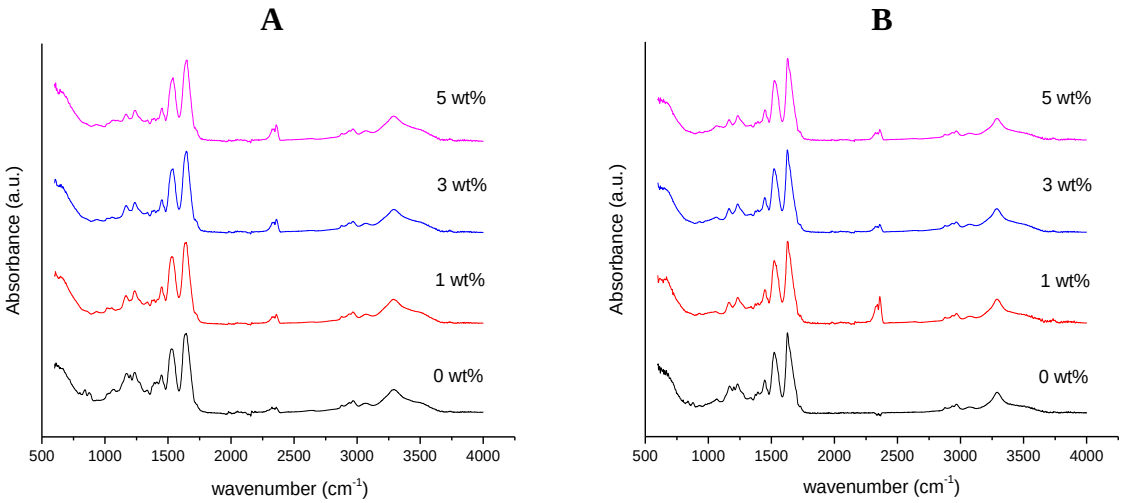

Figure 4.34- (A) FTIR spectra of SELP/LF composite materials. **(B)** FTIR spectra of methanol-treated SELP/LF composite materials.

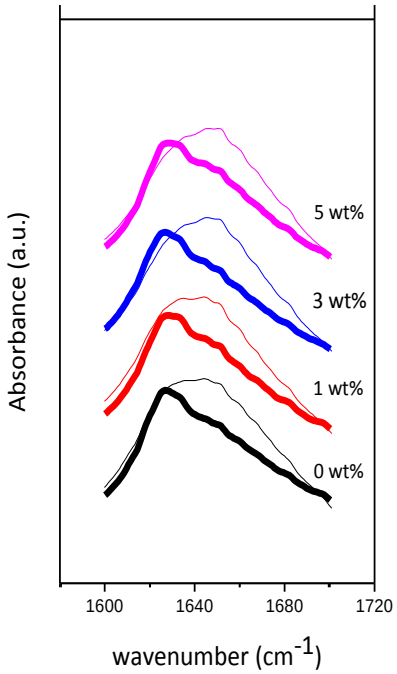

Figure 4.35- FTIR spectra in the amide I region of non-treated (normal line) and methanol-treated (intense line) for the different lactoferrin concentrations (0, 1, 3, 5 wt%).

4.4.1. Degree of swelling and hydrolytic degradation

Degree of swelling

The degree of swelling of a material is its capacity to absorb water. The swelling capability of antibacterial composite materials is an important property for their antibacterial activity, in wound healing processes and other biomedical applications (Vimala *et al.*, 2010).

The samples were immersed in water for different time intervals, according to the procedure described in the chapter 3 (3.3.5).

Figure 4.36 shows the swelling degree profile for SELP, SELP/Ag and SELP/LF fibre mats. It was observed that the SELP fibre mats rapidly swelled after immersion in water with a value of approximately 600% and remaining constant practically throughout all the experiment. In the end of the experiment (1 h), the fibre mats reached its maximum degree of swelling of 704%. A similar behaviour was observed for SELP/Ag fibre mats that rapidly swelled within the first minute of immersion in water, reaching its maximum absorption capacity of 1427% after 5 min. At the end of the experiment (1 h), the degree of swelling of the fibres was 1055%. Regarding the SELP/LF fibre mats, a swelling degree of 838% was observed after 5 min of immersion, reaching a value of 807% in the end of the experiment (1 h). Comparing the results, both the SELP and SELP/LF fibre mats present values for the degree of swelling within the same range except for the greater value obtained for the SELP/Ag fibre mats. This can be attributed to the presence of AgNPs that may enhance water absorption due to the large surface area of the nanoparticles. AgNPs can combine with oxygen atoms present in the aqueous solution and thereafter, the united oxygen could bind to hydrogen and form hydrogen bonds which results in an increase in fibre hydrophilicity (An *et al.*, 2009).

The degree of swelling was also determined for free standing films of H_2O-SELP, H_2O-SELP/Ag and H_2O-SELP/LF (Figure 4.37). When compared with the fibres, the films presented similar swelling degrees except for the silver-containing sample. Indeed, the H_2O-SELP/Ag film demonstrated a lower degree of swelling with values almost half of those obtained with the fibres.

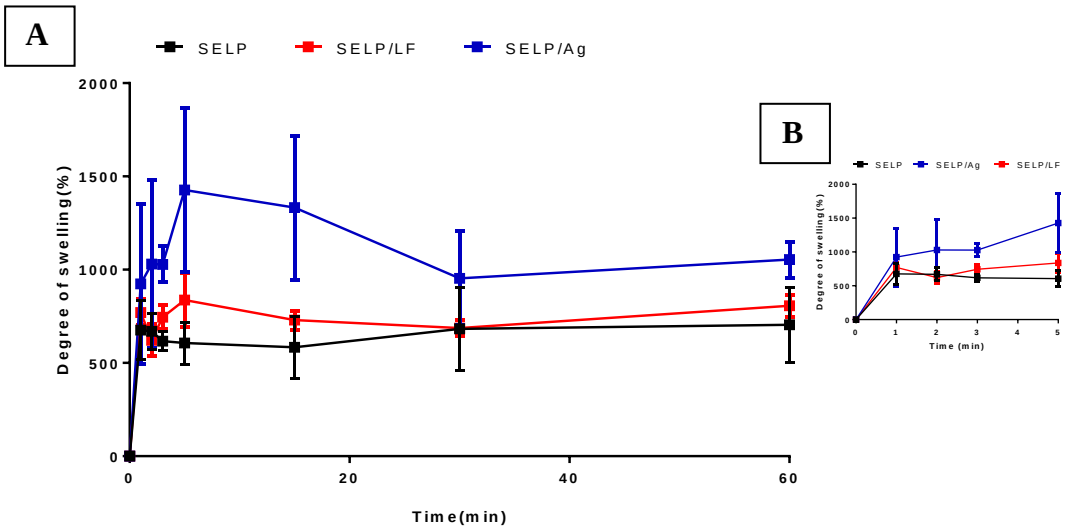

Figure 4.36- (A) Degree of swelling obtained for SELP, SELP/Ag (3 wt%) and SELP/LF (5 wt%) fibres for a total of 60 min of immersion in deionized water at room temperature. **(B)** Inset graphic represents the degree of swelling determined during the first 5 min of immersion.

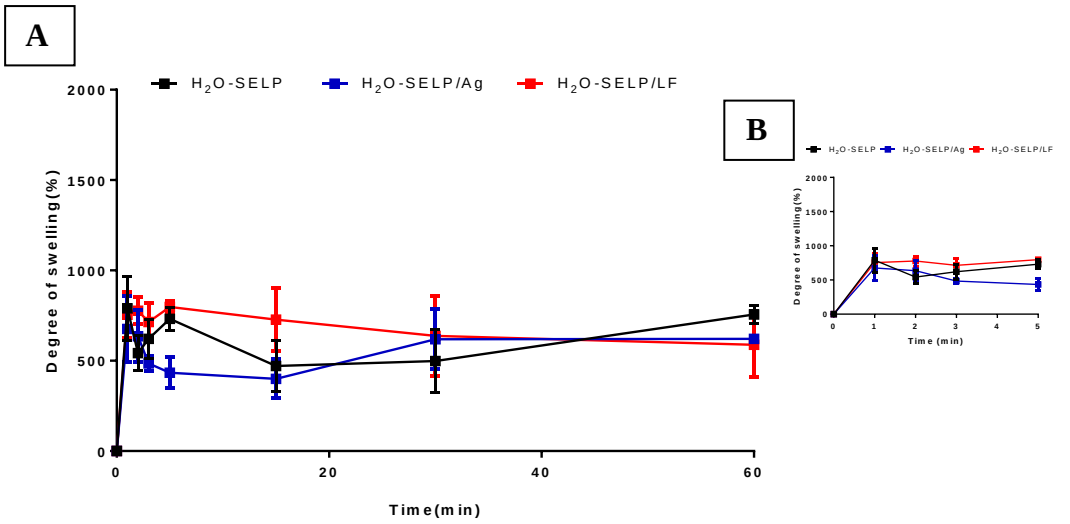

Figure 4.37- (A) Degree of swelling obtained for H_2O-SELP, H_2O-SELP/Ag (5 wt%) and H_2O-SELP/LF (5 wt%) films for a total of 60 min of immersion in deionized water at room temperature. **(B)** Inset graphic represents the degree of swelling determined during the first 5 min of immersion.

In general, the swelling ability demonstrated by the composite materials reveals to be promising for biomedical applications. An application example is as a dressing for skin regeneration, where an effective dressing should control the water loss from the wound at an optimal rate, and avoid excessive dehydration (Padrão *et al.*, 2014; Machado *et al.*, 2013b).

Hydrolytic degradation

The hydrolytic degradation of the composite materials namely pristine SELP, SELP/Ag and SELP/LF fibre mats (Figure 4.38), as well as free standing films (Figure 4.39) was evaluated by immersion in PBS at 37 ºC.

In pristine SELP fibres there was no weight loss in the first days of incubation. After 15 days of incubation there was a weight loss of about 5% (Figure 4.38A) and remarkably, maintained their integrity after 15 days of incubation (data not shown). In opposition, the SELP/Ag fibres showed a rapid weight loss on the first day of incubation with a remaining 88% of residual mass. This mass stayed constant over the 15 days of incubation suggesting that the initial mass loss can be attributed to the rapid diffusion of silver into the medium, whereas SELP maintained a constant weight over time. The diffusion of silver ions was probably favoured by the swelling demonstrated by the sample as the presence of water generates a greater diffusion of Ag^+ ions (Kumar and Münstedt, 2005a). The water molecules incorporate the fibres by intramolecular forces widening the space between the polymer chains and consequently, facilitating the ionic migration of silver through the sample (Kumar and Münstedt, 2005b). In a similar way, the SELP/LF fibre mats also demonstrated a rapid mass loss (15%) and remained constant for the rest of experiment. This rapid weight loss can be associated with the release of lactoferrin into the medium. Despite the observed weight loss, the SELP/Ag and SELP/LF fibres remained intact after the 15 days of incubation (Figure 4.38B and 4.38C, respectively).

Regarding H_2O-SELP, H_2O-SELP/Ag and H_2O-SELP/LF films, it was found that there was only minor or no weight loss for all the samples throughout the 15 days of incubation (Figure 4.39). In fact, the weight of the H_2O-SELP and H_2O-SELP/LF films remained constant throughout the entire period of the experiment suggesting that these materials are very stable. For the H_2O-SELP/Ag film, a weight loss of about 5% was observed after the first day of incubation. This weight loss could once again be attributed to the diffusion of the filler. When compared with the fibre mats, these constrasting results may be a consequence of the availability of the filler to diffuse into the solution. In the films, the filler is more tightly mixed and constrained within the structure and thus is not so accessible to contact with water and diffuse.

However, it should be noted that the higher hydrolytic degradation of the fibre mats when compared with the films may be associated with the handling of the material. The fibre mats are not as uniform as films and during the assay it is possible that some fibres may be lost, resulting in higher degradation values when compared to the films.

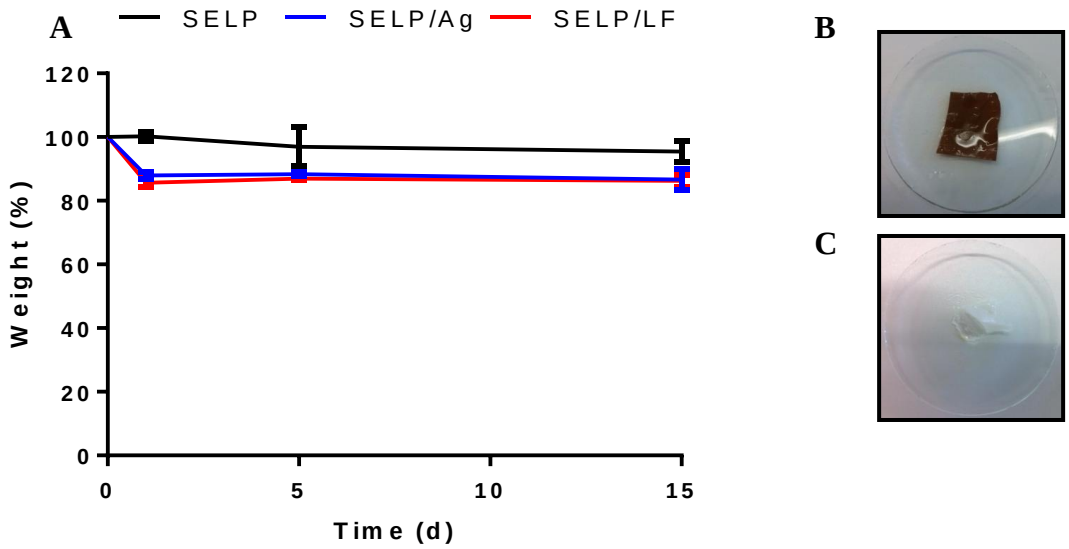

Figure 4.38 – Hydrolytic degradation profile of SELP, SELP/Ag (3 wt%) and SELP/LF (5 wt%) fibres in PBS at different time periods. **(B)** SELP/Ag membranes removed from the PBS after 15 days of incubation. (**C)** SELP/LF membranes removed from the PBS after 15 days of incubation.

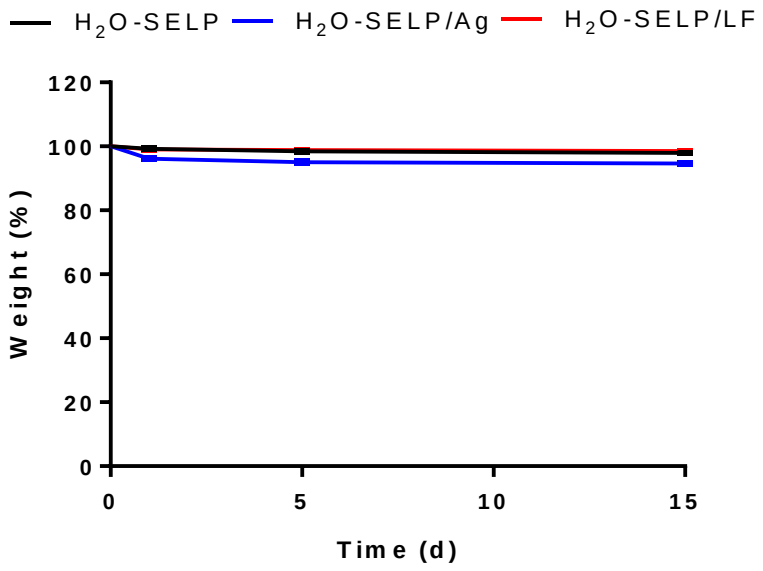

Figure 4.39 – Hydrolytic degradation profile of SELP, SELP/Ag (5 wt%) and SELP/LF (5 wt%) films in PBS at different time periods.

4.5. Evaluation of antimicrobial activity

4.5.1. Growth curves

The antimicrobial performance of the composite materials was evaluated through antimicrobial assays against bacteria and fungi.

Before proceeding to the antimicrobial assays and in order to maintain the same biological conditions such as the number of colony forming units, the growth profile of the microorganisms was plotted (Figure 4.40). The growth curves were determined for each microorganism and a correlation of the number of colonies and the optical density was calculated in order to have the desired number of cells for the realization of antimicrobial assays.

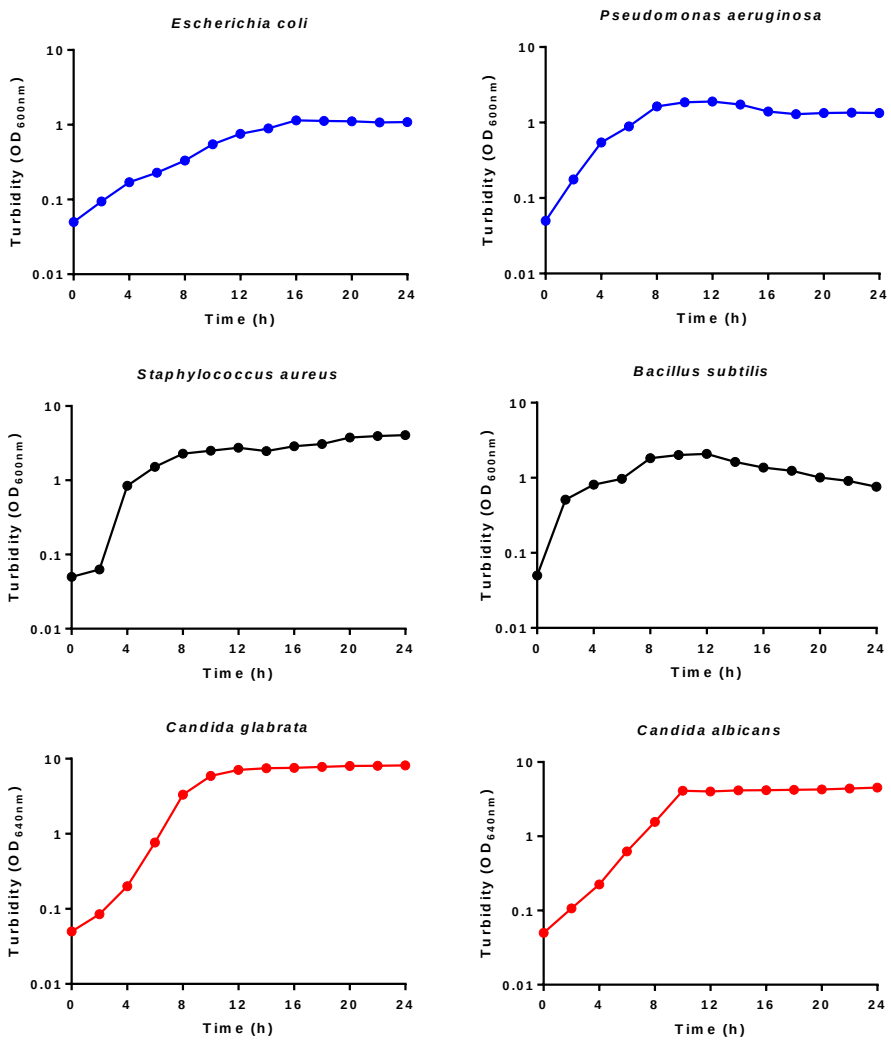

Figure 4.40- Growth curves of *Gram-negative bacteria* (*Escherichia coli* and *Pseudomonas aeruginosa*) (blue), *Gram-positive bacteria* (*Staphylococcus aureus* and *Bacillus subtilis*) (black) and yeast (*Candida glabrata* and *Candida albicans*) (red).

4.5.2. Antimicrobial assays for silver composites

The evaluation of the antimicrobial activity was performed by three different methods: direct contact assay; dynamic shake test and agar diffusion methods as described in the Materials and Methods section.

Direct contact assay

The antibacterial performance of SELP/Ag composite materials against *E. coli* was explored by direct contact assay by counting the number of viable cells. The results of the antibacterial assay for the composite materials containing 0-5 wt% silver is shown in Figure 4.41. The results show that there is 100% growth inhibition for *E. coli* for all the different materials and all the silver concentrations used. This effective growth inhibition was found in other studies using other types of composites containing silver (Wei *et al.*, 2009; Xu *et al.*, 2006). The effectiveness of the composite materials can be clearly attributed to the silver nanoparticles in the materials as the pure SELP showed no antimicrobial activity.

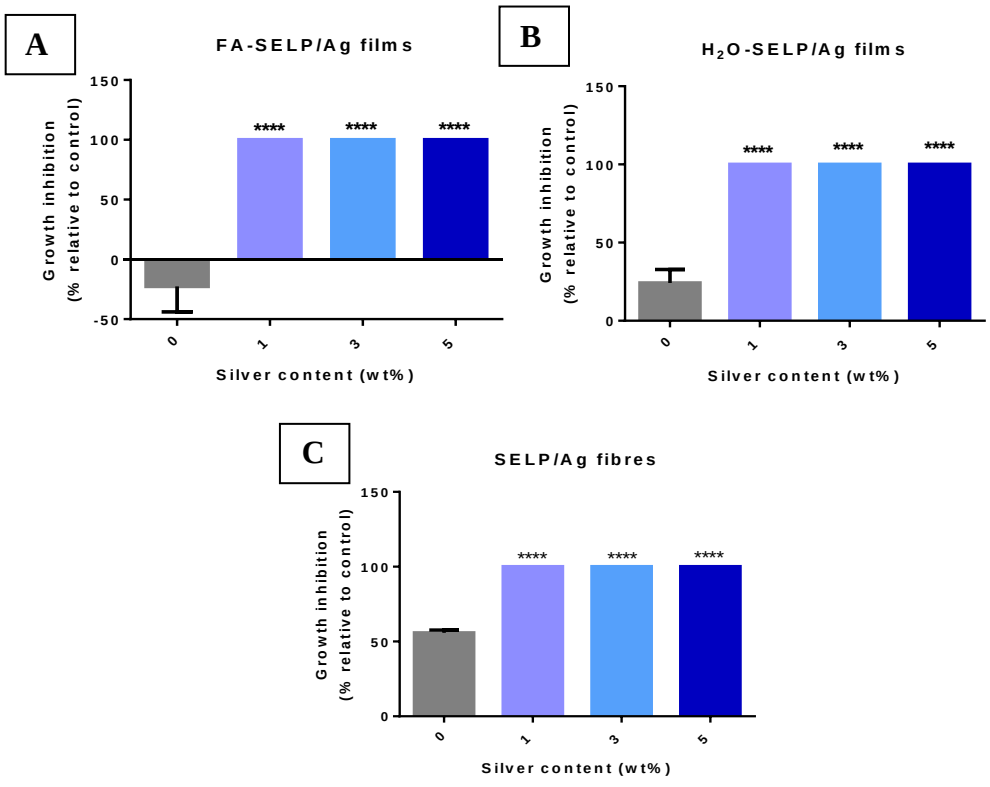

Figure 4.41- Growth inhibition against *E .coli* for **(A)** FA-SELP/Ag films, **(B)** H_2O-SELP/Ag films and **(C)** SELP/Ag fibre mats. Bars represent means ± SD. **** $p<0.0001$.

Due to the nature and properties of the materials especially considering the high degree of swelling, other antimicrobial assays were considered to check the consistency of the results.

Dynamic shake tests

In this antimicrobial assay, the samples are subjected to a physical stress due to the agitation which could result in an increase in the release of AgNPs from the materials. The antimicrobial performance of the composites was evaluated in shaking flasks against *E. coli* and *P. aeruginosa* (Figure 4.42). Again, and as previously observed with the direct contact assay, the SELP/Ag fibre mats were highly effective showing 100% of growth inhibition.

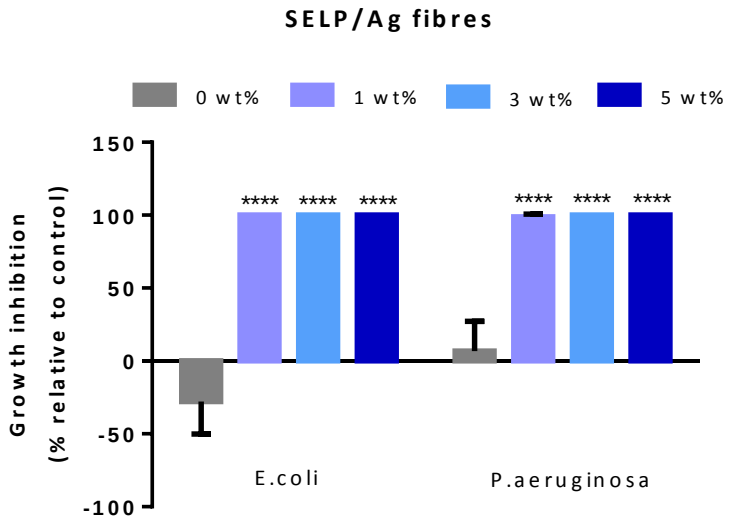

Figure 4.42- Growth inhibition rates against *E. coli* and *P. aeruginosa* by SELP/Ag fibre mats. Bars represent means ± SD. **** $p<0.0001$.

Halo of inhibition/diffusion method

Together with the results obtained with the hydrolytic degradation, the antimicrobial tests suggest that silver diffuses into the medium. This was further confirmed by performing antimicrobial susceptibility diffusion assays as described in the Materials and Methods. In this analysis, the antimicrobial activity of a material is reflected by the formation of a halo of inhibition in which there is no bacterial cell

growth. The diameter of the inhibition halo is thus dependent of the antimicrobial efficacy of the antimicrobial agent as well as of its ability to diffuse into the surroundings.

The halo of inhibition found for SELP/Ag composites against *E. coli*, *P. aeruginosa*, *S. aureus* and *B. subtilis* is shown in figures 4.43, 4.45 and 4.47; and graphically represented in terms of diameter in figures 4.44, 4.46 and 4.48. When compared with the control (SELP 0 wt%) in which no halo of inhibition was found, all the SELP/Ag composite materials were effective against all the bacteria tested, independently of the solvent used. Comparing all the bacteria tested, the composite materials demonstrated a greater antibacterial activity against the Gram-positive *Staphylococcus aureus* whereas the Gram-positive *Bacillus subtilis* showed to be the most resistant specie to the silver impregnated materials. The resistance exhibited by *B. subtilis* may be due to its ability to form endospores resistant to a broad spectrum of antimicrobial agents (Park *et al.*, 2009).

The antibacterial activity of different composites impregnated with silver have been previously described by other authors. However, for a silver content equal to or less than that used by other authors, the composite materials evaluated in this study showed a greater activity, reflected in a higher average diameter (Oraby *et al.*, 2013; Xu and Zhou, 2008).

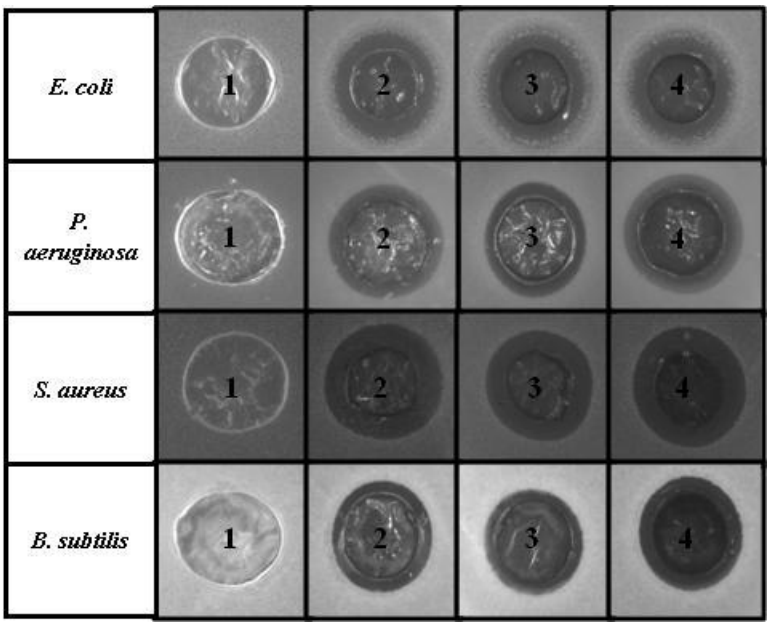

Figure 4.43- Halo of inhibition of FA-SELP/Ag films (1- 0 wt%; 2- 1 wt%); 3- 3 wt%); 4- 5 wt%) against *E. coli*, *P. aeruginosa*, *S. aureus* and *B. subtilis*.

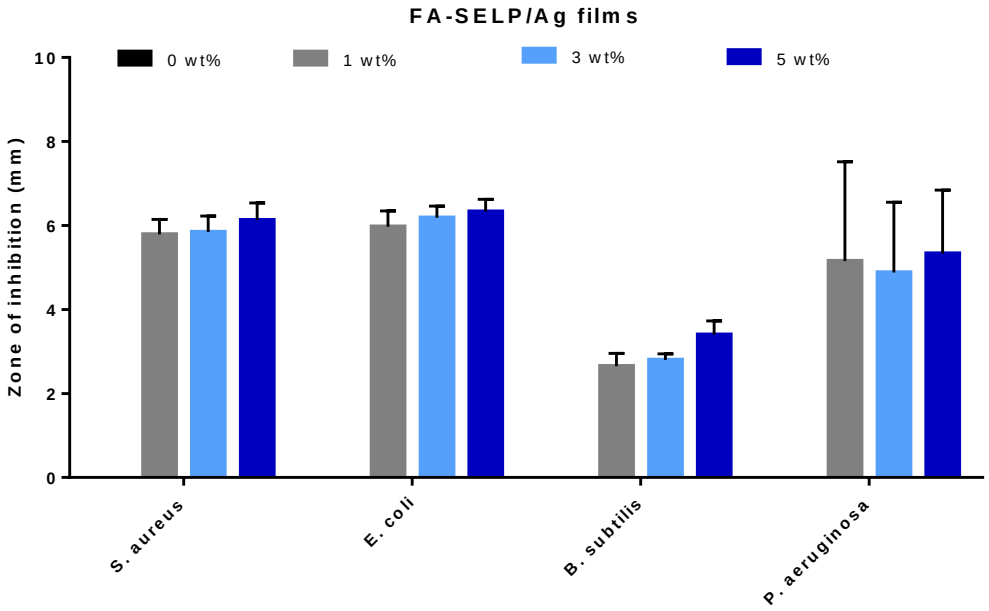

Figure 4.44– Graphical representation comparing the diameter of the halos of inhibition found for FA-SELP/Ag films against different bacteria. Results are expressed by calculating the diameter of zones of inhibition (mm).

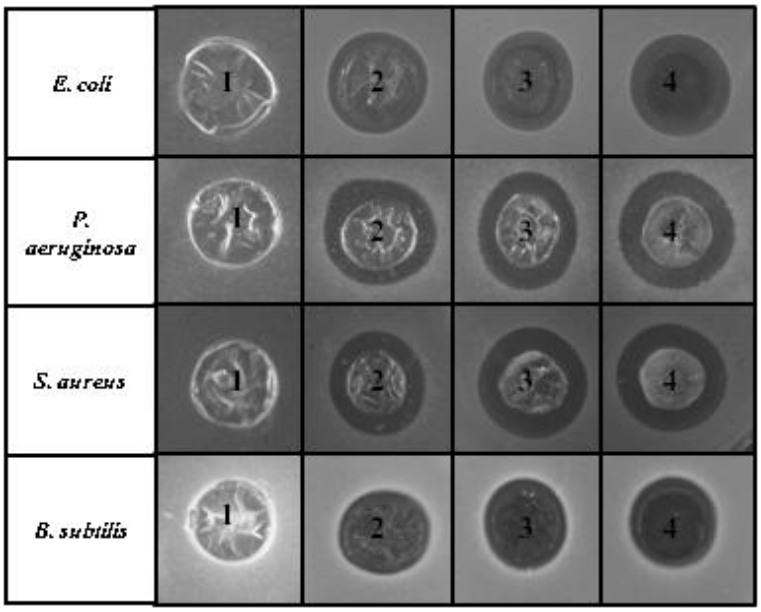

Figure 4.45- Halo of inhibition of H_2O-SELP/Ag films (1- 0 wt%; 2- 1 wt%); 3- 3 wt%); 4- 5 wt%) against *E. coli*, *P. aeruginosa*, *S. aureus* and *B. subtilis*.

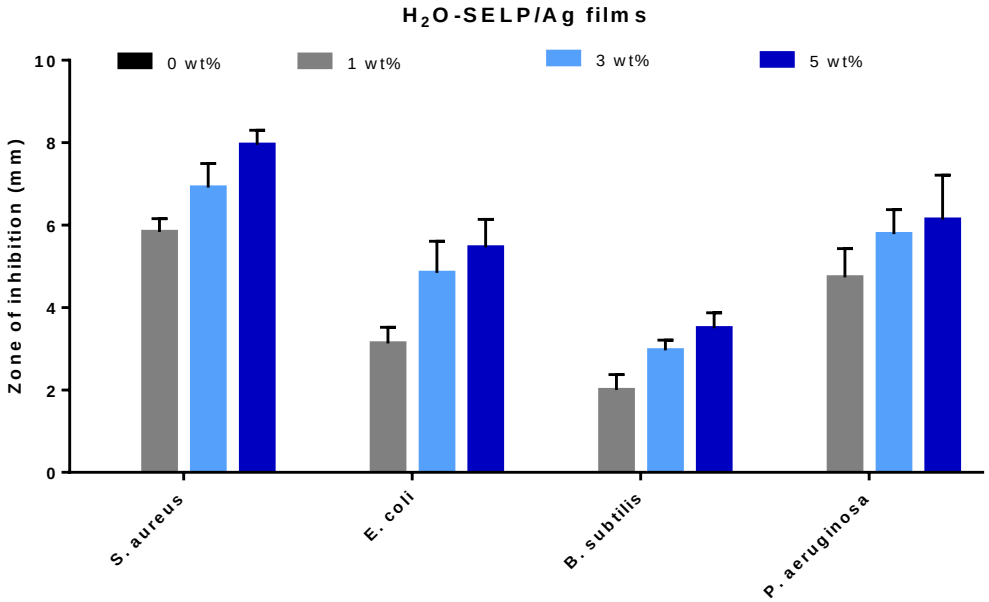

Figure 4.46 – Graphical representation comparing the diameter of the halos of inhibition found for H_2O-SELP/Ag films against different bacteria. Results are expressed by calculating the diameter of zones of inhibition (mm).

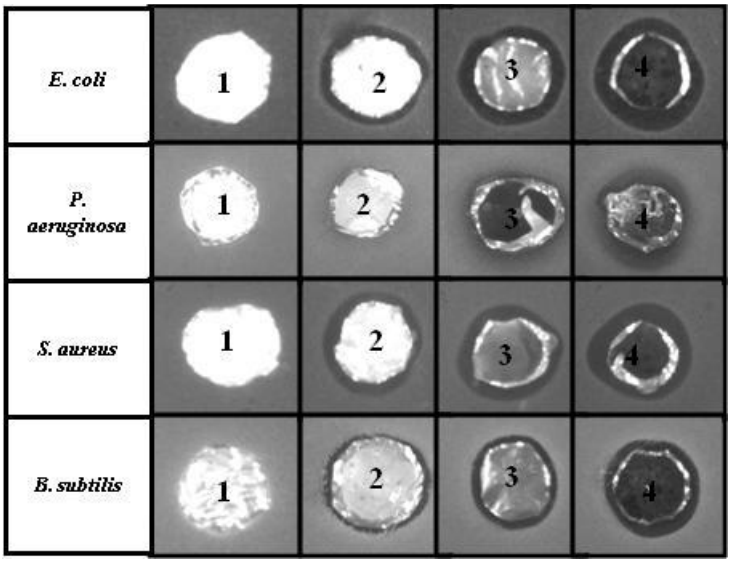

Figure 4.47- Halo of inhibition of SELP/Ag fibres (1- 0 wt%; 2- 1 wt%); 3- 3 wt%); 4- 5 wt%) against *E. coli*, *P .aeruginosa*, *S. aureus* and *B. subtilis*.

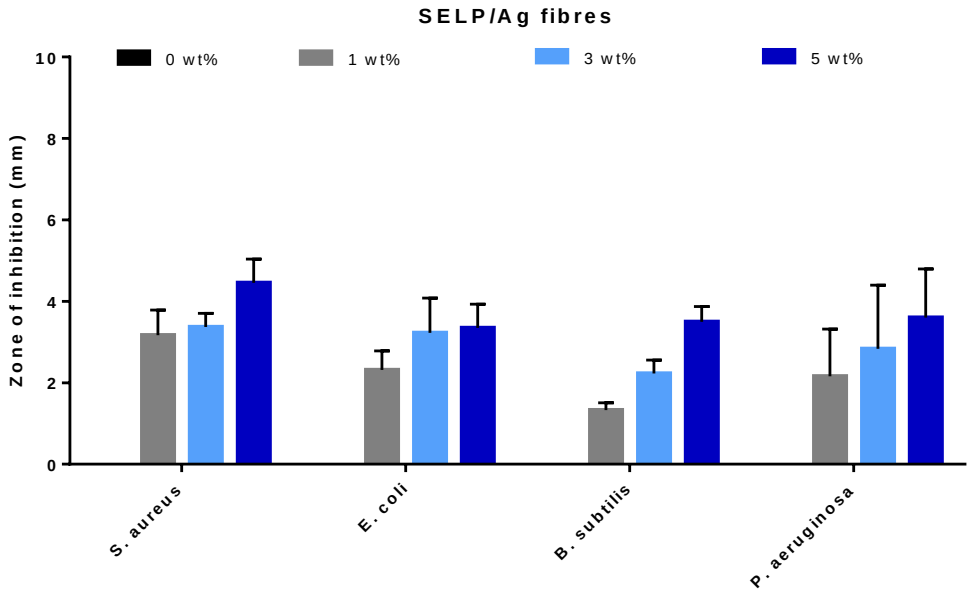

Figure 4.48– Graphical representation comparing the diameter of the halos of inhibition found for SELP/Ag fibres against different bacteria. Results are expressed by calculating the diameter of zones of inhibition (mm).

In this study, the activity of the composite materials containing silver was also evaluated against yeast strains (Figures 4.49, 4.51 and 4.53). The average diameters of the assay when compared to the control (SELP 0 wt%) are shown in Figures 4.50 and 4.52. Interestingly, the films showed a clear halo of inhibition while the fibre mats displayed a diffuse zone of inhibition. Comparing the diameters of the halos of inhibition, the activity demonstrated by the films against *C. albicans* and *C. glabrata* is smaller than the previously demonstrated against bacteria, suggesting that yeasts are more resistant to AgNPs than bacteria. This may occur due to the complexity of the yeast cell in which it is required a higher concentration of silver (Kumar *et al.*, 2012). In fact, similar results, in which the antibacterial activity was stronger than the antifungal activity, have been previously reported (Kumar *et al.*, 2012).

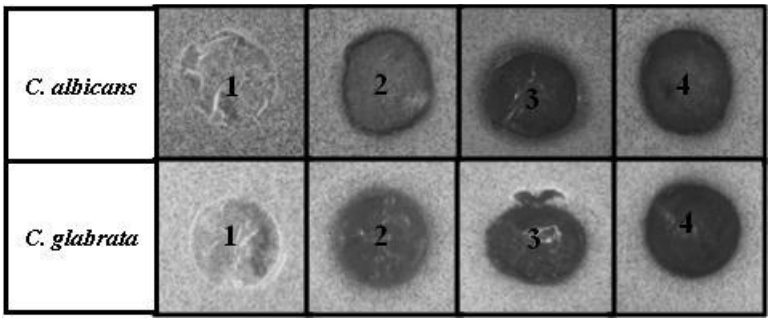

Figure 4.49- Halo of inhibition of FA-SELP/Ag films (1- 0 wt%; 2- 1 wt%); 3- 3 wt%); 4- 5 wt%) against *C. albicans* and *C. glabrata*.

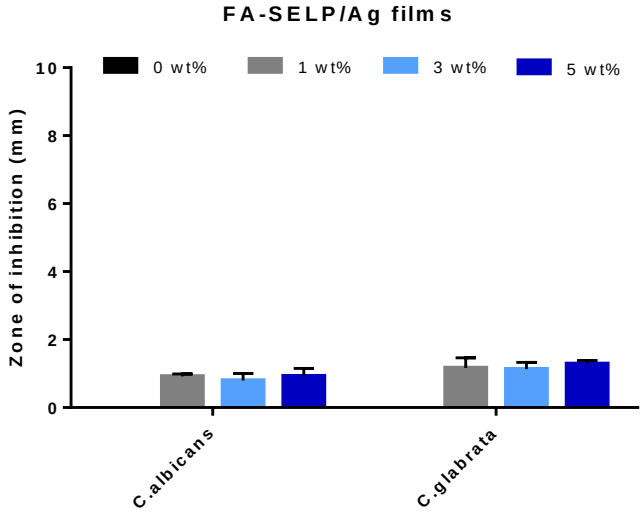

Figure 4.50– Graphical representation comparing the diameter of the halos of inhibition found for FA-SELP/Ag films against two different yeast. Results are expressed by calculating the diameter of zones of inhibition (mm).

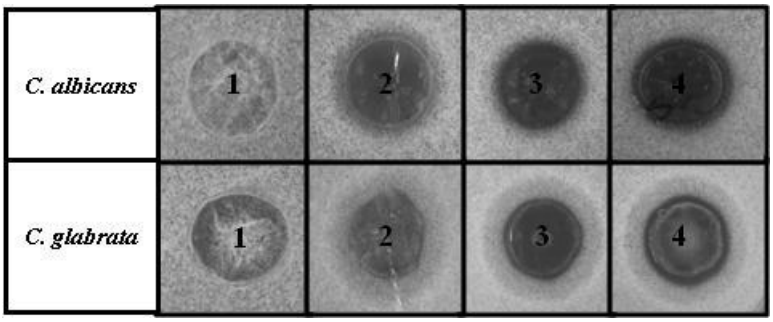

Figure 4.51- Halo of inhibition of H_2O-SELP/Ag films (1- 0 wt%; 2- 1 wt%); 3- 3 wt%); 4- 5 wt%) against *C. albicans* and *C. glabrata*.

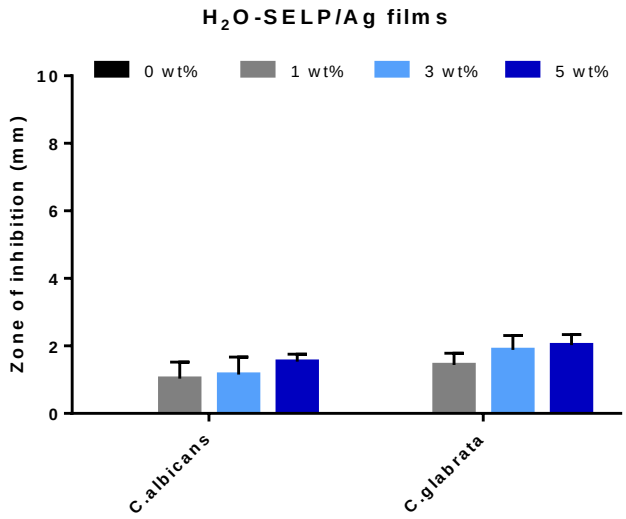

Figure 4.52– Graphical representation comparing the diameter of the halos of inhibition found for H_2O-SELP/Ag films against two different yeast species. Results are expressed by calculating the diameter of zones of inhibition (mm).

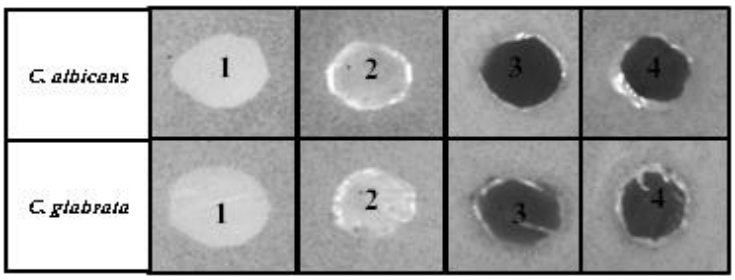

Figure 4.53- Halo of inhibition of SELP/Ag fibres (1- 0 wt%; 2- 1 wt%); 3- 3 wt%); 4- 5 wt%) against *C. albicans* and *C. glabrata*.

Antifungal assay

Further studies were performed with SELP/Ag materials against *Aspergillus nidulans* (Figures 4.54 and 4.55). However, no visible activity was found for all the materials tested indicating that this microorganism is resistant to silver within the range of the concentrations used. This may be due to the fact that the concentration of silver used is not sufficient to enter the fungus cells but sufficient to be adsorbed on the bacterial surface. Thus, silver ions immobilize dehydrogenation because respiration occurs across the cell membrane in bacteria rather than across the mitochondrial membrane as in eukaryotic cells of fungi (Nabikhan *et al.*, 2010).to enter the fungus cells but sufficient to be adsorbed on the bacterial surface, thus silver ions immobilize dehydrogenation because respiration occurs across the cell membrane in bacteria rather

than across the mitochondrial membrane as in eukaryotic cells of fungi (Nabikhan *et al.*, 2010).

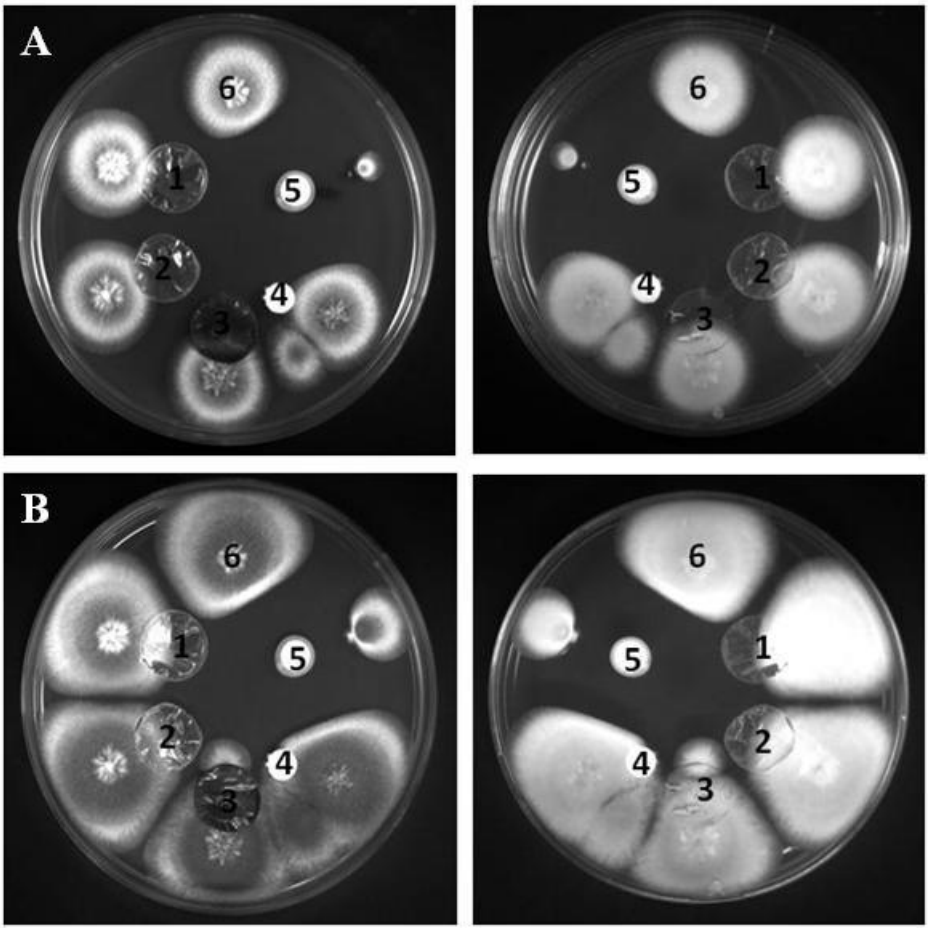

Figure 4.54- Assay of direct contact of H_2O-SELP/Ag films against *Aspergillus nidulans*. **(A)** Two days at 37 ° C after performing these assays **(B)** Three days at 37 ° C after performing these assays. 1-H_2O-SELP ;2- H_2O-SELP/Ag (1 wt%);3- H_2O-SELP/Ag (5 wt%) ,4- sterile disc ;5- itraconazole and 6-positive control.

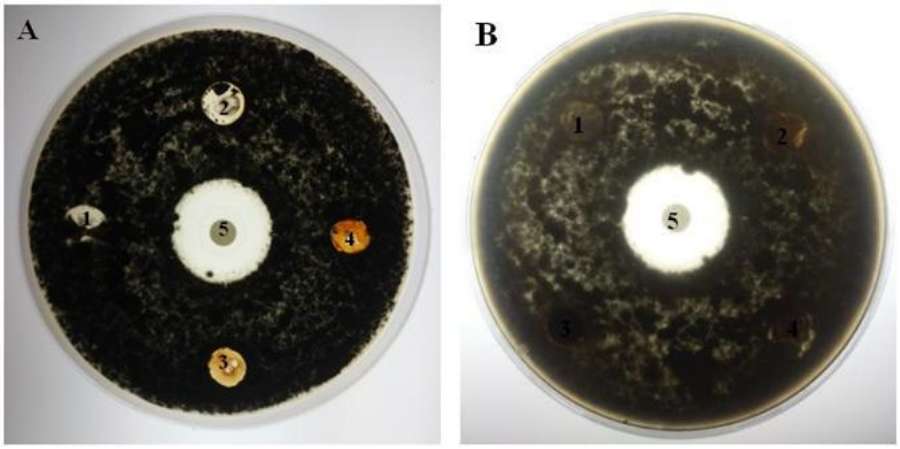

Figure 4.55- Diffusion assay of SELP/Ag materials against *Aspergillus nidulans*. **(A)** FA-SELP/Ag films **(B)** SELP/Ag fibres 1- SELP (0 wt%) ;2- SELP/Ag (1 wt%);3- SELP/Ag (3 wt%) ,4- SELP/Ag (5 wt%) and 5- itraconazole.

4.5.3. Antimicrobial assays for lactoferrin composites

Direct contact assay

The ability of the SELP/LF materials to inhibit the growth of *E. coli* is shown in Figure 4.56. The SELP/LF composites were effective to promote a bacterial growth inhibition higher than 50% which is in agreement with other studies (Kutila *et al.*, 2003; Yekta *et al.*, 2010).

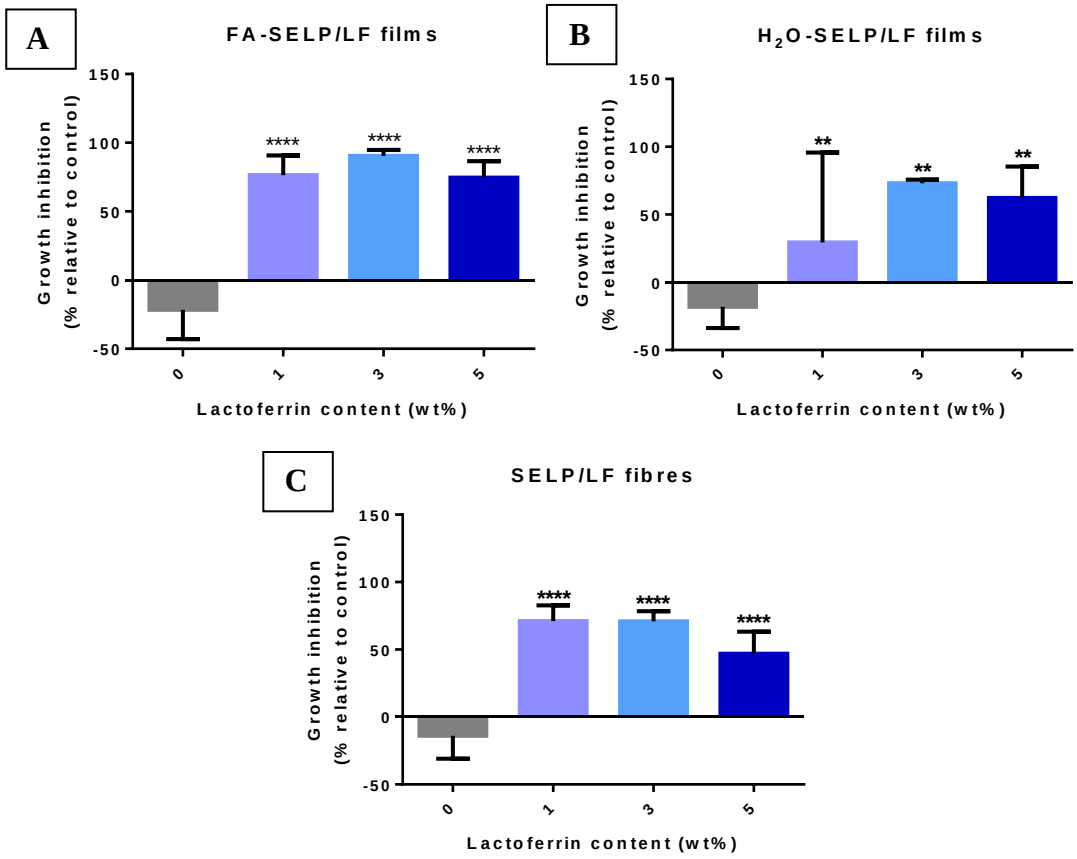

Figure 4.56- Growth inhibition against *E.coli* of **(A)** FA-SELP/LF films, **(B)** H_2O-SELP/LF films and **(C)** SELP/LF fibre mats. Bars represent means ± SD. ** p<0.01and **** p<0.0001.

Halo of inhibition/diffusion method

The results for the antimicrobial activity of lactoferrin-containing composite materials are shown in the Figures 4.57, 4.58 and 4.59. No halo of inhibition or diffuse halos were detected for all concentrations and materials tested, indicating that these materials do not exhibit diffusible antimicrobial activity. These results are contrary to

those previously reported by Rastogi *et al.*, which demonstrated zones of inhibition against different bacteria, included *E. coli* (Rastogi *et al.*, 2014). However, the results presented here are in accordance with those obtained in hydrolytic degradation as no weight loss was detected. This strongly suggests that lactoferrin is tightly packed within the structure of the SELP materials and therefore, is not able to diffuse to the outside.

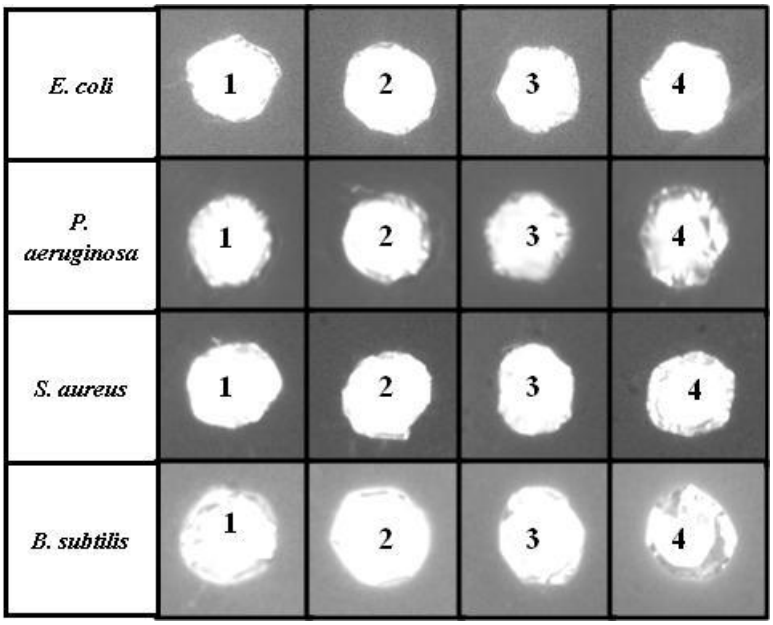

Figure 4.57- Halo of inhibition of SELP/LF fibres (1- 0 wt%; 2- 1 wt%); 3- 3 wt%); 4- 5 wt%) against *E. coli*, *P. aeruginosa*, *S. aureus*, and *B. subtilis*.

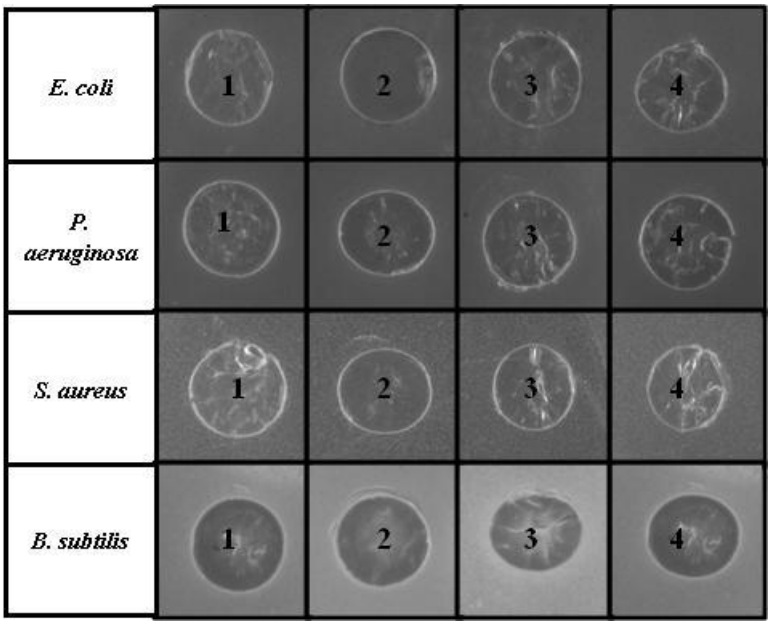

Figure 4.58- Halo of inhibition of FA-SELP/LF films (1- 0 wt%; 2- 1 wt%); 3- 3 wt%); 4- 5 wt%) against four *E. coli*, *P. aeruginosa*, *S. aureus* and *B. subtilis*.

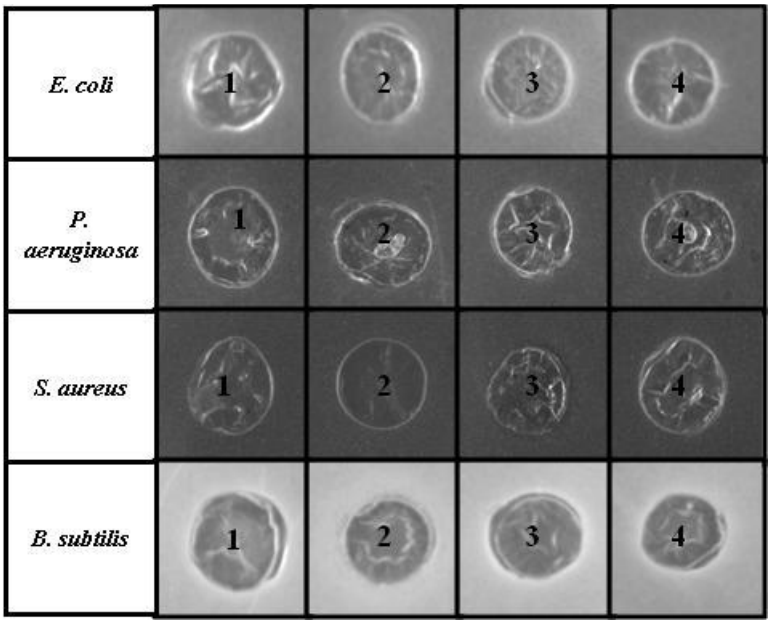

Figure 4.59- Halo of inhibition of H_2O-SELP/LF films (1- 0 wt%; 2- 1 wt%); 3- 3 wt%); 4- 5 wt%) against four *E. coli*, *P. aeruginosa*, *S. aureus* and *B. subtilis*.

4.5. Cytotoxicity evaluation

The SELP/Ag materials demonstrated to have a good antibacterial activity but the biocompatibility of a material is fundamental for any bioapplication (Ghosh *et al.*, 2011). The *in vitro* cytotoxic effects of SELP/Ag materials in BJ-5ta cell line (telomerase-immortalized normal human skin fibroblasts) were evaluated by an indirect contact assay and the viability of the fibroblast cells was confirmed using the MTS assay (Figures 4.60, 4.61 and 4.62). In general, after 24 h, the silver-containing materials showed no toxicity to the BJ-5ta cells and only a slight decrease in cell viability was observed after a prolonged exposure to 72 h. Comparing the concentrations tested, the concentration of 5 wt% for the H_2O-SELP/Ag film, showed a slight decrease in cell viability. The silver cytotoxicity in eukaryotic cells has been reported by several authors. However, some authors (Alt *et al.*, 2004; Wen *et al.*, 2007) observe that low concentration of compounds containing silver are not cytotoxic to fibroblasts, which is in agreement with the results obtained for the SELP/Ag composite materials.

However, it must be noted down that with a concentration of 1 wt% and for all the materials, no cytotoxicity was found. Taking into account that this concentration

showed to be highly effective against bacteria, this strongly suggests that SELP/Ag materials are promising materials for medical applications.

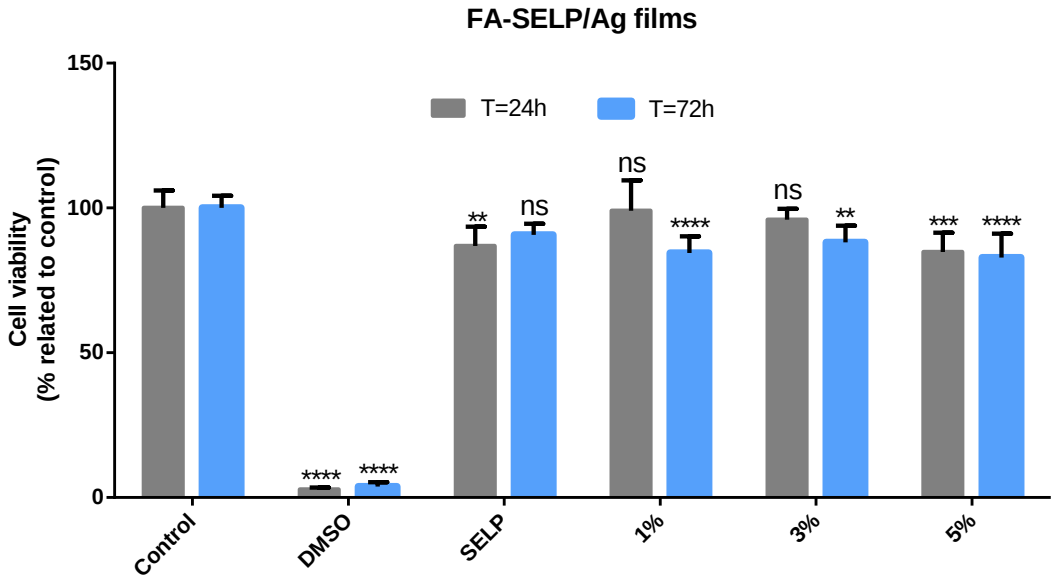

Figure 4.60- Indirect contact cytotoxicity test of pristine FA-SELP and FA-SELP/Ag films on normal human skin fibroblasts (BJ-5ta cell line) with positive (control) and negative controls (30% DMSO) for cell viability after 24 and 72 h of cell culture. Results are expressed as % of viability compared to the control. Bars represent means ± SD. ns- non-significant,* p<0.05,** p<0.01, *** p<0.001 and **** p<0.0001.

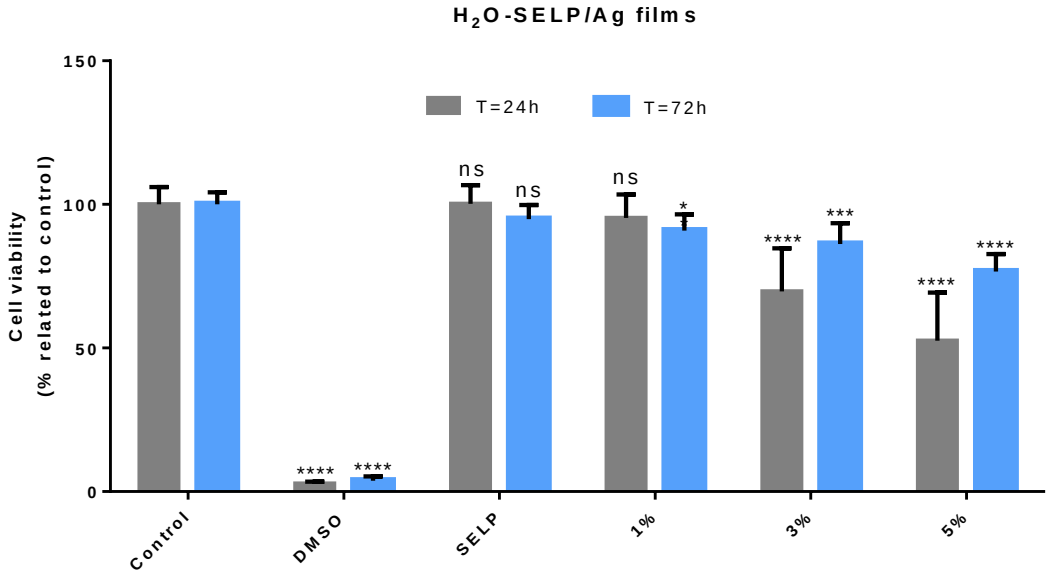

Figure 4.61- Indirect contact cytotoxicity test of pristine H_2O-SELP and H_2O-SELP/Ag films on normal human skin fibroblasts (BJ-5ta cell line) with positive (control) and negative controls (30% DMSO) for cell viability after 24 and 72 h of cell culture. Results are expressed as % of viability compared to the control. Bars represent means ± SD. ns- non-significant,* p<0.05,** p<0.01, *** p<0.001 and **** p<0.0001.

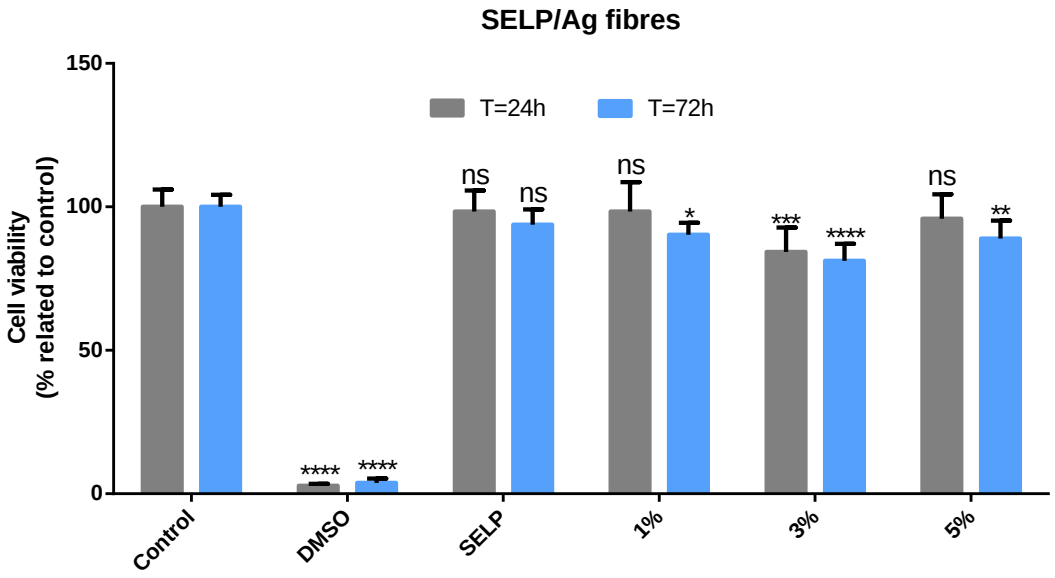

Figure 4.62- Indirect contact cytotoxicity test of pristine SELP and SELP/Ag fibres on normal human skin fibroblasts (BJ-5ta cell line) with positive (control) and negative controls (30% DMSO) for cell viability after 24 and 72 h of cell culture. Results are expressed as % of viability compared to the control. Bars represent means ± SD. ns- non-significant,* $p<0.05$,** $p<0.01$, *** $p<0.001$ and **** $p<0.0001$.

5. FINAL REMARKS AND FUTURE PERSPECTIVES

The first objective of this study was the production and purification of SELPs, which was achieved successfully, enabling the production of SELPs composites with antimicrobial agents (lactoferrin and silver nitrate) by electrospinning and solvent cast techniques. The composite materials (fibers and film) impregnated with an antimicrobial agent (silver or lactoferrin) were successfully produced. Structure stabilization of the composite materials was obtained with chemical treatment with methanol vapor phase conferred stability in aqueous solutions, without major changes in the fibrous structure and comparable to the pure SELP material

The composite materials were characterized by SEM, EBS, EDS, ESEM, XRD, UV-visible and FTIR. The average fibres diameters are similar, regardless of the compound used, with diameters around 100 nm. The results demonstrated that there was the formation of nanoparticles during the process used to obtain the composite material and that silver nanoparticles were distributed throughout the fibers and films. The XRD pattern shows that the solvent used in the processing conditions could affect the crystallinity of the polymer matrix. The UV–vis spectrum features spherical silver nanoparticles as shown by the single plasmon peak at approximately 420 nm. The FTIR results of the materials after treatment with methanol demonstrated that insolubility in aqueous solutions is mediated through a mechanism based on β-sheet conformation in expense of random coil structure. FTIR analysis of composite materials showed also that the presence of silver or lactoferrin, regardless of the concentration used, has no effect on the chemical composition of the composite materials.

The antimicrobial activity of the composite materials impregnated with lactoferrin was evaluated through disk diffusion assays and no visible antibacterial activity was observed, contrary to the direct contact assays. Additional studies have to be carried out to better understand the antimicrobial activity of lactoferrin, perhaps by using a higher concentration of lactoferrin. The results of diffusion assays showed that the composite materials containing silver had strong antibacterial activities against *Gram+ and Gram– bacteria* namely *Staphylococcus aureus, Bacillus subtilis, Escherichia coli* and *Pseudomonas aeruginosa*. Both SELP/Ag fibre mats and films were effective against all the bacteria tested, independently of the solvent used. The films impregnated with silver also showed antifungal effect against *Candida albicans* and *Candida glabrata*.

Finally, the SELP/Ag materials showed no adverse cytotocity and inhibited the growth of microorganisms without significantly affecting the viability of human skin fibroblasts.

These results thus suggest that SELP/Ag composite materials can be used as effective inhibitors of microorganism growth, making them promising materials as biomedical devices such as wound dressings.

6. REFERENCES

Adlerova, L., Bartoskova, A., Faldyna, M. 2008. "Lactoferrin: a Review." *Veterinarni Medicina* 53(7): 457–68.

Alanis, A. J. 2005. "Resistance to Antibiotics: Are We in the Post-Antibiotic Era?" *Archives of medical research* 36(6): 697–705.

Alekshun, M. N. and Levy, S. B. 2007. "Molecular Mechanisms of Antibacterial Multidrug Resistance." *Cell* 128(6): 1037–50.

Alt, V., Bechert, T., Steinrücke, P., Wagener, M., Seidel, P., Dingeldein, E., Domann, E. and Schnettler, R. 2004. "An in Vitro Assessment of the Antibacterial Properties and Cytotoxicity of Nanoparticulate Silver Bone Cement." *Biomaterials* 25(18): 4383–91.

An, J., Zhang, H., Zhang, J., Zhao, Y. and Yuan, X. 2009. "Preparation and Antibacterial Activity of Electrospun Chitosan/poly (ethylene Oxide) Membranes Containing Silver Nanoparticles." *Colloid and Polymer Science* 287(12): 1425–34.

Andersson, D. I. and Hughes, D. 2010. "Antibiotic Resistance and Its Cost: Is It Possible to Reverse Resistance?" *Nature Reviews Microbiology* 8(4): 260–71.

Azam, A., Ahmed A. S., Oves, M., Khan, M. S., Habib, S. S. and Memic, A. 2012. "Antimicrobial Activity of Metal Oxide Nanoparticles Against Gram-Positive and Gram-Negative Bacteria: a Comparative Study." *International journal of nanomedicine* 7: 6003–9.

Baker, H. M. and Baker, E. N. 2012. "A Structural Perspective on Lactoferrin Function." *Biochemistry and Cell Biology* 90(3): 320–28.

Beachley, V. and Wen, X. 2010. "Polymer Nanofibrous Structures: Fabrication, Biofunctionalization, and Cell Interactions." *Progress in polymer science* 35(7): 868–92.

Behera, S., Ghanty,S., Ahmad, F., Santra, S. and Banerjee, S. 2012. "UV-Visible Spectrophotometric Method Development and Validation of Assay of Paracetamol Tablet Formulation." *Journal of Analytical & Bioanalytical Techniques* 03(06):1-6.

Bhardwaj, N. and Kundu, S. C. 2010. "Electrospinning: a Fascinating Fiber Fabrication Technique." *Biotechnology advances* 28(3): 325–47.

Bossche, V. H. 1997. "Mechanisms of Antifungal Resistance." *Revista iberoamericana de micologia* 14: 44–49.

Byun, Y., Whiteside, S., Thomas, R., Dharman, M., Hughes, J. and Kim, Y. T. 2011. "The Effect of Solvent Mixture on the Properties of Solvent Cast Polylactic Acid (PLA) Film." *Journal of Applied Polymer Science* 124(5): 3577–82.

Cao, H. and Liu, X. 2010. "Silver Nanoparticles-Modified Films Versus Biomedical Device-Associated Infections." *Wiley interdisciplinary reviews. Nanomedicine and nanobiotechnology* 2(6): 670–84.

Cappello, J., Crissman, J. W., Crissman, M., Ferrari, F. A., Textor, G., Wallis, O., Whitledge, J. R., Zhou, X., Burman, D., Aukerman, L. and Stedronsky, E. R. 1998. "In-Situ Self-Assembling Protein Polymer Gel Systems for Administration , Delivery , and Release of Drugs." *Journal of Controlled Realease* 53(1-3): 105–17.

Schneider, C. A., Rasband, W. S. and Eliceiri, K. W. 2012. "NIH Image to ImageJ: 25 Years of Image Analysis." *Nature Methods* 9(7): 671–75.

Celis, J. E. 2006. *Cell Biology: A Laboratory Handbook*. 3rd ed. Elsevier Academic Press.

Chong, M. K., Chua, A. J. S., Tan, T. T. T., Tan, S. H. and Ng, M. L. 2014. "Microscopy Techniques in Flavivirus Research." *Micron* 59: 33–43.

Chul, I., Kweon, H. Y., Lee, K. G. and Park, Y. H. 2003. "The Role of Formic Acid in Solution Stability and Crystallization of Silk Protein Polymer." *International Journal of Biological Macromolecules* 33(4-5): 203–13.

Chul, I., Kweon, H. Y., Park, Y. H. and Hudson, S. 2001. "Structural Characteristics and Properties of the Regenerated Silk Fibroin Prepared from Formic Acid." *International Journal of Biological Macromolecules* 29: 91–97.

Da Costa, A. M. A., Machado, R., Ribeiro, A., Collins, T., Thiagarajan, V., Petersen, M. T. N., Rodríguez-Cabello, J. C., Gomes, A. C. and Casal, M. 2015. "Development of Elastin Like Recombinamer Films with Antimicrobial Activity." *Biomacromolecules*.

Dinerman, A. A., Cappello, J., Ghandehari, H. and Hoag, S. W. 2002. "Swelling behavior of a genetically engineered silk-elastinlike protein polymer hydrogel." *Biomaterials* 23:4203–4210

Du, W., Niu, S., Xu, Y., Xu, Z. and Fan, C. 2009. "Antibacterial Activity of Chitosan Tripolyphosphate Nanoparticles Loaded with Various Metal Ions." *Carbohydrate Polymers* 75(3): 385–89.

Duygu, D., Baykal, T., Açikgöz, I., and Yildiz, K. 2009. "Fourier Transform Infrared (FT-IR) Spectroscopy for Biological Studies." *G.U. Journal of Science* 22(3): 117–21.

Egger, S., Lehmann, R. P., Height, M. J., Loessner, M. J. and Schuppler, M. 2009. "Antimicrobial Properties of a Novel Silver-Silica Nanocomposite Material." *Applied and environmental microbiology* 75(9): 2973–76.

García-Montoya, I.A., Cendón, T. S., Arévalo-Gallegos, S. and Rascón-Cruz, Q. 2012. "Lactoferrin a Multiple Bioactive Protein: An Overview." *Biochimica et biophysica acta* 1820(3): 226–36.

Garg, K. and Bowlin, G. 2011. "Electrospinning jets and nanofibrous structures." *Biomicrofluidics* 5(1): 013403.

Gavanji, S. 2013. "The Effects of Silver Nano Particles on Microorganisms : A Review." *Applied Science Reports* 1(2): 50–56.

Ghannoum, M. A. and Rice, L. B. 1999. "Antifungal Agents: Mode of Action, Mechanisms of Resistance, and Correlation of These Mechanisms with Bacterial Resistance." *Clinical microbiology reviews* 12(4): 501–17.

Ghosh, S., Ranebennur, T. K. and Vasan, H. N. 2011. "Study of Antibacterial Efficacy of Hybrid Chitosan-Silver Nanoparticles for Prevention of Specific Biofilm and Water Purification." *International Journal of Carbohydrate Chemistry* 2011: 1–11.

González-Chávez, S. A., Arévalo-Gallegos, S. and Rascón-Cruz, Q. 2009. "Lactoferrin: Structure, Function and Applications." *International journal of antimicrobial agents* 33(4): 301.e1–301.e8.

Gustafson, J. A., Price, R. A., Greish, K., Cappello, J. and Ghandehari, H. 2010. "Silk-Elastin-Like Hydrogel Improves the Safety of Adenovirus-Mediated Gene-Directed Enzyme− Prodrug Therapy." *Molecular Pharmaceutics* 7(4): 1050–56.

Gustafson, J., Greish, K., Frandsen, J., Cappello, J. and Ghandehari, H. 2009. "Silk-Elastinlike Recombinant Polymers for Gene Therapy of Head and Neck Cancer: From Molecular Definition to Controlled Gene Expression." *Journal of controlled release : official journal of the Controlled Release Society* 140(3): 256–61.

Haider, M., Cappello, J., Ghandehari, H. and Leong, K. W. 2008. "In Vitro Chondrogenesis of Mesenchymal Stem Cells in Recombinant Silk-Elastinlike Hydrogels." *Pharmaceutical research* 25(3): 692–99.

Haider, M., Leung, V., Ferrari, F., Crissman, J., Powell, J., Cappello, J. and Ghandehari, M. 2005. "Molecular Engineering of Silk-Elastinlike Polymers for Matrix-Mediated Gene Delivery: Biosynthesis and Characterization." 2(2): 139–50.

Harbottle, H., Thakur, S., Zhao, S. and White, D. G. 2006. "Genetics of Antimicrobial Resistance." *Animal biotechnology* 17(2): 111–24.

Hogan, D. and Roberto K. 2002. "Why Are Bacteria Refractory to Antimicrobials?" *Current opinion in microbiology* 5(5): 472–77.

Hu, X., Kaplan, D. and Cebe, P. 2006. "Determining Beta-Sheet Crystallinity in Fibrous Proteins by Thermal Analysis and Infrared Spectroscopy." *Macromolecules* 39(18): 6161–70.

Huang, Z., Zhang, Y. Z., Kotaki, M. and Ramakrishna, S. 2003. "A Review on Polymer Nanofibers by Electrospinning and Their Applications in Nanocomposites." *Composites Science and Technology* 63(15): 2223–53.

Jenkins, R. 2000. "X-Ray Techniques : Overview." Encyclopedia of Analytical Chemistry 13269–13288.

Jenssen, H. and Hancock, R. E. W. 2009. "Antimicrobial Properties of Lactoferrin." *Biochimie* 91(1): 19–29.

Jeong, L. and Park, W. H. 2014. "Preparation and Characterization of Gelatin Nanofibers Containing Silver Nanoparticles." *International journal of molecular sciences* 15(4): 6857–79.

Jung, W. K., Koo, H. C., Kim, K. W., Shin, S., Kim, S. H. and Park, Y. H. 2008. "Antibacterial Activity and Mechanism of Action of the Silver Ion in Staphylococcus Aureus and Escherichia Coli." *Applied and environmental microbiology* 74(7): 2171–78.

Greish, K., Frandsen, J., Scharff, S., Gustafson, J., Cappello, J., Li, D., O'Malley, B. W., H. and Ghandehari, H. 2010. "Silk-Elastinlike Protein Polymers Improve the Efficacy of Adenovirus Thymidine Kinase Enzyme Prodrug Therapy of Head and Neck Tumors." *The Journal of Gene Medicine* 12(7): 572–79.

Kenneth, R. and Ray, G. 2004. *Sherris Medical Microbiology - An Introduction to Infectious Diseases*. 4th ed.

Kim, S. H., Nam, Y. S., Lee, T. S. and Park, W. H. 2003. "Silk Fibroin Nanofiber. Electrospinning, Properties, and Structure." *Polymer Journal* 35(2): 185–90.

Klepser, M. E., Ernst, E. J. and Pfaller, M. A. 1997. "Update on Antifungal Resistance." *Trends in Microbiology* 5(9): 2251–53.

Knetsch, M. L. W. and Koole, L. K. 2011. "New Strategies in the Development of Antimicrobial Coatings: The Example of Increasing Usage of Silver and Silver Nanoparticles." *Polymers* 3(4): 340–66.

Kumar, P., Selvi, S. S. and Govindaraju, M. 2012. "Seaweed-Mediated Biosynthesis of Silver Nanoparticles Using Gracilaria Corticata for Its Antifungal Activity Against Candida Spp." *Applied Nanoscience* 3(6): 495–500.

Kumar, R. and Münstedt, H. 2005. "Polyamide/silver Antimicrobials: Effect of Crystallinity on the Silver Ion Release." *Polymer International* 54(8): 1180–86.

Kundu, B., Rajkhowa, R., Kundu, S. C. and Wang, X. 2013. "Silk Fibroin Biomaterials for Tissue Regenerations." *Advanced drug delivery reviews* 65(4): 457–70.

Kutila, T., Pyörälä, S., Saloniemi, H. and Kaartinen, L. 2003. "Antibacterial Effect of Bovine Lactoferrin Against." *Acta Veterinaria Scandinavica* 44(1-2): 35–42.

LaFayette, S. L., Collins, C., Zaas, A. K., Schell, W. A., Betancourt-Quiroz, M., Gunatilaka, A. A. L., Perfect, J. R and Cowen, L. E. 2010. "PKC Signaling Regulates Drug Resistance of the Fungal Pathogen Candida Albicans via Circuitry Comprised of Mkc1, Calcineurin, and Hsp90." *PLoS pathogens* 6(8): 1-23.

Legrand, D., Pierce, A., Elass, E., Carpentier, M., Mariller, C. and Mazurier, J. 2008. "Lactoferrin Structure and Functions." *Advances in experimental medicine and biology* 606: 163–94.

Lewis, R. E., Viale, P. and Kontoyiannis, D. P. 2012. "The Potential Impact of Antifungal Drug Resistance Mechanisms on the Host Immune Response to Candida." *Virulence* 3(4): 368–76.

Lin, W., Li, Q. and Zhu, T. 2012. "Study of Solvent Casting/particulate Leaching Technique Membranes in Pervaporation for Dehydration of Caprolactam." *Journal of Industrial and Engineering Chemistry* 18(3): 941–47.

Loeffler, J., and Stevens, D. A. 2003. "Antifungal Drug Resistance." *Clinical Infectious Diseases* 36(Suppl 1): 31–41.

Machado, R., Ribeiro, A. J., Padrão, J. Silva, D., Nobre, A., Teixeira, J. A., Arias, F. J., Cunha, A. M., Rodríguez-Cabello, J. C. and Casal, M. 2009. "Exploiting the Sequence of Naturally Occurring Elastin : Construction , Production and Characterization of a Recombinant Thermoplastic Protein- Based Polymer." 6: 133–45.

Machado, R., Azevedo-Silva, J., Correia, C., Collins, T., Arias, F. X., Rodríguez-Cabello, J. C. and Casal, M. 2013a. "High Level Expression and Facile Purification of Recombinant Silk-Elastin-Like Polymers in Auto Induction Shake Flask Cultures." *AMB Express* 3(1): 11.

Machado, R., da Costa, A., Sencadas, V., Garcia-Arévalo, C. Costa, C. M., Padrão, J., Gomes, A., Lanceros-Méndez, S., Rodríguez-Cabello, J. C. and Casal, M. 2013b. "Electrospun Silk-Elastin-Like Fibre Mats for Tissue Engineering Applications." *Biomedical materials (Bristol, England)* 8(6): 065009.

Machado, R. M. R. 2012. "Design , Bioproduction and Characterization of Protein Recombinant Silk-Elastin-Based Polymers – a New Class of Nano-Biomaterials." *Universidade do Minho Escola de Ciências*.

Marie, C., and White, T. C. 2009. "Genetic Basis of Antifungal Drug Resistance." *Current fungal infection reports* 3(3): 163–169.

Martins, A., Reis, R. L. and Neves, N. M. 2008. "Electrospinning: Processing Technique for Tissue Engineering Scaffolding." *International Materials Reviews* 53(5): 257–274.

Megeed, Z., Cappello, J. and Ghandehari, H. 2002. "Controlled release of plasmid DNA from a genetically engineered silk-elastinlike hydrogel." *Pharm. Res.* 19: 954–959

McCann, J. T., Li, D. and Xia, Y. 2005. "Electrospinning of Nanofibers with Core-Sheath, Hollow, or Porous Structures." *Journal of Materials Chemistry* 15: 735–738.

Mijnendonckx, K., Leys, N., Mahillon, J., Silver, S. and Houdt, R. V. 2013. "Antimicrobial Silver: Uses, Toxicity and Potential for Resistance." *Biometals : an international journal on the role of metal ions in biology, biochemistry, and medicine* 26(4): 609–621.

Mishra, N. N., Prasad, T., Sharma, N., Payasi, A., Prasad, R., Gupta, D. K. and Singh, R. 2007. "Pathogenicity and Drug Resistance in Candida Albicans and Other Yeast Species. A Review." *Acta microbiologica et immunologica Hungarica* 54(3): 201–235.

Montazer, M. and Malekzadeh, S. B. 2012. "Electrospun Antibacterial Nylon Nanofibers through in Situ Synthesis of Nanosilver: Preparation and Characteristics." *Journal of Polymer Research* 19(10): 9980.

Monteiro, D. R., Gorup, L. F., Silva, S., Negri, M., de Camargo, E. R., Oliveira, R., Barbosa, D. B. and Henriques, M. 2011. "Silver Colloidal Nanoparticles: Antifungal Effect Against Adhered Cells and Biofilms of Candida Albicans and Candida Glabrata." *Biofouling* 27(7): 711–719.

Monteiro, D. R., Gorup, L. F., Takamiya, A. S., Ruvollo-Filho, A. C., de Camargo, E, R. and Barbosa, D. B. 2009. "The Growing Importance of Materials That Prevent Microbial Adhesion: Antimicrobial Effect of Medical Devices Containing Silver." *International journal of antimicrobial agents* 34(2): 103–110.

Muñoz-Bonilla, A. And Fernández-García, M. 2012. "Polymeric Materials with Antimicrobial Activity." *Progress in Polymer Science* 37(2): 281–339.

Nabikhan, A., Kandasamy, K., Raj, A. and Alikunhi, N. M. 2010. "Synthesis of Antimicrobial Silver Nanoparticles by Callus and Leaf Extracts from Saltmarsh Plant, Sesuvium Portulacastrum L." *Colloids and surfaces. B, Biointerfaces* 79(2): 488–493.

Nagarsekar, A., Crissman, J., Crissman, M., Ferrari, F., Cappello, J. and Ghandehari, H. 2002. "Genetic Synthesis and Characterization of pH-and Temperature-sensitive Silk-elastinlike Protein Block Copolymers." *Journal of Biomedical Materials Research* 62(2): 195–203.

Ner, Y., Stuart, J. A., Whited, G. and Sotzing, G. A. 2009. "Electrospinning Nanoribbons of a Bioengineered Silk-Elastin-Like Protein (SELP) from Water." *Polymer* 50(24): 5828–5836.

Oraby, M. A., Waley, A. I., El-dewany, A. I., Saad, E. A. and El-hady, B. M. A. 2013. "Electrospinning of Gelatin Functionalized with Silver Nanoparticles for Nanofiber Fabrication." *Modeling and Numerical Simulation of Material science* 3(4): 95–105.

Oudhia, A. 2012. "UV-VIS Spectroscopy as a Nondestructive and Effective Characterization Tool for II-VI Compounds." *Recent Research in Science and Technology* 4(8): 109–111.

Padrão, J., Silva, J. P., Rodrigues, L. R., Dourado, F., Lanceros-Méndez, S. and Sencadas, V. 2014. "Modifying Fish Gelatin Electrospun Membranes for Biomedical Applications: Cross-Linking and Swelling Behavior." *Soft Materials* 12(3): 247–252.

Pal, S., Tak, Y. K. and Song, J. M. 2007. "Does the Antibacterial Activity of Silver Nanoparticles Depend on the Shape of the Nanoparticle? A Study of the Gram-Negative Bacterium Escherichia Coli." *Applied and environmental microbiology* 73(6): 1712–1720.

Park, S., Bae, H., Xing, Z., Kwon, O. H. and Huh, M. 2009. "Preparation and Properties of Silver-Containing Nylon 6 Nanofibers Formed by Electrospinning." *Journal of Applied Polymer Science* 112: 2320–2326.

Perea, S. and Patterson T. F. 2002. "Antifungal Resistance in Pathogenic Fungi." *Clinical Infectious Diseases* 35(9): 1073–1080.

Pfaller, M. A. 2012. "Antifungal Drug Resistance: Mechanisms, Epidemiology, and Consequences for Treatment." *The American journal of medicine* 125(1 Suppl): S3–13.

Pinto, R. J. B., Fernandes, S. C. M., Freire, C. S. R., Sadocco, P., Causio, J., Neto, C. P. and Trindade, T. 2012. "Antibacterial Activity of Optically Transparent Nanocomposite Films Based on Chitosan or Its Derivatives and Silver Nanoparticles." *Carbohydrate research* 348: 77–83.

Poole, K. 2002. "Mechanisms of Bacterial Biocide and Antibiotic Resistance." *Journal of Applied Microbiology* 92(S1): S55–S64.

Prabhu, S. and Poulose, E. K. 2012. "Silver Nanoparticles: Mechanism of Antimicrobial Action, Synthesis, Medical Applications, and Toxicity Effects." *International Nano Letters* 2(32): 1–10.

Prasad, R. and Kapoor, K. 2004. "Multidrug Resistance in Yeast Candida." *International review of cytology* 242: 215–248.

Price, R., Gustafson, J., Greish, K., Cappello, J., McGill, L. and Ghandehari, H. 2012. "Comparison of Silk-Elastinlike Protein Polymer Hydrogel and Poloxamer in Matrix-Mediated Gene Delivery." *International journal of pharmaceutics* 427(1): 97–104.

Rai, M. K., Deshmukh, S. D., Ingle, A. P and Gade, A. K. 2012. "Silver Nanoparticles: The Powerful Nanoweapon Against Multidrug-Resistant Bacteria." *Journal of applied microbiology* 112(5): 841–852.

Rai, M., Yadav, A. and Gade, A. 2009. "Silver Nanoparticles as a New Generation of Antimicrobials." *Biotechnology advances* 27(1): 76–83.

Rai V, R. and Bai A, J. 2011. "Nanoparticles and Their Potential Application as Antimicrobials." *Science against microbial pathogens: communicating current research and technological advances*: 197–209.

Raja, K., Saravanakumar, A. And Vijayakumar, R. 2012. "Spectrochimica Acta Part A : Molecular and Biomolecular Spectroscopy Efficient Synthesis of Silver Nanoparticles from Prosopis Juliflora Leaf Extract and Its Antimicrobial Activity Using Sewage." *Spectrochimica Acta Part A: Molecular and Biomolecular Spectroscopy* 97: 490–494.

Rasband, W. S. "ImageJ", US National Institutes of Health, Bethesda, Maryland, EUA. http://imagej.nih.gov/ij/.

Rastogi, N., Nagpal, N., Alam, H., Pandey, S., Gautam, L., Sinha, M., Shin, K., Manzoor, N., Virdi, J., Kaur, P., Sharma, S. and Singh, T, P. 2014. "Preparation and Antimicrobial Action of Three Tryptic Digested Functional Molecules of Bovine Lactoferrin." *PloS one* 9(3): e90011.

Reidy, B., Haase, A., Luch, A., Dawson, K. and Lynch, I. 2013. "Mechanisms of Silver Nanoparticle Release, Transformation and Toxicity: A Critical Review of Current Knowledge and Recommendations for Future Studies and Applications." *Materials* 6(6): 2295–2350.

Ruparelia, J. P, Chatterjee, A. K., Duttagupta, S. P. Mukherji, S. 2008. "Strain Specificity in Antimicrobial Activity of Silver and Copper Nanoparticles." *Acta Biomaterialia* 4(3): 707–716.

Rutledge, G. C. and Fridrikh, S. V. 2007. "Formation of Fibers by Electrospinning." *Advanced drug delivery reviews* 59(14): 1384–1391.

Saengmee-Anupharb, S., Srikhirin, T., Thaweboon, B., Thaweboon, S., Amornsakchai, T., Dechkunakorn, S. and Suddhasthira, T. 2013. "Antimicrobial Effects of Silver Zeolite, Silver Zirconium Phosphate Silicate and Silver Zirconium Phosphate Against Oral Microorganisms." *Asian Pacific journal of tropical biomedicine* 3(1): 47–52.

Sahay, R., Kumar, P. S., Sridhar, R., Sundaramurthy, J., Venugopal, J., Mhaisalkar, S. G. and Ramakrishna, S. 2012. "Electrospun Composite Nanofibers and Their Multifaceted Applications." *Journal of Materials Chemistry* 22(26): 12953–12971.

Scheller, J., Guhrs, K. H., Grosse, F. and Conrad, U. 2001. "Production of Spider Silk Proteins in Tobacco and Potato." *Nature Biotechnology* 19(6): 573–577.

Schmid, F. 2001. "Biological Macromolecules : Spectrophotometry Concentrations." Encyclopedia of Life Sciences *Biological Macromolecules : Spectrophotometry Concentrations*.

Shahverdi, A. R., Minaeian, S., Shahverdi, H. R., Jamalifar, H. and Nohi, A. 2007. "Rapid Synthesis of Silver Nanoparticles Using Culture Supernatants of

Enterobacteria: A Novel Biological Approach." *Process Biochemistry* 42(5): 919–923.

Shanks, C. R. and Peteroy-Kelly, M. A. 2009. "Research Article: Analysis of Antimicrobial Resistance in Bacteria Found at Various Sites on Surfaces in an Urban University." *Bios* 80(3): 105–113.

Shi, Q., Vitchuli, N., Nowak, J., Noar, J., Caldwell, J. M., Breidt, F., Bourham, M., McCord, M. and Zhang, X. 2011. "One-Step Synthesis of Silver Nanoparticle-Filled Nylon 6 Nanofibers and Their Antibacterial Properties." *Journal of Materials Chemistry* 21(28): 10330–10335.

Spížek, J., Novotná, J., Rezanka, T. and Demain, A. L. 2010. "Do We Need New Antibiotics? The Search for New Targets and New Compounds." *Journal of industrial microbiology & biotechnology* 37(12): 1241–1248.

Strate, B. W. A., Beljaars, L., Molema, G., Harmsen, M. C. and Meijer, D. K. F. 2001. "Antiviral Activities of Lactoferrin." *Antiviral Research* 52(3): 225–239.

Teng, W., Cappello, J. and Wu, X. 2009. "Recombinant Silk-Elastinlike Protein Polymer Displays Elasticity Comparable to Elastin." *Biomacromolecules* 10(11): 3028–3036.

Tenover, F. C. 2006. "Mechanisms of Antimicrobial Resistance in Bacteria." *American Journal of Infection Control* 34(5S): S3–S10.

Urry, D. W. 2006. "*What Sustains Life? Consilient Mechanisms for Protein-Based Machines and Materials"* (New York: Springer)

Vandeputte, P., Ferrari, S. and Coste, A. T. 2012. "Antifungal Resistance and New Strategies to Control Fungal Infections." *International journal of microbiology* 2012: 1–26.

Varesano, A., Vineis, C., Aluigi, A. and Rombaldoni, F. 2011. "Antimicrobial Polymers for Textile Products." 99–110.

Vimala, K., Mohan, Y. M., Sivudu, K. S., Varaprasad, K., Ravindra, S., Reddy, N. N., Padma, Y., Sreedhar, B. and MohanaRaju, K. 2010. "Fabrication of Porous Chitosan Films Impregnated with Silver Nanoparticles: a Facile Approach for Superior Antibacterial Application." *Colloids and surfaces. B, Biointerfaces* 76(1): 248–258.

Wakabayashi, H., Yamauchi, K. and Takase, M. 2006. "Lactoferrin Research, Technology and Applications." *International Dairy Journal* 16(11): 1241–1251.

Ward, P. P. 2002. "Lactoferrin and Host Defense." *Biochemistry and cell* 102(1): 95–102.

Wei, D., Sun, W., Qian, W., Ye, Y. and Ma, X. 2009. "The Synthesis of Chitosan-Based Silver Nanoparticles and Their Antibacterial Activity." *Carbohydrate research* 344(17): 2375–2382.

Wen, H., Lin, Y., Jian, S., Tseng, S., Weng, M., Liu, Y., Lee, P., Chen, P., Hsu, R., Wu, W. and Chou, C. 2007. "Observation of Growth of Human Fibroblasts on Silver Nanoparticles." *Journal of Physics: Conference Series* 61: 445–449.

Xia, X., Qian, Z., Ki, C. S., Park, Y. H., Kaplan, D. L. and Lee, S. Y. 2010. "Native-Sized Recombinant Spider Silk Protein Produced in Metabolically Engineered Escherichia Coli Results in a Strong Fiber." *Proceedings of the National Academy of Sciences of the United States of America* 107(32): 14059–14063.

Xu, X., Yang, Q., Wang, Y., Yu, H., Chen, X. and Jing, X. 2006. "Biodegradable Electrospun Poly(l-Lactide) Fibers Containing Antibacterial Silver Nanoparticles." *European Polymer Journal* 42(9): 2081–2087.

Xu, X. and Zhou, M. 2008. "Antimicrobial Gelatin Nanofibers Containing Silver Nanoparticles." *Fibers and Polymers* 9(6): 685–690.

Yekta, M. A., Verdonck, F., Van Den Broeck, W., Goddeeris, B. M., Cox, E. and Vanrompay, D. 2010. "Lactoferrin Inhibits E . Coli O157 : H7 Growth and Attachment to Intestinal Epithelial Cells." *Veterinarni Medicina* 55(8): 359–368.

Zeng, L., Jiang, L., and Teng, W., Cappello, J., Zohar, Y. and Wu, X. 2014. "Engineering Aqueous Fiber Assembly into Silk-Elastin-Like Protein Polymers." *Macromolecular Rapid Communications* 35(14): 1273–1279.

7. ANNEXES

Table A1- Vibrational band assignments in the Amide I region (Hu *et al.*, 2006; R. Machado *et al.*, 2013).

Wavenumber (cm^{-1})	Secondary structure assignment
1605-1615	aggregated strands
1616-1621	aggregated beta-strand/beta-sheets (weak)[1]
1622-1627	beta-sheets (strong)[1]
1628-1637	beta-sheets (strong)[2]
1638-1655	random coils
1656-1662	alpha-helices
1663-1696	turns and bends
1697-1703	beta-sheets (weak)[1]

1 Intermolecular beta-sheets
2 Intramolecular beta-sheets

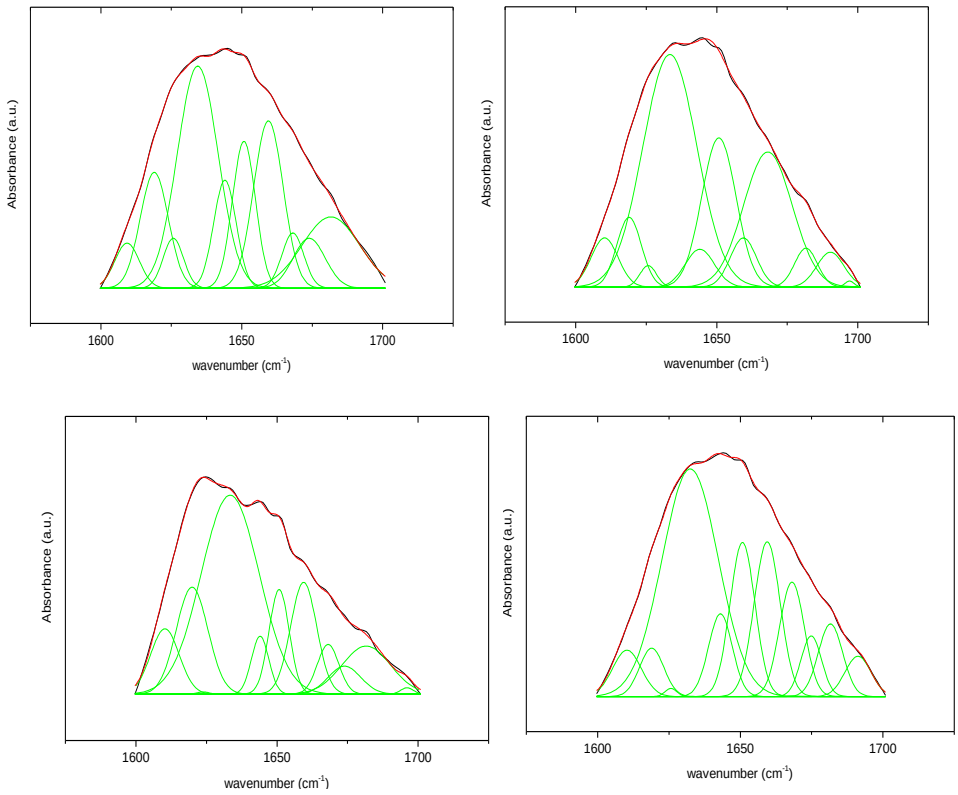

Figure A1- Curve-fitted spectra (upper) of silver fibres of non-treated. Gaussian bands (green line) were fitted iteratively to the amide I band (black line).

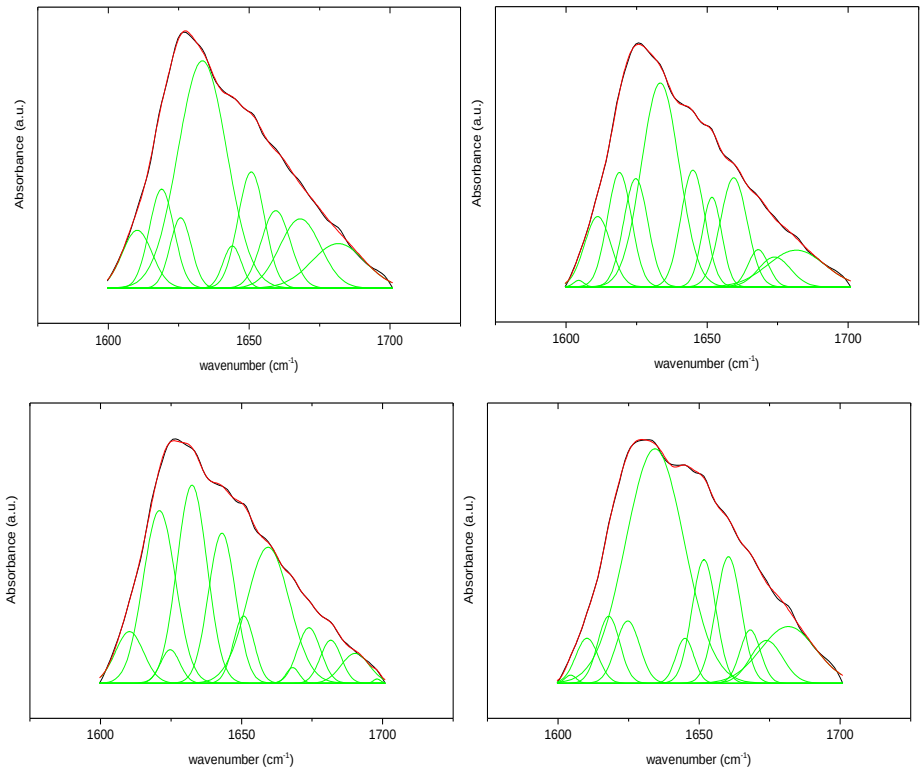

Figure A2- Curve-fitted spectra (upper) of silver fibres of methanol-treated. Gaussian bands (green line) were fitted iteratively to the amide I band (black line)**.**

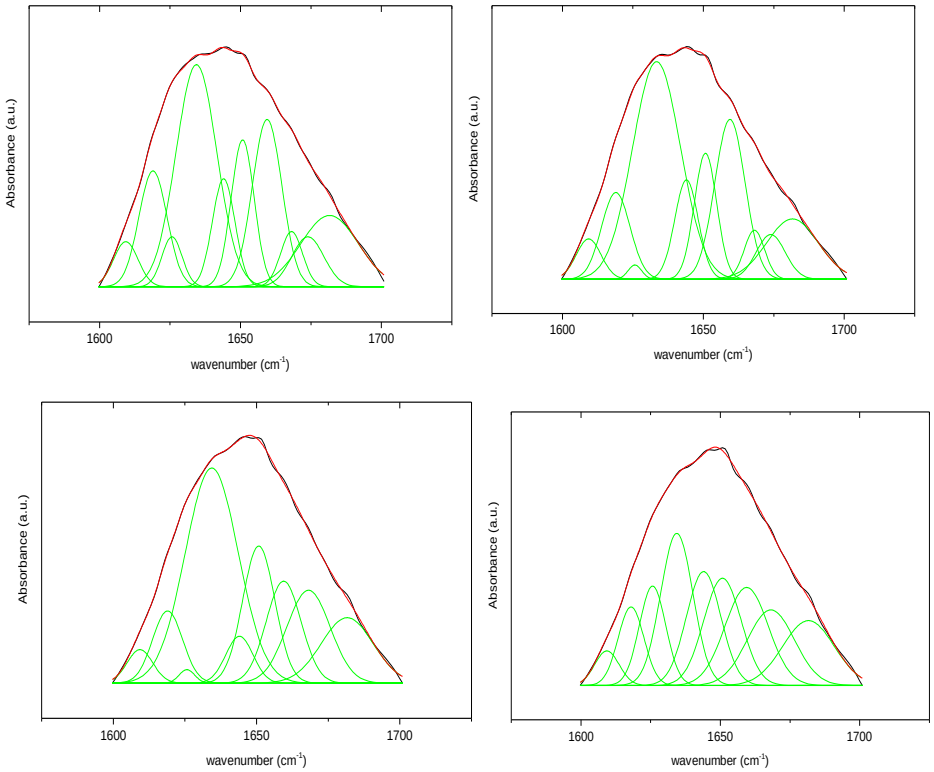

Figure A3- Curve-fitted spectra (upper) of lactoferrin fibres of without treatment. Gaussian bands (green line) were fitted iteratively to the amide I band (black line).

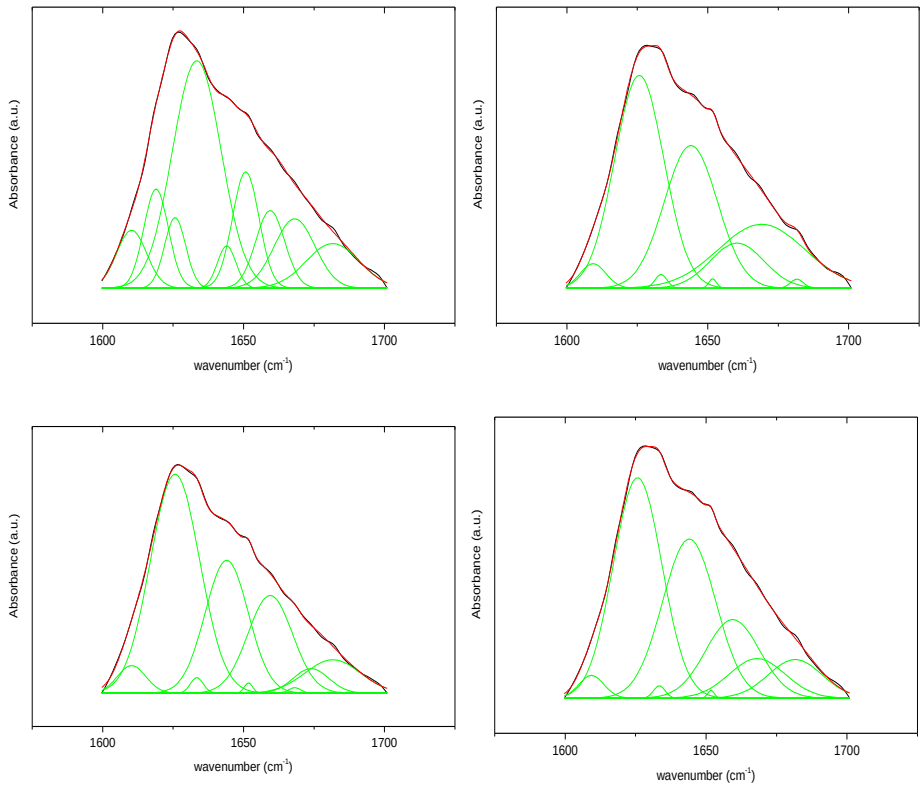

Figure A4- Curve-fitted spectra (upper) of lactoferrin fibres of methanol-treated. Gaussian bands (green line) were fitted iteratively to the amide I band (black line).

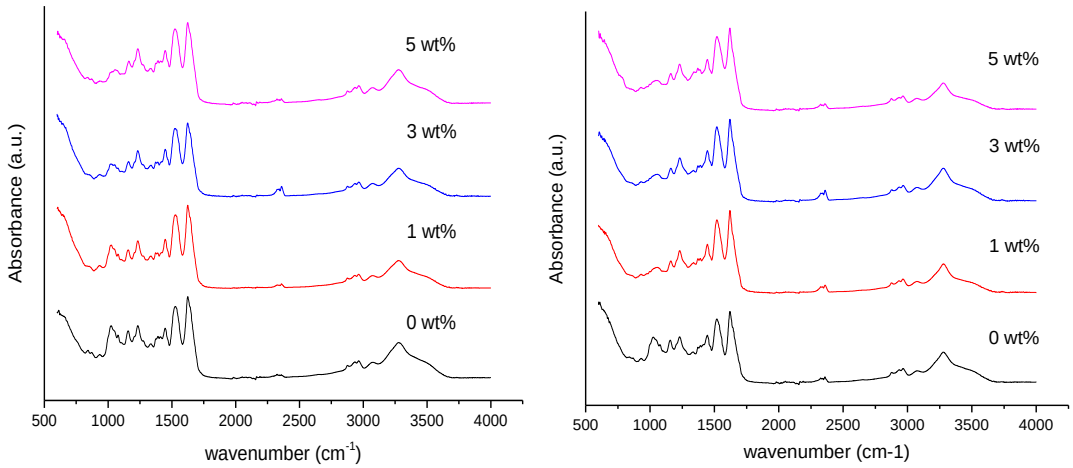

Figure A5- (A) FTIR spectra of FA-SELP/Ag films. **(B)** FTIR spectra of methanol-treated FA-SELP/Ag films.

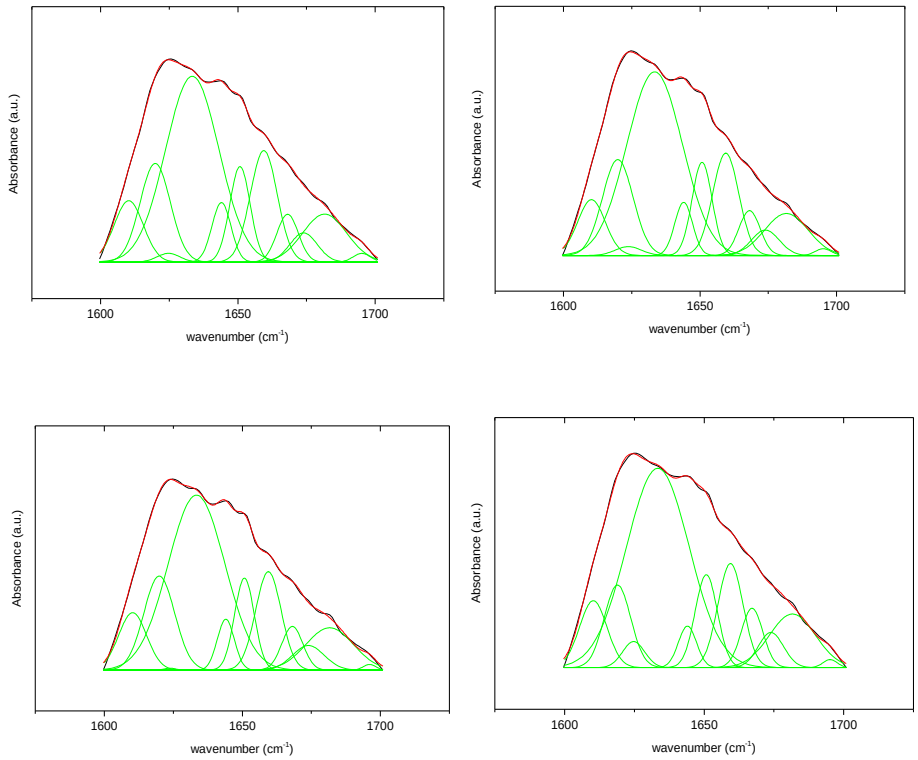

Figure A6- Curve-fitted spectra (upper) of FA-SELP/Ag of non-treated. Gaussian bands (green line) were fitted iteratively to the amide I band (black line).

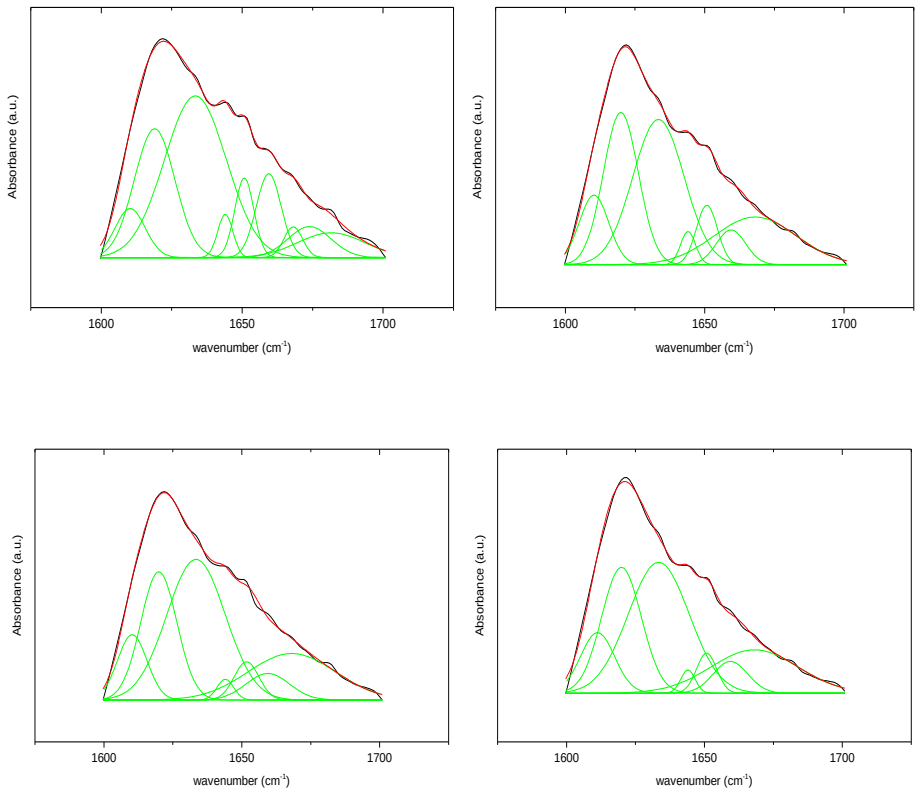

Figure A7- Curve-fitted spectra (upper) of FA-SELP/Ag films of methanol-treated. Gaussian bands (green line) were fitted iteratively to the amide I band (black line)**.**

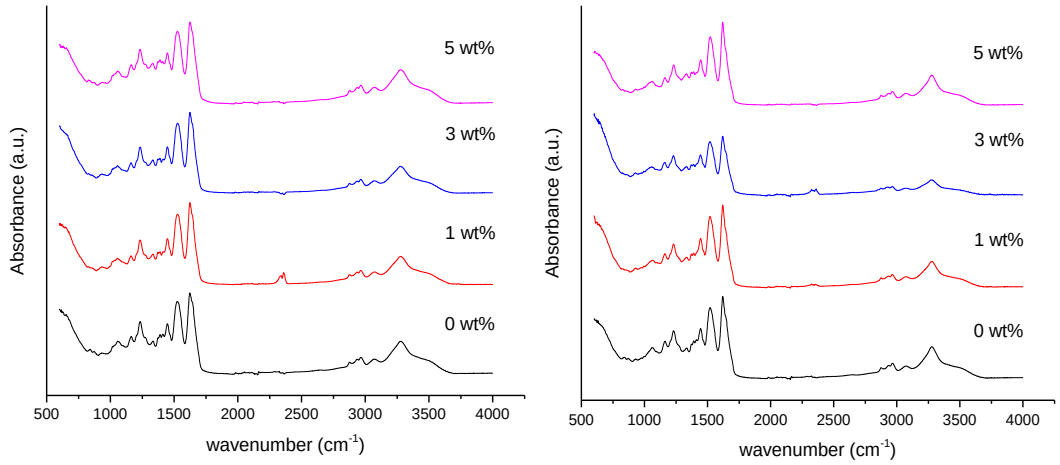

Figure A8- (A) FTIR spectra of H2O-SELP/Ag films. (**B)** FTIR spectra of methanol-treated H2O-SELP/Ag films.

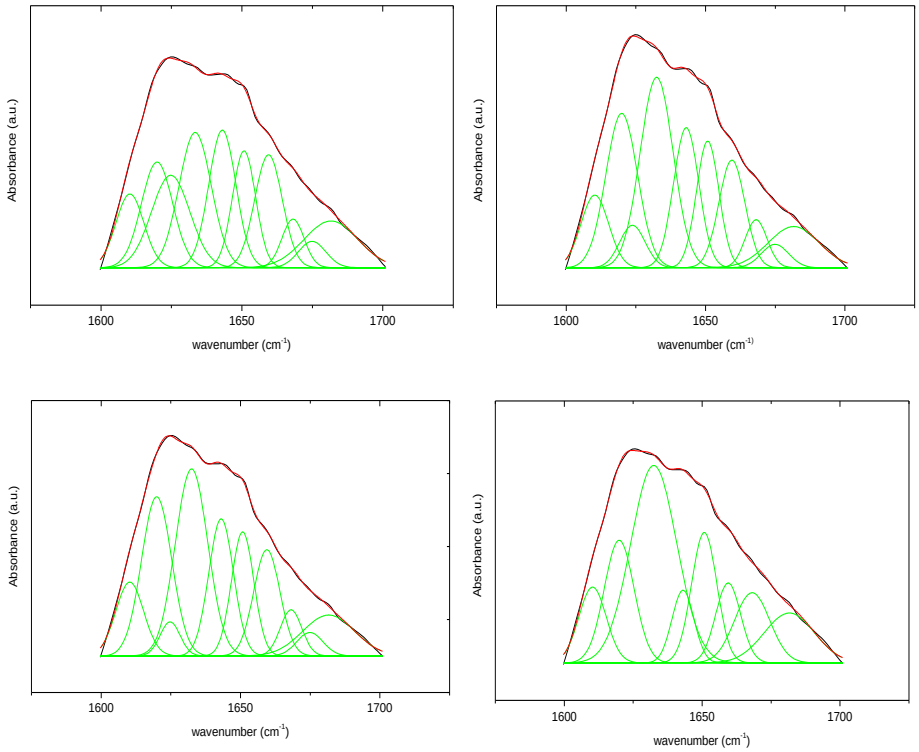

Figure A9- Curve-fitted spectra (upper) of H2O-SELP/Ag of non-treated films. Gaussian bands (green line) were fitted iteratively to the amide I band (black line).

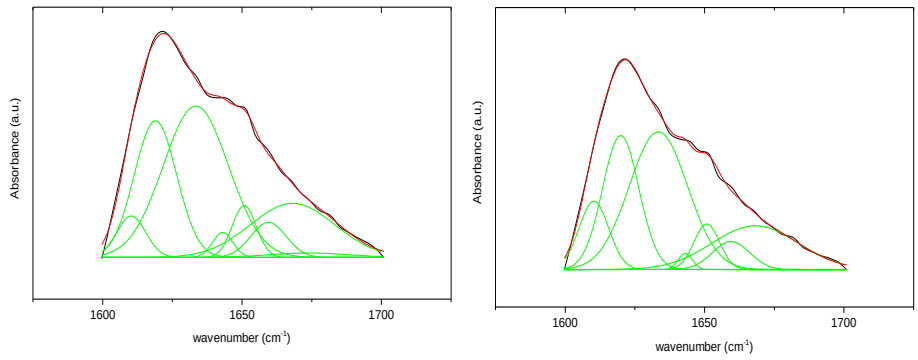

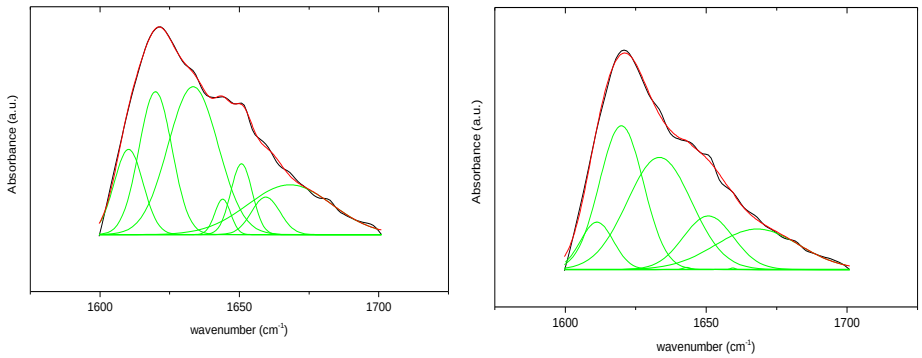

Figure A10- Curve-fitted spectra (upper) of H2O-SELP/Ag of methanol-treated methanol-treated . Gaussian bands (green line) were fitted iteratively to the amide I band (black line).

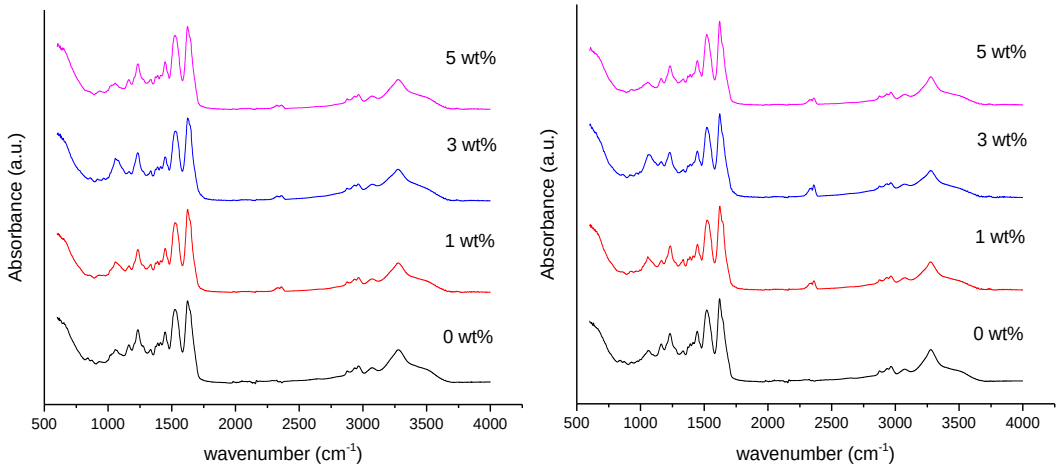

Figure A11- (A) FTIR spectra of H2O-SELP/LF films. **(B)** FTIR spectra of methanol-treated H2O-SELP/LF films.

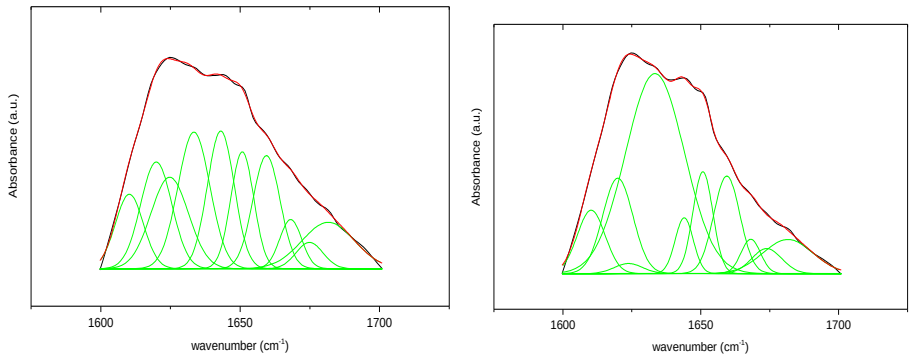

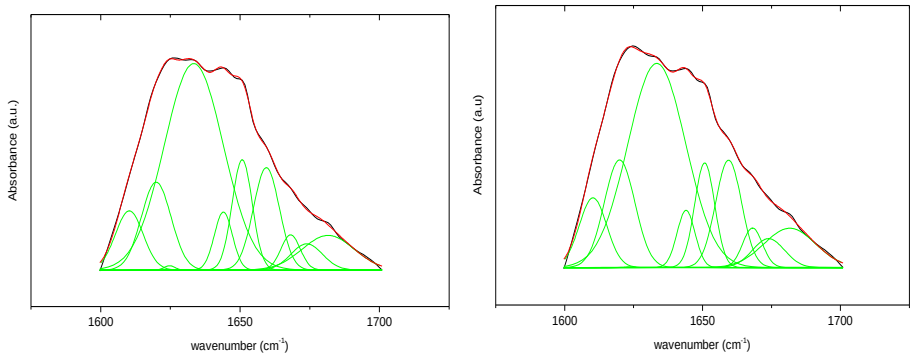

Figure A12- Curve-fitted spectra (upper) of H2O-SELP/LF of non-treated films. Gaussian bands (green line) were fitted iteratively to the amide I band (black line).

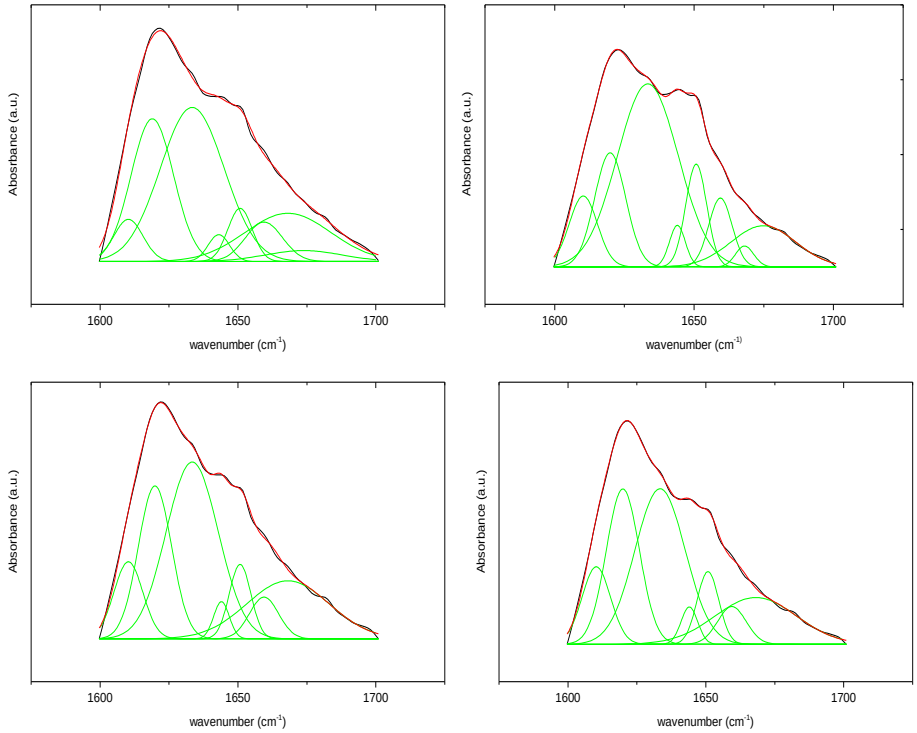

Figure A13- Curve-fitted spectra (upper) of H2O-SELP/LF of methanol-treated methanol-treated . Gaussian bands (green line) were fitted iteratively to the amide I band (black line).

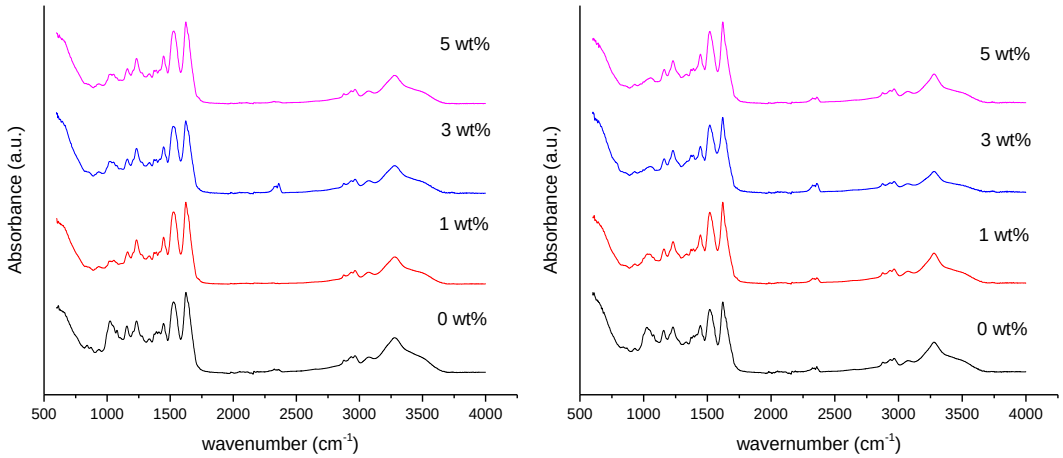

Figure A14.- (A) FTIR spectra of FA-SELP/LF films. **(B)** FTIR spectra of methanol-treated FA-SELP/LF films.

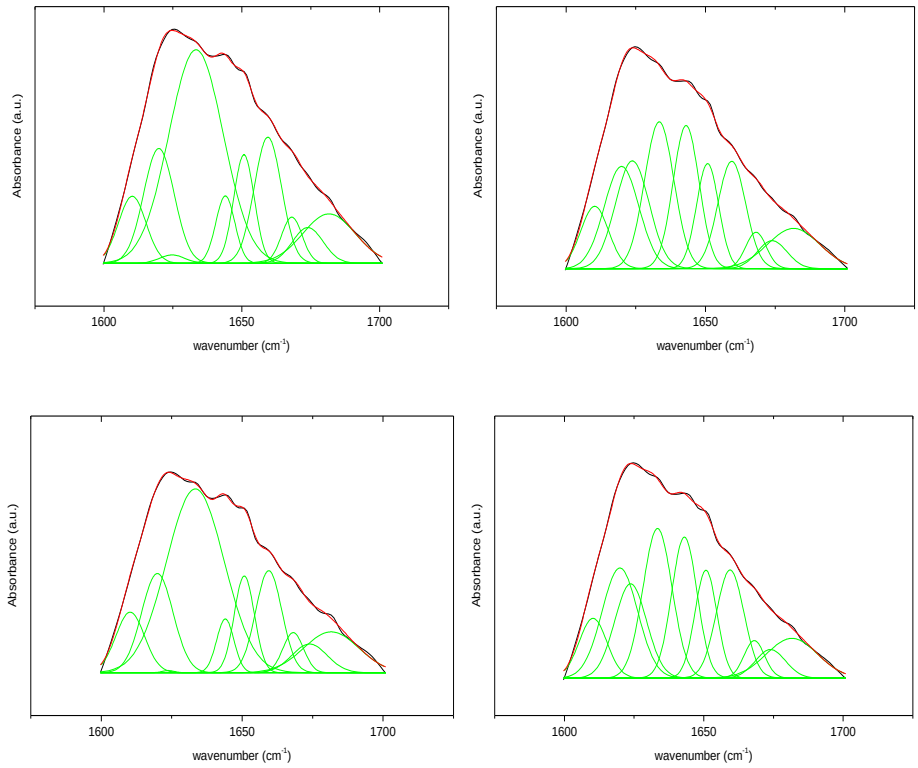

Figure A15- Curve-fitted spectra (upper) of FA-SELP/LF of non-treated films. Gaussian bands (green line) were fitted iteratively to the amide I band (black line).